University of Southampton

AUTOMATIC GAIT RECOGNITION BY SYMMETRY ANALYSIS

By

James Ben Hayfron-Acquah

A thesis submitted for the degree of

Doctor of Philosophy

Faculty of Engineering and Applied Science

Department of Electronics and Computer Science

University of Southampton

United Kingdom

June 2003

University of Southampton

Abstract

FACULTY OF ENGINEERING AND APPLIED SCIENCE
DEPARTMENT OF ELECTRONICS AND COMPUTER SCIENCE

Doctor of Philosophy

Automatic gait recognition by symmetry analysis

by James Ben Hayfron-Acquah

This work describes a new method for automatic gait recognition based on analysing the symmetry of human motion, by extending an established symmetry operator. This operator, rather than relying on the borders of a shape or on general appearance, is able to locate features by their symmetrical properties. Essentially, it accumulates the symmetries between image points to give a symmetry map. This approach is reinforced by the psychologists' view that gait is a symmetrical pattern of motion. It is also supported by works that suggest pendular motion is an appropriate model for automatic gait recognition.

This research is the first application of symmetry to images of moving objects. We have developed approaches to temporal symmetry and refined earlier approaches not only in terms of temporal issues but also in terms of basic capability. Accordingly, the new approaches generate symmetry maps of moving subjects by extension and refinement of the earlier operator to include time. As such, the resulting maps obtain information concerning not only body shape, but also the way it moves. The Fourier transform is used to derive the gait signatures from the symmetry maps, in view of its invariance and coding properties, and also its descriptive capability.

As a new technique, a large part of the research was devoted to experimentation. The approach was applied to a number of disparate databases from different institutions. We first applied our method to compare animals' gait and then to different databases of at least twenty subjects, with each subject in the database having four or more image sequences. For all databases, we derive gait signatures for silhouette information. We also derive gait signatures from optical flow information as alternative inputs to our approach, for some of the databases. For the silhouette information four different approaches namely spatial, spatio-temporal, extended spatio-temporal and temporal symmetry are used. Two other forms of symmetry are also considered. Symmetry projection is used in searching for symmetries in a given orientation or direction. Radial symmetry is used in detecting points that are highly symmetric in multiple distinct orientations, by emphasising contributions in the directions normal to the main symmetry. The results show that the symmetry properties of an individual's gait appear to be unique and can indeed be used for analysis and recognition.

We have so far achieved a Correct Classification Rate exceeding 95% by the k-nearest neighbour rule with $k = 1$ and $k = 3$, and that is a very promising start. The extensive experimentation carried out on the performance analysis of the symmetry operator also suggests that symmetry enjoys practical advantages in automatic gait recognition such as relative immunity to noise and missing frames, with capability to handle occlusion, and as such might prove suitable for applications such as video-clip database browsing. Naturally, the new approach is generic, with potential application in domains other than behavioural biometrics.

Table of Contents

List of figures

List of tables

To my family and especially my little girl, Miss Emmanuella Aba Hayfron-Acquah

Acknowledgements

My foremost and greatest appreciation goes to my supervisors Prof. Mark S. Nixon and Dr John N. Carter for their encouragement, constructive criticisms, suggestions and assisting in getting the much needed academic materials throughout this work.

I would like to thank my family for their encouragement and partial financial support. I am also very grateful to the Image, Speech and Intelligent Systems (ISIS) research group especially Dr Jamie Shutler and Dr Mike Grant for the role they playing in setting up the Southampton University's databases used in this work.

I would also like to acknowledge the financial support of the Association of Commonwealth Universities, United Kingdom, the Scholarship Secretariat, Accra-Ghana and the partial support of the European Research Office of the US Army under contract number N68171-01-C-9002. I am grateful to anyone who played any role during my stay in England especially Mrs Anne D. Donohue.

Above all, I am most grateful to God for everything that has ever happened to me.

Chapter 1

CONTEXT AND CONTRIBUTIONS

1.1 Introduction

Gait is an emergent biometric aimed essentially to recognise people by the way they walk. It is a basic requirement for daily activity [1] and is known to be one of the most universal and complex of all human activities [2]. It is determined by the muscular and the skeletal structure, thus a person can be seen as an individual comprising of several components. These components range from a subject's thigh rotation and leg swing patterns. Gait as a biometric has a number of advantages. It requires no contact, like automatic face recognition, and that it is less likely to be obscured than other biometrics. It also has allied subjects including medical studies, psychology and human body modelling and tracking. All these subjects lend support to the view that gait has clear potential as a biometric. Gait in able-bodied people has received considerable attention. It is therefore not surprising that the Defence Advanced Research Projects Agency (DARPA) of the United States is currently providing funds to a number of institutions to research into Automatic Gait Recognition for Human Identification at a Distance. The participating institutions focussing specifically on gait are the University of Southampton (SOTON), Massachusetts Institute of Technology (MIT), Georgia Technical Research Institute (GTRI), University of South Florida (USF), University of Maryland (UM), Carnegie Mellon University (CMU) and the National Institute for Standards in Technology (NIST).

1.2 Contributions

The majority of current approaches to gait recognition analyse image sequences to derive a gait signature from human motion characteristics and then use them for recognition. Early results from the different approaches to gait recognition confirm that there is rich potential in gait recognition. However, only further development will confirm whether its performance can match or better that of other biometrics.

Early tests from the different approaches were carried out on small number of subjects, usually up to 10 people. We have since generated a much larger database, which is currently the largest gait database of its kind consisting of over 100 subjects with each subject having at least four image sequences for each direction of walk (from left to right and vice-versa). We will use these databases to show that our approach can perform well on both smaller and larger databases.

There is a literature supporting the notion of symmetry of gait. We started by reviewing in detail the current position for gait as a biometric and whether or not symmetry of gait can be used to recognise people. We have, since the start of this work, continued to show that symmetry can indeed be used in gait recognition. We started by first applying the discrete symmetry operator on a small gait database [3, 4] and the symmetry operation here is new to gait analysis. In both works, we showed that the symmetrical properties of an individuals' gait appear to be unique and that humans can be recognised by the symmetry of their gait. The results obtained were very promising. An extended version of this early work [4] was invited for the special issue of Pattern Recognition Letters on Multi-Modal Biometrics. We later extended our approach to analyse animal motions and showed that animals can equally be identified by symmetry of their movements [5]. The concern here was the distinction between quadrupeds. We then included temporal information in the spatial approach [6], the first such approach to include time within a symmetry operation. The inclusion of the temporal information in our symmetry calculation improved on our earlier results. The extension is a very new approach. Further modifications of our spatio-temporal approach include extensions to projection and radial symmetry, as well as novel reformulation of the

temporal symmetry operator. These continue to confirm our earlier results and reaffirmed the appropriateness of symmetry as a cue for gait recognition.

Comparisons of our approach with others working on gait recognition using the same databases have shown that our new approaches perform very well and in most cases better.

1.3 Thesis overview

The thesis is divided into eight chapters. The remaining chapters will be arranged as follows.

- Chapter 2: Introduction

  This chapter presents a brief introduction to gait recognition and some of its advantages over the other known biometrics. Some of the allied studies of gait are also discussed to show the importance of gait as well as how gait is perceived by psychologists as a symmetrical pattern of motion.

- Chapter 3: Approaches to automatic gait recognition

  This chapter reviews some of the approaches to automatic gait recognition. We show how early and current approaches have shown that it is possible to recognise people by their gait even though most of the approaches were tested on smaller databases. The main approaches considered include the spatio-temporal pattern of motion, holistic or statistical measurement and model based approaches, pointing out some of the advantages and disadvantages of the various approaches. We also look at how some of these approaches suggest that symmetry is an appropriate cue for gait recognition.

- Chapter 4: Gait and symmetry

  This chapter looks at the relationship between gait and symmetry. A review of literature that provides support for gait symmetry and gait asymmetry is also presented. We also introduce the symmetry operator as used in this work and justify its choice. The symmetry contribution depends on only two parameters. Here, we discuss the effects that these parameters have on the overall symmetry

contributions. The operator is also applied to human and animal silhouettes. Our main contribution of including temporal information in the symmetry calculation shows that people can be recognised not only by their body shape but also by their body dynamics. Other forms of symmetry computations are discussed. These include projection symmetry and radial symmetry. The symmetry projection is very useful in looking for symmetries in a given direction. It has been used to detect facial features. We show how the formulation can be modified to suit gait recognition as well as how the direction of symmetry should be selected to improve on subject recognition. Radial symmetry is also used to detect points that are highly symmetric in multiple distinct orientations by emphasising contributions in the directions normal to the main symmetry. This will be described briefly in this chapter. Results of the application of the radial symmetry and projection symmetry will be presented later.

- Chapter 5: Symmetry extraction

This chapter provides an overview of how symmetry can be extracted from both silhouette and optical flow information as alternative inputs to our approach. We also show how a gait signature is derived and also observe the possibility of separating animal movements by symmetry analysis. The concluding part of this chapter explains how subjects are recognised by using the Fourier transform and the k-nearest neighbour rule.

- Chapter 6: Results of Human gait recognition by symmetry

Chapter 6 provides the results obtained from the different databases. The databases used include those captured at the University of Southampton, University of California San Diego and Carnegie Mellon University. A description of the processes involved in the data capture at University of Southampton as well as the chroma-key silhouette extraction is also provided. The appropriate number of Fourier descriptions needed for good recognition rates is also investigated.

- Chapter 7: Performance analysis of the symmetry operator

This chapter is on performance analysis of the symmetry operator. Here, we look at how our approaches perform with respect to missing frames, noise, occlusion and

low resolution images. These factors determine how practicable our approach can be, especially for visual surveillance, security applications or video-clip database browsing. We also compare our results with those obtained by other approaches on same databases.

- Chapter 8: Conclusion and further works.

We draw overall contributions and assess generalization capability for this new approach.

1.4 Publications resulting from this work

i. Hayfron-Acquah, J.B., M.S. Nixon, and J.N. Carter, *Automatic Gait Recognition via the Generalised Symmetry Operator.* BMVA Workshop Understanding Visual Behaviour, 2001.

ii. Hayfron-Acquah, J.B., M.S. Nixon, and J.N. Carter, *Automatic Gait Recognition by Symmetry Analysis.* Proc. Audio-and-Video-Based Biometric Person Authentication, 2001: p. 272-277.

iii. Hayfron-Acquah, J.B., M.S. Nixon, and J.N. Carter, *Recognising Human and Animal Movement by Symmetry.* Proc. IEEE International Conference on Image Processing, 2001: p. 290-293.

iv. Hayfron-Acquah, J., M. Nixon, and J. Carter, *Human Identification by Spatio-Temporal Symmetry.* 16th International Conference on Pattern Recognition, 2002: p. 632-635.

v. Hayfron-Acquah, J.B., M.S. Nixon, and J.N. Carter, *Automatic Gait Recognition by Symmetry Analysis.* Pattern Recognition Letters on Multi-Modal Biometrics, 2003: 24(**13**), p. 2175 – 2183.

Chapter 2

INTRODUCTION

Recently there has emerged a new application domain of computer vision dealing with the analysis of human images. This includes ear recognition, face recognition, body tracking and hand gesture recognition, just to mention a few. Recognising people automatically is of increasing interest, and recently, gait recognition has been added to this domain. For example, the Defence Advanced Research Projects Agency (DARPA) of the United States is currently providing funds to a number of institutions to research into Automatic Gait Recognition for Human Identification at a Distance. This programme concerns developing new technologies for recognising people at a distance. This is especially appropriate forum for identification by gait, as it allows not only for use of gait as a biometric, but also provides a capability for developing other biometrics once a human subject has been located.

Gait recognition has recently generated a considerable amount of media interest (in national and international TV, radio and the press). As a biometric, gait concerns recognising people by the way they walk and the aim of gait recognition is to recognise people by the way they walk from the changes in the human body, regardless of the clothes worn or the differing backgrounds. Humans perceive gait by observing a person's overall shape and how the body changes as they walk.

One major advantage of gait as a biometric over others (e.g. fingerprint recognition) is that it does not require contact with the subjects nor does it require the subject to be near sensors. There are a number of motivations for using gait as a biometric with the main one being that gait is less likely to be obscured. Moreover, it is very difficult to conceal or disguise gait whilst maintaining apparent normal movement. An increasing

demand for research into automatic gait recognition may be illustrated by the following real time application scenario involving armed robbers (see Figure 2.1). They usually wear helmets, face-mask, spectacles and/or gloves thus making it very difficult to use most of the well established biometrics such as the fingerprint or face from their video footage. However, aiming not to attract attention by walking suspiciously or impeding their own gait in achieving their targets, the robbers will have to walk naturally thus exposing their own normal gait.

Figure 2.1: An armed robber as captured on CCTV camera walking away from a crime scene [Discovery channel news, 25 January, 2000]

Currently, gait is also the only biometric effective at a distance. This is because at a distance other biometrics will find the image quality or resolution to be too low to be perceived with any accuracy. However, given a sufficient view of the human subject video footage, the gait might be perceived and recognised. This would not be possible without motorised zoom cameras, but even this requires location of the human subject and this also could be achieved by automatic gait analysis.

Even though it could be argued that physical condition factors such as drunkenness, pregnancy and injuries can affect an individual's motion, these factors are similar in principle to factors affecting other biometrics and most of these may have only a short

term effect. For example, face recognition, which is considered one of the most acceptable biometrics, suffers from the effects of ageing, facial expressions, facial hair, make-up, etc.

From a psychological perspective, most people are able to recognise acquaintances from familiarity cues such as clothes, size, body shape, hair colour/style, or having seen a face before. The aim of gait recognition is to recognise people by the way they walk regardless of the clothes worn or differing backgrounds.

There have been allied studies of gait, notably among these are medical studies, psychological studies, modelling human motion and tracking people. Psychologists, medical researchers and mathematicians suggest gait is a symmetrical pattern of motion [7-9] as well as suggesting that humans perceive gait as unique for human identification. This is also suggested by recent studies in Computer Vision. We capitalised on these to show that we can distinguish human and animal movement, and further use this to recognise people by the way they walk.

It is worth mentioning that even though there is a substantial body of literature on the application of symmetry [10-14] and on gait recognition [15-19], no attempt has before been made to use the symmetrical properties of an individual's gait for recognition. This work, therefore, uses the Generalised Symmetry operator in deriving gait signatures from the symmetrical properties of human walk. The operator essentially aims to detect features that have spatially symmetric properties. It is considered to be a pre-attentive feature that enhances recognition and reconstruction of shapes and objects [20]. Symmetry detection is a low level operation and can be applied to shapes and objects without prior knowledge of their shape for recognition.

2.1 Medical studies of gait

Medical studies use gait as a clinical tool for the treatment of pathologically abnormal gait. For example, Murray *et al.* [21] conducted a research involving sixty pathologically normal men aged between 20 and 65 years. The men were placed in five

age groups. The data collection system used required markers to be attached to the subject. This form of data collection is typical within the medical field and although practical in that domain, it is not suitable for identification or gait recognition. Each subject was filmed walking for a repeated number of trials. Murray *et al.* observed that the standard movement patterns of the men were strikingly similar for a repeated number of trials of the same subject. They suggested that if all gait movements are considered then gait is unique. However, some of the measurements are available from an overhead view, capable of reducing the apparent value of this observation. Gait was considered as 'a total walking cycle'. A gait cycle is the time interval between successive instances of initial foot-to-floor contact 'heel strike' for the same foot, that is a gait cycle starts and ends with the heel strike of the same foot (*see appendix B*). The results obtained [21] were used in Murray's later work [22] to compare the gait patterns of pathologically abnormal patients for treatment. Though there is an extensive literature on studies of gait for medical use, none is primarily concerned with biometrics. Nixon *et al.* [23] are of the view that measurements by gait researchers could prove to be of benefit in biometrics, though there is concern that the system of data collection cannot be used in biometrics.

2.2 Psychological studies of gait

Psychologists [2, 7] have long suggested the ability of humans to recognise and distinguish between different types of human motion. For example, in Johansson's work [24], he attached reflectors at the major joints of his subjects and filmed them walking in a dark environment. These were then played to observers who immediately recognised the few moving dots as a human walking. The viewers initially failed to recognise the points when viewed in static images as they could not perceive them to be in the human form but rather as a picture of a Christmas tree. Later work by Dittrich [25] showed how by point light displays a human could be rapidly extracted to discriminate the different types of human motion including jumping and dancing. Bingham *et al.* [26], also used point light displays to confirm that they are sufficient for the discrimination of different types of object motion and that discrete movements of parts of the body can be perceived. Cutting *et al.* [16] later conducted a similar

experiment. The aim of the research was to show how viewers can recognise themselves as well as others from an abstract display of human movements. The viewers were able to identify themselves and others. Most of the viewers admitted using familiarity cues such as body size, amount of arm swing, manner of walk. Cutting *et al.* [7] also suggest gait as a synchronous symmetric pattern of movement as such giving a pointer to the use of symmetry in automatic recognition by gait. In another work by Kozlowski *et al.* [27] from similar experiments involving six subjects; 3 males and 3 females, who knew each other, they were able to recognise the sex of a walker from the dynamic point light display. The six subjects were made to walk ten times. The same six subjects served as viewers a month later including one other person that knew the other six subjects. The walkers were referred to as Walker 1, Walker 2, etc. "Walkers 4, 5, and 6 were correctly identified as male on an average of 72% of trials, and walkers 2 and 3 were correctly identified as female on 67% of trials ... Walker 1 ... only 32% of trials."

In a recent study by Stevenage *et al.* [19], they concluded that it is possible to recognise people by they way they walk, and can learn their gait for recognition purposes from their video footage. They also observed that even under adverse conditions, humans can still perceive human gait as a cue to identity.

From the above works and other related psychological studies of gait, it is clear that psychological studies clearly support gait as a potential biometric, with some suggesting that symmetry of human motion can be used to recognise individuals.

2.3 Modelling the human body and its motion

There are studies concerning human motion and extraction. The primary aim of these studies was not usually for biometric purposes. Different models are used to represent the human body; notable among these are stick model, blob model, cylinder model, etc. Stick figure models represent the human body by connecting sticks at various joints of the human body. It is the simplest representation of the human body. The motion of the joints gives the key to motion estimation and analysis. For example, Akita [28] used a

six segment model to represent the two arms, two legs, the torso and the head of the human body to model the movements of the body using a sequence of stick figures. Other works use different number of joints and segments.

The walking model of Lee *et al.* [29] uses 14 joints and 17 segments while Guo *et al.* [30] used a ten stick model articulated with six joints to represent the human body structure in silhouette. Recently, Dockstader *et al.* [31] used the fusion of a fifteen-parameter stick model and a ten-parameter bounding volume for the human body. Each component of the model is measured in 3-D, body centred coordinates. These measurements were used to obtain estimates of certain gait variables such as the stride length, arm swing, cadence, gait velocity and stance.

Cylinders have also been used to represent the feet, legs, thighs, arms, upper-arms, head and torso to model the human body. The works by Hogg [32] and Rohr [33] use 14 cylinders to represent the above listed human body parts in their walking models. Kurakake *et al.* [34] treated the human body as an articulated object having parts that can be considered as almost rigid and connected through articulations. They use a two dimensional version (ribbon) of the cylinder to represent the parts.

The blob model was developed by Kauth *et al.* [35] and Azarbayejani [36] used this model in human motion tracking. Azarbayejani modelled the human body as a connected set of blobs, each of which serves as one class.

Campbell *et al.* [37] proposed techniques for representing movements based on space curves in subspaces of a 'phase space', a symbolic description that translates the continuous domain of human motion into a discrete sequence of symbols. The phase space has axes of joint angles and torso location and attitude, and the axes of the subspaces are subsets of the axes of the space phase.

2.4 Tracking people

Tracking people is an important aspect of visual surveillance or security applications. Body tracking basically involves finding and following the human body model in each frame of a video footage. This is usually achieved by defining a set of body features and finding those same features in each image frame of a sequence. By finding these features, it is possible to calculate changes between frames such as body shape, velocity, position, etc.

Hogg [32] used a model based approach where images are mapped into a description in which a person was represented using a series of hierarchical levels. His model, the WALKER, was illustrated by superimposing the machine-generated picture over the original photographic images. Gavrila *et al.* [38] presented a 3-D model-based approach of tracking humans using multi-view images. On a large Humans-In-Action database of subjects the model successfully tracked some demanding postures.

Most tracking approaches naturally lack the accuracy required for recognition as this was not their original purpose. However, it appears reasonable to assume that tracking procedures could be deployed to develop a gait signature or at least to derive a human silhouette for later recognition purposes. It is certainly evident that tracking approaches can deliver estimates of the human body for analysis by a recognition approach.

2.5 Conclusions

Each of the allied studies continues to support the notion that gait can be used as a biometric. The physical characteristics of gait are established and viewed as unique, humans can perceive gait and gait can be modelled and extracted by computer vision techniques. Equally, there are suggestions from many of these studies that symmetry is attributable to gait. Much of this work has been of benefit to the approaches to automatic gait recognition.

Chapter 3

APPROACHES TO AUTOMATIC GAIT RECOGNITION

Although gait recognition is a fairly new area of research, there are already several approaches to automatic gait recognition [16, 17, 23, 39-48]. The approaches that extract motion information from a sequence of images for recognition are said to be motion-based while the other approaches that extract features of images are known as feature-based. The two approaches are sometimes classified as the model-based approach and the holistic approach. Model-based approaches are those that use models such as the stick figure to represent the human body. Gait signatures are then derived from measurements such as the orientation of the human thigh. The holistic approaches on the other hand are those that use a set of measurements such as height and distance between two parts of the human body to distinguish between different people.

3.1 Model based approaches

The spatio-temporal approach is considered probably the earliest approach to automatic gait recognition. In this model-based approach, the gait signature was derived from the spatio-temporal patterns of a walking person [49]. The different patterns of the motions of the head and the legs in XY-translation and time were extracted. The patterns were then processed to determine the motion of the bounding contours to which a five-stick model was fitted. The gait signature was then derived by normalising the fitted model in terms of velocity, by linear interpolation. In [49], the approach was applied to a database of five subjects each having twenty-six image sequences. The recognition

rates obtained were between 60 percent and a little over 90 percent. The rates were dependent on the weighting factors in the Euclidean distance metric.

Nash *et al.* [50] also developed another model-based approach that uses the simple pendulum model as a basis for searching a scene to locate a moving person using the Velocity Hough Transform (VHT). Cunado *et al.* [41] developed a model-based approach in which the legs are considered as interlinked pendulums. Gait signatures are derived from the spectra of measurements of the orientation of the thigh accumulated from the image sequence using an extension of the VHT. This model provides enough information for recognition. Using Fourier weighted magnitude spectra, encouraging recognition rates were obtained on a small database of subjects. This approach suggest symmetry analysis to be an appropriate approach for gait recognition

The idea of Cunado *et al.* was later extended by Yam *et al.* [48, 51] to include the motion of the lower leg thus producing a coupled oscillator gait model which they applied to a database of walking and running image sequences to give very promising recognition rates. The approach extracts leg motion during walking and running using temporal template matching, with a model defined by forced coupled oscillators. Fourier transform analysis of the variations in the leg (thigh and lower leg) is used to generate gait signatures. The k-nearest neighbour classifier is then used to classify the subjects. On a database of 25 subjects having 5 image sequences each, individuals' recognition rates of over 90% were obtained. This approach explicitly uses bilateral symmetry in its formulation. This is used primarily to derive a model from which leg data is derived from the angles. Again, this emphasises the notion that symmetry is an appropriate cue for recognition by gait.

Bhanu *et al.* [39] also adopted a model-based approach that models the various parts of the human body based on their geometrical representations. Using the least squares fit of the 3D kinematics model to the 2D silhouette extracted from image sequences, the walking parameters (cadence, step length, stride length, velocity, etc) are then extracted from the 3D silhouette. The main advantage of this approach is that it does not rely on

subjects walking normal to the plane view of the camera. On a database of 30 image sequences, a recognition rate of 77% was achieved.

In [17], a new approach to automatic gait recognition that does not use a model of the human walking was presented. Rather, optical flow was used to derive the gait signature by analysing the motion content (shape of motion) of a human walking. The features of the motion were derived as the variation of the first and second-order moments of a dense optical flow. The periodic structure obtained from the gait features was described by using the relative phase of the spectral components. The approach was applied to a database of six subjects with seven image sequences each and a recognition rate exceeding 90 percent was obtained. Here also, the recognition rate was dependent on the type and the number of motion features considered.

3.2 Holistic approaches

Holistic or statistical approaches aim to find a set of measurements from a gait sequence to distinguish between subjects. Generic object-motion characterisation is also another approach where the gait signature is derived from a parametric eigenspace [52]. In terms of functionality, this approach is similar to spatio-temporal image correlation, but essentially reduces the computational requirement. Here, adjacent images are subtracted to obtain a body silhouette, which is then processed to reduce noise. The images are then projected onto eigenspace. Eigenvalue decomposition is then performed on the silhouette sequence. The order of the eigenvectors obtained corresponds to the frequency content. In [52], the approach was applied to a database of seven subjects with ten image sequences each. The recognition rates were 88 and 100 percent for eight and sixteen eigenvectors, respectively for the spatio-temporal image correlation approach.

The eigenspace approach was extended [43, 53] to use canonical analysis, a model-free approach. One of the major differences between the approach and the others is that the image sequence is described as a whole. It essentially combines the Canonical Space Transformation (CST) based on the canonical analysis with the Eigenspace Transform

(EST). The effect of combining the eigenspace transformation and the canonical space transformation is to reduce the dimensionality of the input data and also to optimise class separability of different gait sequences. The canonical space approach was applied to a database of five subjects with five image sequences each and a recognition rate of 80% was achieved. When EST and CST were combined and applied to the same database, a recognition rate of 100% was achieved. The popularity of eigenspace approaches [23] is reflected in a recent approach [54] where Principal Component Analysis is applied to generate eigengaits. Supervised clustering then groups the training set into different classes. Similarity plots are then assigned to the various eigengaits for recognition, obtaining a recognition rate of 93% on a database of six subjects.

Johnson *et al.* presented a multi-view gait recognition method using recovered static body parameters (activity-specific biometric) of subjects [55]. The technique extracts some identifying properties of an individual's behaviour and is only applicable when a person is performing that action. The body parts are first labelled by analysing the binary silhouette of the subject in each video frame after background segmentation. A bounding box is placed around the silhouette and then divided into three sections namely head section, pelvis section and foot section. The static body parameters used for identification are the set of measured distances in pixels between the body parts locations, that is (i) the height of the subject, (ii) the distance between the head and the pelvis locations, (iii) the maximum distance between the pelvis and left foot location, and between the pelvis and the right foot location and (iv) the distance between the left and the right foot. These measurements are taken when the subjects' feet are maximally spread during walking action. Using these four measurements on a database of six subjects, individuals' recognition rate of over 90% was achieved.

Recently, Shutler *et al.* extended statistical gait recognition via temporal (velocity) moments [46, 56]. Statistical moments were applied to image sequences resulting in a temporal shape descriptor. The advantage here is the temporal moments have an intimate relationship with gait itself, unlike earlier approaches. The velocity moments up to order four were computed, and successfully applied to a database of four subjects

with four image sequences each. More recently, Shutler *et al.* used the Zernike velocity moments [57] to describe motion for recognition. The approach aims to describe a shape by its motion from an image sequence by capturing independent descriptors. The statistical ANOVA technique is then used to classify the features selected as gait signature. Using the k-nearest neighbour approach, recognition rates of 100% were obtained on a small database of subjects. Performance analysis shows that the approach is good at handling occlusion.

The approach to gait recognition by Foster *et al.* [42, 58, 59] involves deriving a gait signature from the area of the silhouette within a mask. Different masks are used depending on the area of the silhouette required. For example, the bottom half mask selects only the legs of the subject. For a given image sequence, the mask is applied to each image in a sequence. One of the main advantages of this method is that it is independent of the direction of motion. It is also relatively fast, however, whenever a new subject is added to the database, the entire process has to be run again. On a large database of subjects, the recognition rates obtained were very promising.

Collins' *et al.* recent approach presented a baseline method for human identification based on the body shape and gait [60]. This is supposed to provide a lower bound against which to evaluate gait techniques. Their viewpoint dependent approach is based on template matching of body silhouettes. Cyclic gait analysis is then used to extract key frames from a test sequence which are later used to compare with training frames using normalised correlation. The template matching was done by using a test subject from a probe set with templates in the gallery set [61]. The subject is then classified by using the nearest neighbour matching among the correlation scores. Basically, their approach captures features such as body height, size, stride length and the amount of arm swing. The approach was applied to different databases of different viewing angles (0 and 45 degrees), background conditions (indoor and outdoor) and walking speeds (slow and fast) achieving recognition rates of 76 – 100% by considering up to the top 10% of the matches.

Phillips *et al.* [61] developed a simple algorithm composed of three parts based on issues involved in gait recognition such as the effect of view, shoes and surface. The first part of the algorithm defines bounding boxes around the moving subject in each frame of a sequence. The second part begins with the background estimation from the mean and covariance of the RGB channels at each pixel, using the pixel values outside the bounding boxes. The silhouette of the subject in the bounding boxes is then extracted. The third stage involves the computation of the similarity between silhouette pairs of frames. This is done by computing the ratio of the number of pixels in their intersection to their union. The sum of the similarity measures throughout an entire sequence defines the correlation between two sets of silhouettes. These are then used for classification. On a database of 74 subjects, individuals' recognition correct classification rate of over 70% was obtained.

3.3 Conclusions

The model based approaches and the holistic approaches have their own merits and demerits. The model based methods are more open to re-deployment to different camera views, or even different applications. Most of the statistical approaches are not intimately related to gait as they just produce raw numbers to distinguish between different subjects. Moreover, most of them fail to take into account the temporal component of gait and instead focus on distinguishing between collection of silhouettes rather than a sequence as a whole. However, some of the holistic approaches have improved capability over application problems such as noise as they do use more subject information as compared with a model description of only the human legs.

It is clear from the review of the existing approaches that most of the early techniques used databases usually containing up to 10 subjects with good recognition rates. Some of the recent techniques have used much larger databases. All these different approaches have been tried on different databases and the results have shown that it is possible to recognise people by their gait. However, in order to test new developments (such as different approaches or improvements in existing techniques), gait would benefit from having an established database.

Chapter 4

GAIT AND SYMMETRY

4.1 Support for gait symmetry

Gait requires continuing ground reaction forces at each step and propelling the body forward in the direction of progression. Some researchers have defined gait symmetry in different ways. Herzog *et al.* [62] and Soudan [63] defined gait symmetry as a perfect agreement between the actions of the lower limbs. Hesse *et al.* [64], Gundersen *et al.* [65], Griffin *et al.* [9] and Gabbard [66] on the other hand suggest that the term 'gait symmetry' be used when there are no statistical differences on parameters measured bilaterally during a human walk. Anatomical or physiological criteria have also been used to describe symmetrical or asymmetrical behaviour in able-bodied gait. What all these different definitions have in common is that the term 'gait symmetry' can be used when both limbs behave identically.

Presently, there is a literature that provides support for gait symmetry. When the term was first used, it was assumed for the simplicity in data collection and analysis where direction of motion was ignored [2], and this provides one of the main reasons that many gait studies relied on unilateral data collection [20–22] or in some cases pooled right and left limb data [16, 23–26]. Moreover, the idea of gait symmetry was not tested in any of these works, since it was assumed. However, some experiments where both lower extremities were included in the observations confirmed the presence of gait symmetry.

Giakas *et al.* [67] investigated variability and symmetry of ground reaction force (GRF) measurement during walking using time and frequency domain analysis. Means and

standard deviations of the selected ground force reaction time and frequency domain parameters for the left and right sides were calculated from 10 trials of each side and their results confirm the hypothesis of gait symmetry.

Menard *et al.* [68] did not find significant asymmetry in any averaged ground reaction force patterns at natural walking speed in nine able-bodied subjects. This confirmed Hamil *et al.* [69] results that there are no significant differences between the limbs in eleven vertical, five anterior-posterior and four medio-lateral characteristics of the ground reaction forces during walking and running. Chou *et al.* [70] also reported perfect symmetry in energy efficiency between both limbs during walking. Hesse *et al.* [64] and Wall *et al.* [71] claim that normal gait is symmetrical.

In a more recent work by Perthunen [72], the normal gait of twelve adults was examined. In his experiment, measurements were taken immediately after the familiarization on a 30m long walkway. The subjects were examined at target velocities of 4.0km/h, 5.5km/h and 7.0km/h. These correspond to slow, normal and fast walking respectively. The margin for accepting a trial was $\pm 2.5\%$ of the selected speed. The subjects' walking speeds were measured and controlled by photocells. The order of the walking speeds was randomized. Each subject walked three times at each speed. All subjects were made to wear the same walking shoes to reduce the effect of footwear. He concluded that the foot loading patterns of healthy subjects demonstrated symmetrical gait in the natural walking conditions. No statistically significant differences were found between the left and the right ground reaction force in the vertical and the medio-lateral directions of the slow, normal and fast walking speeds.

4.2 Support for gait asymmetry

Sadeghi *et al.* [2] provides an intensive review on the support of gait asymmetry. Their review paper summarises the work done over the last few decades suggesting lower limb symmetry during able bodied gait. Though we have shown that there is good support for gait symmetry, there is actually far more support for gait asymmetry. Gait asymmetry is often considered to indicate gait pathology. In pathological gait, marked

differences have been identified between people with affected and unaffected limbs [2]. Some researches have shown that in able-bodied gait, there are differences between the right and the left limbs. For example, Singh [73] noted that during walking, the right and the left limbs are not used equally. Researchers have used a number of kinematics and spatio-temporal parameters such as velocity, stride, maximum knee flexion, foot placement angle, joint motion, step, etc to show the asymmetry in human gait. Rosenrot *et al.* [74], observed that the duration of the initial and terminal double support periods showed marked differences as expected in healthy asymmetry subjects. Gundersen *et al.* [65] also reported gait asymmetry in temporal and kinematic parameters. Wheelwright *et al.* [75] studied 134 normal children by looking at the spatio-temporal parameters of their gait. They reported asymmetrical behaviour of the lower limbs of their subjects aged between 3-18 years.

Other works also found gait asymmetry in able-bodied subjects. Herzog *et al.* [70] conducted an experiment on 62 able-bodied subjects for peak vertical, anterior-posterior and the medio-lateral components of the ground reaction force. Differences were noted between the right and the left lower limbs of the subjects. Later, Herzog *et al.* [4] found that asymmetry were much larger in 34 ground reaction force data of a control group than expected. Dickey *et al.* [76] identified an asymmetrical contribution in able-bodied subjects for the muscular work done at the hip level. Giakas *et al.* [67] confirm that human gait is a symmetrical movement based on harmonic analysis while substantial asymmetries characterised time domain variables in the medio-lateral component of ground reaction force. They carried out a study on the variability and symmetry of ground reaction force measurements during walking of ten healthy young male subjects.

Sadeghi *et al.* [2], in summarising their review of support for gait symmetry, stated that gait symmetry has been reported in only a few studies using quantitative biomechanics, and that there are not enough studies where a substantial number of subjects participated. They are of the view that using a single gait parameter or applying simple statistical methods for comparisons, are additional limitations to studies on support for gait symmetry. On the support for gait asymmetry, they concluded from their review

that able-bodied gait seems to be naturally asymmetrical and this asymmetrical behaviour could be associated with the different contributions of the lower limb in carrying out propulsion and control task. Therefore, accepting that gait is asymmetrical in the able-bodied population is important for medical studies and the study of physical activities, gait analysis and evaluation, etc. It is clear from all the above that asymmetry is more potent for gait recognition. Pure symmetry (for example simple harmonic motion) is insufficient for recognition by gait. It implies a lack of forward movement as well.

4.3 Symmetry Operator and the Discrete Symmetry Transform

Symmetry is considered as a feature that enhances the recognition and the reconstruction of shapes and images. It is also said to be one of the basic features of shapes and objects. Every object, be it natural or artificial often gives rise to the human perception of symmetry [20] thereby suggesting symmetry as a fundamental principle. An object is said be to symmetric when the response to symmetry operators is invariant. An example is mirror symmetry. Boolean symmetry operators require the shape of the object to be known in advance to be able to extract its features, rendering them inefficient in most cases. A simple symmetry operator would return a true result when given a precisely symmetric figure. The discrete symmetry operator on the other hand can be used to estimate symmetricity without the knowledge of the object's shape. Unlike other feature extraction operators that find a shape by relying on the border of the shape, the symmetry operator locates shapes according to their symmetrical properties. It essentially performs local operations on the edges of the image to determine whether a given shape is symmetric or not. The symmetry transform assigns a continuous symmetry measure to each point in the image. The symmetry transform of a shape is determined with respect to a given point-symmetry group. It appears that the performance of the symmetry transform is not affected by the existence of several objects in the scene[20].

In [23], gait signatures were derived from the frequency components of the variations in the inclination of the human thigh. Due to the periodic nature of the thigh during walking, a bi-pendular model was used. As pendular modelled the periodic motion of the thigh during walking, this again suggests that symmetry is suited to gait recognition. In [56], the moments derived from silhouettes had symmetry properties. These suggest the use of symmetry to be appropriate for automatic gait recognition. Symmetry has also been used to detect regions of interest for face recognition [77, 78]. Symmetrical shapes can be described on either a global or local scale. Global scale symmetry is normally used for true symmetrical shapes [79] and the most general shape description requires local symmetry evaluation [80, 81]. Symmetrical features of objects have been used for shape descriptions, shape matching, model-based object matching and object recognition [77, 82-84].

A symmetry operator extracts symmetrical properties of objects and shapes to describe and recognise objects. Bonneh *et al.* [13] used a generalised symmetry operator to distinguish between different textures. This was done by first applying the symmetry operator to the different textures and then using a discriminability measure to distinguish the different textures. In the same work, they also applied their symmetry operator to a person in portrait to detect the regions of interest.

The choice of the discrete symmetry transform (DST) appears most appropriate for gait analysis and this is its first use here. Some of the main reasons for this are as follows. Its operation is very transparent since the parameters are related to the way image content is exploited. It is also discrete since it operates on pixel grids rather than an approximation calculated from image points. Most of the early low-level attentional mechanisms were based on either grey-level variance, rapid changes in grey levels or junctions [85]. However, the DST does not depend on object segmentation and does not need to be found a priori. It uses low-level edge data and it appears to generalise many of the existing cues such as image intensity used in computer vision models for detecting regions of interest in an image. It is also based on psychophysical observation [20].

In [13], the performance of the DST was compared with the transforms proposed by Fogel [86], Krose [87], Rubenstein [88], Malik [89], Bergen [90], Buf [91], etc. The DST was found to perform much better than all these transforms. Recently, Loy *et al.* [92], inspired by the results of the DST, also evaluated the performance of most of the existing popular symmetry transforms for detecting regions of interest within a scene or an image. These transforms included that of Gesu [93], Lin [94], Minor [95], Reisfeld [20] and Sela [96]. The performance evaluation was carried out on a range of images. They concluded that of the existing transforms, the DST used in this work provided the best results. Moreover, they found that though the other existing transforms were able to highlight important regions they tend to highlight many other points, reducing their overall effectiveness. It is worth mentioning that though Gesu's transform was found to have lower complexity than that of Reisfeld, it did not appear as effective for locating points of interest.

The popularity of the technique is reflected in the interest it has generated, with high volume of citations [13, 18, 97-104]. Moreover, the potency or appeal of Reisfield's technique is reflected in its frequent use as a baseline [13, 99] for comparison against new approaches. These new approaches have not been used here since skew symmetry or axis of symmetry is their common target and that is not an issue here. The DST lends itself to specific deployment as reflected in its original presentation, and here in moving object analysis. It also allows for the possibility of extension. For example, it was extended by Parsons *et al.* [18] by introducing a focus into the distance weighting function of the transform as will be used later. We have also extended the DST. These extensions are discussed in detail under the following sections. Also, Sun *et al.* [97] used a simplified version of Reisfeld's local symmetry measure to detect faces and facial features in 2D images using colour and local symmetry information. The colour was used to estimate the area of the image containing the face, and this in turn was used to set the window sizes for the symmetry detection and measurements. Also, Li *et al.* [98] to detect facial features in 2D images. As such, it appears well-suited to the basis of a new approach for recognising moving people using their shape and movement.

Although the DST appears well-suited for our work, its main disadvantage is that it is computationally demanding.

4.3.1 Spatial Symmetry Calculation

Let P_i and P_j be any two different points in the edge map of an image, where $i, j \in 1..n$ with n being the number of pixels in the edge map; (x_1,y_1) and (x_2,y_2) are their respective coordinates. θ_i and θ_j denote the orientation of the gradient at P_i and P_j respectively; M_i and M_j are their respective edge magnitudes. α_{ij} is the counter clockwise angle between the horizontal axis and the line passing through P_i and P_j. These are shown in Figure 4.1.

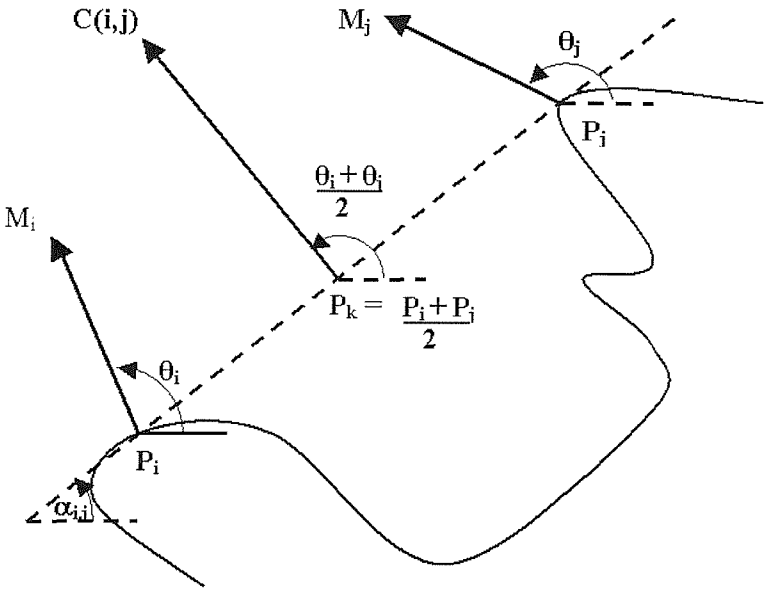

Figure 4.1: The symmetry contribution of edge points P_i and P_j

Reisfield's symmetry relation or contribution, $C(i,j)$ between any two different points P_i and P_j is defined as:

$$C(i,j) = SD_{i,j} Ph_{i,j} I_i I_j \tag{4.1}$$

where $SD_{i,j}$ and $Ph_{i,j}$ are the symmetry distance and the phase between the two points. I_i and I_j are the logarithm of the intensities at the points P_i and P_j respectively. The symmetry is accumulated at the centre or mid point of each pair of image points.

The function for *SD* is the symmetry distance weighting function. It reflects the distance between two different points $P_i = (x_i, y_i)$ and $P_j = (x_j, y_j)$. Points that are closer have lower distance and hence give higher values while those that are further away give lower values. The symmetry distance, $SD_{i,j}$ between two image points P_i and P_j is calculated as follows:

$$SD_{i,j} = \frac{1}{\sqrt{2\pi\sigma}} \exp^{-\left(\frac{\|P_i - P_j\|}{2\sigma}\right)}, \forall i \neq j \qquad \textbf{(4.2)}$$

where σ controls the scope of the function. Each value of σ implies a different scale thus making it convenient for multi-resolution schemes to be implemented. A large value of σ implies large-scale symmetry which has the advantage of giving distant points similar weighting to those at small spacing. Figure 4.2(b) shows the effect of large value of σ, that is $\sigma = 6$. The distance weight drops less rapidly for points that are widely spaced and allows such points to contribute to the measured symmetry. On the other hand, a small value of σ (shown in Figure 4.2(a), with $\sigma = 0.6$) implies local operation and local symmetry. In other words, small values of σ give closer points much higher values than the distant points. The distance weight in this case drops rapidly for points that are widely spaced and hence minimizing the contributions of such points to the measured symmetry. Thus, the value of σ essentially provides scaling possibilities. The reason for the use of the *SD* weighting function is that it is isotropic, that is, it has no preferred orientation, but we will also consider other forms of symmetry that use preferred orientation such as symmetry projection.

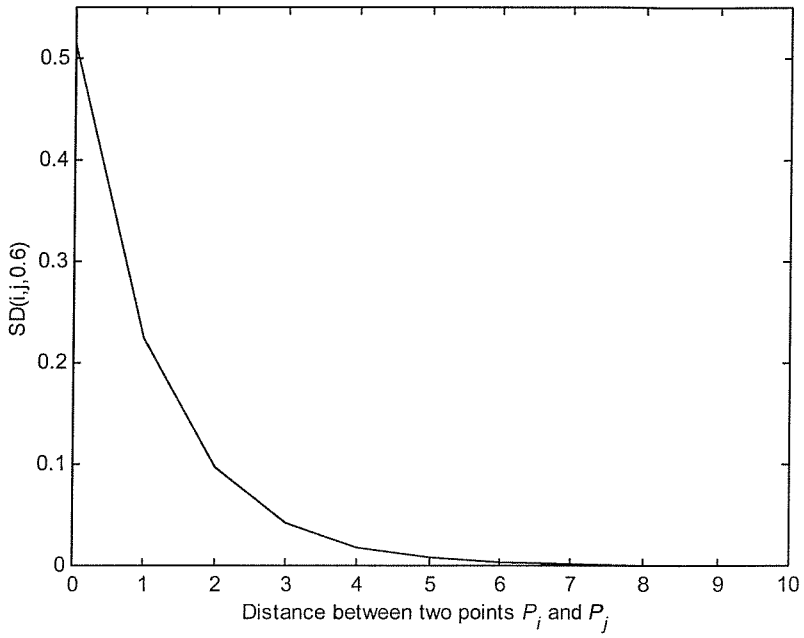

(a) Effect of small sigma ($\sigma = 0.6$)

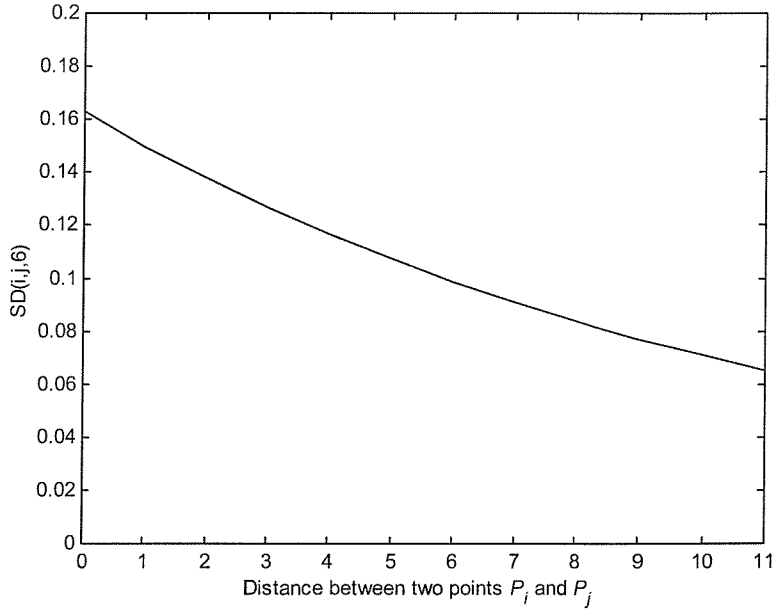

(b) Effect of large sigma ($\sigma = 6$)

Figure 4.2. Effects of sigma on distance weighting.

Recently, Parsons *et al.* [18] observed that increasing the value of σ only increases the weighting given to the more distant points and does not decrease the influence of close points. A comparison with the Gaussian-like function showed that the mean of the distribution locates the function on the mean value of the sample. A focus, μ, was therefore introduced into the distance weighting function. The resulting function is called the focus weighting function. The value of μ controls the focusing capability of the function, hence, the value of μ essentially improves on the scaling possibilities of the symmetry distance function. The modified or focus-weighting function, $FD_{i,j}$ is defined as follows:

$$FD_{i,j} = \frac{1}{\sqrt{2\pi\sigma}} \exp^{-\left(\frac{\|P_i - P_j\| - \mu}{2\sigma}\right)}, \forall i \neq j \tag{4.3}$$

It must be noted that the addition of the focus into the distance weighting function moves the attention of the symmetry operator from points close together to a selected distance. To incorporate this property, equation 4.1 is modified as follows:

$$C(i,j) = FD_{i,j} Ph_{i,j} I_i I_j \tag{4.4}$$

The logarithm intensity function, I_k, of the edge magnitude, M_k at the point k with the coordinate (x,y) is defined as follows:

$$I_k = \log(1 + M_k) \tag{4.5}$$

where

$$M_k = \sqrt{M_x^2(x,y) + M_y^2(x,y)} \tag{4.6}$$

and $M_x(x,y)$ and $M_y(x,y)$ are the vectors given by the Sobel templates for the vertical and the horizontal edge detection respectively which together give the magnitude, M_k and the direction, θ_k of an edge, P_k with coordinate (x_k,y_k). The reason for the use of the logarithm of magnitude rather than the magnitude itself is that it reduces the differences

between high gradients or symmetries resulting from weak edges. This makes the correlation measure less sensitive to very strong edges.

Reisfield's weighting function between the two points P_i and P_j is defined as follows:

$$Ph_{i,j} = \left(1 - \cos\left(\theta_i + \theta_j - 2\alpha_{i,j}\right)\right)\left(1 - \cos\left(\theta_i - \theta_j\right)\right), \quad \forall i \neq j, \tag{4.7}$$

and where

$$\alpha(i,j) = \tan^{-1}\left(\frac{y_i - y_j}{x_i - x_j}\right) \tag{4.8}$$

is the angle between the line joining the two points and the x-axis. θ_i and θ_j are the orientation of the gradient at P_i and P_j respectively.

The phase weighting function attains its minimum when the edge direction at the two points is in the same direction ($\theta_i = \theta_j$), and is maximum when the edge directions are away from each other ($\theta_i = \theta_j + \pi$) and along the line joining the two points $\theta_j = \alpha_{i,j}$. Figure 4.3(a) shows when the phase weighting function attains its maximum and the effect of $\alpha_{i,j}$ on the symmetry measure. Figure 4.3(b) also shows the effect of relative edge direction on the phase weighting. Figure 4.4 shows two different situations with the same phase value.

From equation 4.7, the phase weighting function has two factors. The first factor, $(1-\cos(\theta_i+\theta_j-2\alpha_{i,j}))$ makes it possible for maximum symmetry to be achieved when $(\theta_i - \alpha_{i,j}) + (\theta_j - \alpha_{i,j}) = \pi$. This is when the two gradients at the points P_i and P_j are oriented in the same phase and towards each other. This situation corresponds to a dark object on a light background. The second factor, $(1-\cos((\theta_i - \theta_j))$ is introduced because the case $(\theta_i - \alpha_{i,j}) = (\theta_j - \alpha_{i,j}) = \pi/2$ is included in $(\theta_i - \alpha_{i,j}) + (\theta_j - \alpha_{i,j}) = \pi$ when the first factor attains its maximum. This is when the edge directions are normal to the line joining the points P_i and P_j. This situation also corresponds to a light object on a dark background. The combination of factors makes it possible to achieve the same measure for different object reflectance and lighting conditions. This definition of the phase weighting function therefore allows the symmetry map of a silhouette to be generated irrespective of the image colour and its background colour. This is illustrated in Figure

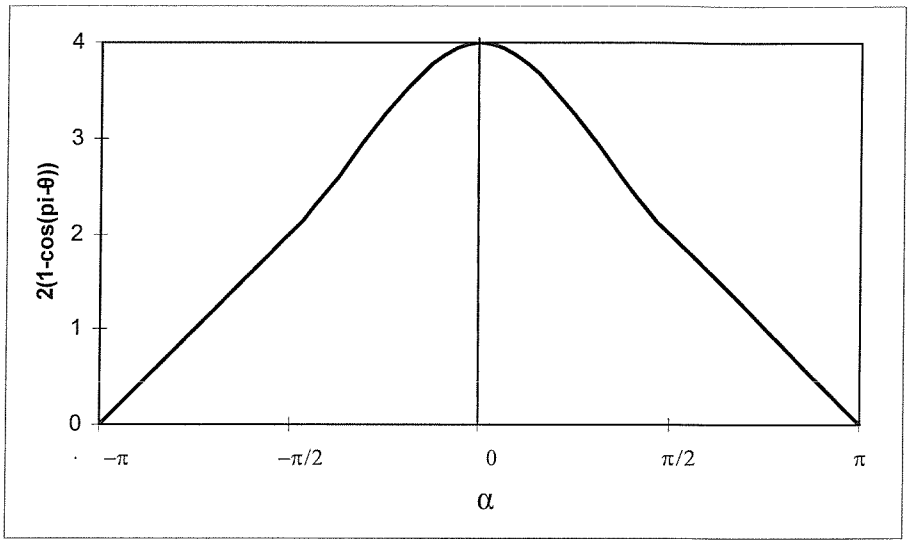

(a) when $\theta_i = \pi$, $\theta_j = 0$ and varying $\alpha_{i,j}$

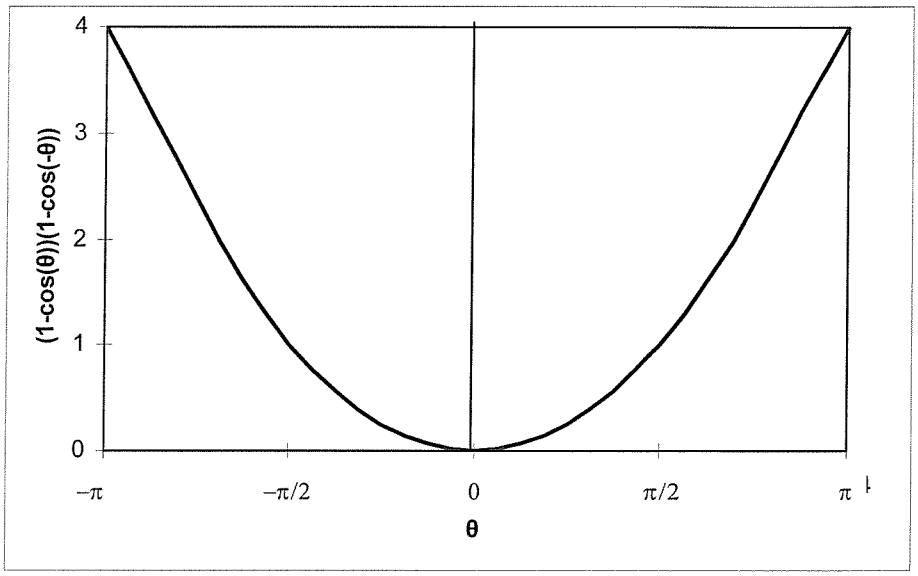

(b) when $\theta_i = \alpha_{i,j} = 0$, varying θ_j

Figure 4.3 Effect of relative edge direction on phase weighting

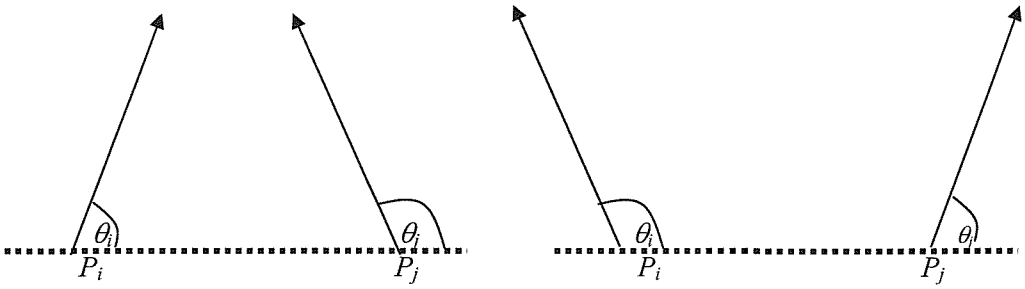

Figure 4.4 Two different situations with same phase value which is maximal

4.5. Figure 4.5(a) is a silhouette and (b) is its negative, (c) and (d) are their respective symmetry maps. These symmetry maps are generated with $\mu = 27$ and $\sigma = 90$. Evidently, the symmetry maps are identical, so the symmetry is invariant to the relationship of an object to its background. We see from the symmetry maps in Figure 4.5 that the legs and the arms are highlighted as the regions of high symmetry. These highlighted regions are those parts of the human body associated with gait. Regions between the legs are also highlighted as regions of high symmetry. We also see that a small part of the head and the torso are also highlighted as regions of interest. The brighter the pixel in a symmetry map, the higher the accumulated symmetry measure at that pixel.

It must be noted that a large value for the product of I_i and I_j implies there is a strong correlation between the two large gradients. Note also that gradients are used instead of intensities since we are interested in edges that relate to objects' borders.

The symmetry contribution value obtained is then plotted at the midpoint of the two points. Thus, the midpoint, $\Gamma(p)$ of the two points P_i and P_j is given by:

$$\Gamma(p_k) = \left\{ (i,j) \middle| \frac{P_i + P_j}{2} = p_k \right\} \tag{4.9}$$

The total symmetry magnitude (or isotropic symmetry), $M\sigma(p)$ of each point P is the sum of the contributions. The accumulated symmetry evidence for all pairs of points i and j having their midpoint at P is given by

(a) Original silhouette

(b) Negative of (a)

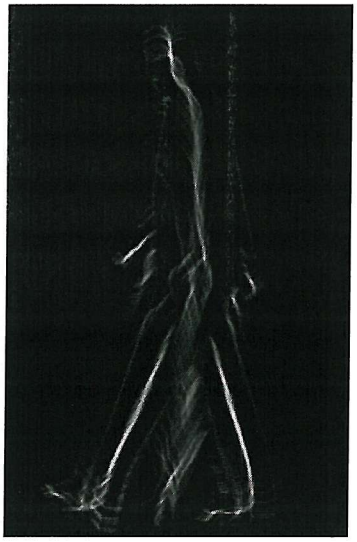

(c) Symmetry map of (a)

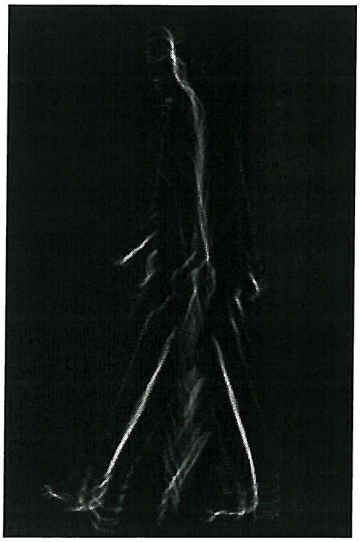

(d) Symmetry map of (b)

Figure 4.5 Same symmetry measures for white silhouette on black and black silhouette on white.

$$M_{\sigma,u}(p_k) = \sum_{(i,j)\in\Gamma(p_k)} C(i,j) \tag{4.10}$$

and the direction of contribution of P_i and P_j is given by

$$\varphi(i,j) = \frac{(\theta_i + \theta_j)}{2} \tag{4.11}$$

The direction of symmetry at the point P_k is therefore defined as

$$\phi(P_k) = \varphi(i,j) \tag{4.12}$$

such that $C(i,j)$ is maximal for $(i,j) \in \Gamma(P_k)$. Hence the symmetry at the mid point P_k is given by

$$S(P_k) = [M(P_k), \phi(P_k)] \tag{4.13}$$

From equation 4.13, the direction of symmetry at any point comes from only one pair of edge points. This may not necessarily give the best possible direction of symmetry for all pairs of points that contributed to the corresponding edge magnitude. We believe that by including the symmetry direction of all pairs of points that contributed to any particular symmetry magnitude should be the best option. For example using the average of the symmetry directions may be better than using the direction of symmetry of the pair of points that contributed most to the symmetry magnitude, i.e. it might be better to use a local average rather than a local maxima. This will be investigated in section 6.5.

The symmetry transform as discussed here detects reflectional symmetry and we will discuss radial and projection symmetry in the following sections. Note that the symmetry of most interest when analysing humans is bilateral symmetry because the human body is approximately bilaterally symmetric. The symmetry is available best in fronto parallel views, but affects limb disposition in the fronto normal views used in this research. This transform reflects the fact that each of its components modulates the other ones. It is invariant under 2D rotation and translation transformations. It is also invariant under change in scaling (similarity transformation) [20], which is of potential

advantage in automatic gait recognition. Equation 4.10 gives isotropic symmetry as it has no preferred orientation, that is, the direction of symmetry is not used.

In Figure 4.6 we show the symmetry maps derived for an image of an elephant. The selection of parameters (σ and μ) by experimentation can highlight the overall symmetry around the centre of mass as shown in Figure 4.6(c), or local symmetry about the legs (as clearly seen in between the legs and even between the tusks) as shown in Figure 4.6(d). A combination of these is used in studying the symmetry of motion.

It is possible to include the direction of symmetry contribution in our symmetry calculations (see equation 4.13). This gives either projection symmetry, radial symmetry or radial projection symmetry depending on how the symmetry magnitude and the symmetry direction are combined (see equations 4.14, 4.15 and 4.16).

4.3.2 Symmetry projection

Symmetry projection is very useful in looking for symmetries in a given direction. Reisfeld *et al.* [80] used this type of symmetry to detect facial features. The symmetry projection, $PS(p, \psi)$ at a point p and an orientation ψ is defined as

$$PS(p,\psi) = M(p)\cos(\phi(p) - \psi) \tag{4.14}$$

where $M(p)$ is the symmetry magnitude as defined by equation 4.10 and $\phi(p)$ as defined by equation 4.12. For gait analysis, we will be interested in emphasising symmetries that point either north or south, that is $\psi = \pm\text{-}\pi/2$. In this case maximum contribution is achieved when $\phi(p) = \psi = \pi/2$ or $\phi(p) = \psi = -\pi/2$. Since the latter points in opposite direction to the former, it means that the latter will yield a minimal contribution according to equation 4.14. The two situations are as shown in Figure 4.7. If this happens, then the above equation will distinguish between a dark object on a light background and a light object on a dark background. Figure 4.8(c) and 4.8(d) are symmetry maps obtained from equation 4.14. It is clear that the two symmetry maps are

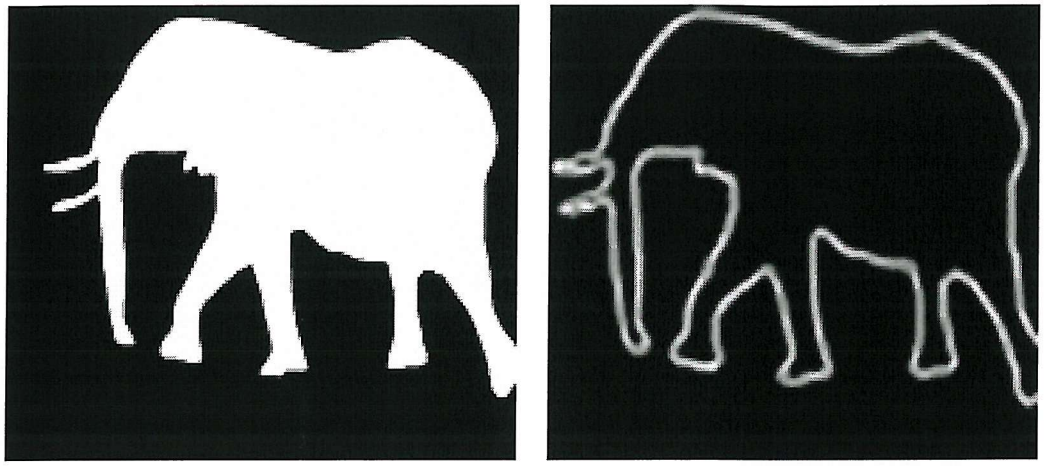

(a) Original image (b) Sobel edge map

(c) Far-symmetry map (d) Close-symmetry map

Figure 4.6: Controlling the action of symmetry operator

different. This is because a white object on a black background has the same edge-map as a black object on a white background but the edge directions are turned by 180 degrees. Thus, equation 4.14 may not be suited for our gait recognition because some researchers prefer to extract their silhouettes as black on white background and others as white on black background and if that happens then the same subject extracted in the two different ways will be considered or classified as different subjects. Moreover, there will be no need to ensure that all images in a database are all white on black or black on white. The symmetry maps generated by Reisfield's formulation do not really show the symmetrical properties of the original image. To turn the above equation into a more useful feature extractor will mean modifying the *PS(p, ψ)* such that it gives a preferred symmetry axis rather than only a preferred direction. Hence equation 4.14 will be replaced as follows:

$$PS(p,\psi) = M(p)\left|\cos(\phi(p) - \psi)\right| \tag{4.15}$$

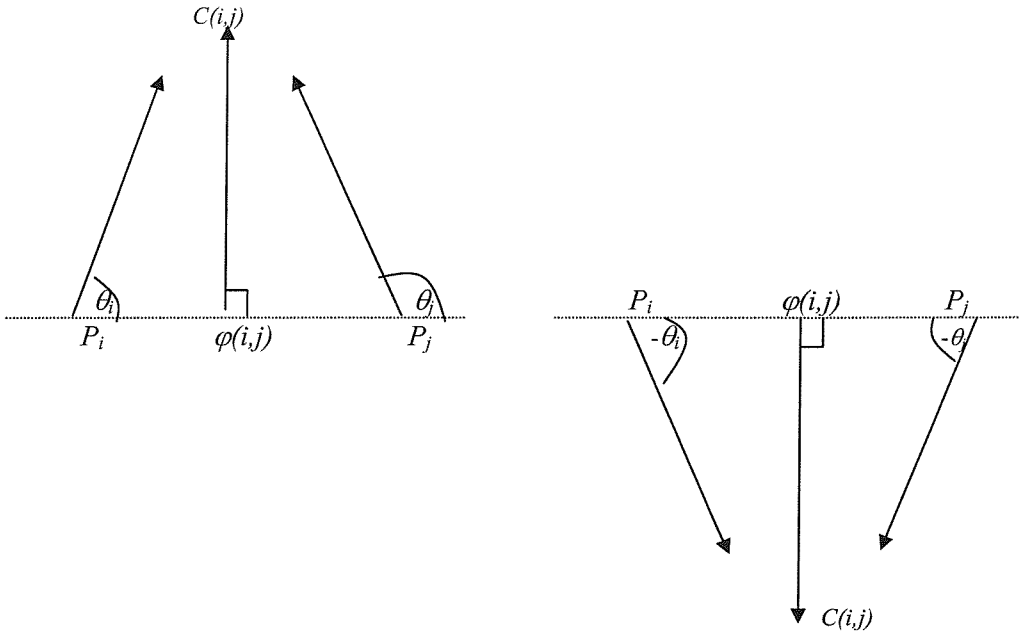

Figure 4.7: The two situations where the symmetry contribution is maximal

This will also ensure that a light object on a dark background and a dark object on a light background will generate identical symmetry maps (see Figure 4.8(e) and (f) generated by equation 4.15). Comparing Figure 4.8(c) and (e), it is clear that the latter

(a) white image on black background

(a) black image on white background

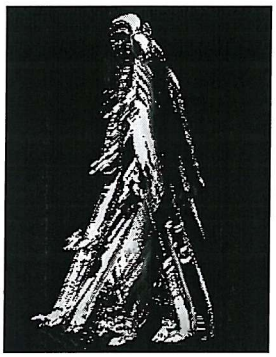

(c) symmetry of (a) using equation 4.14

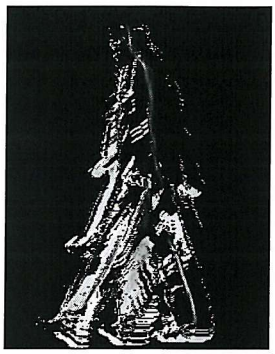

(d) symmetry of (b) using equation 4.14

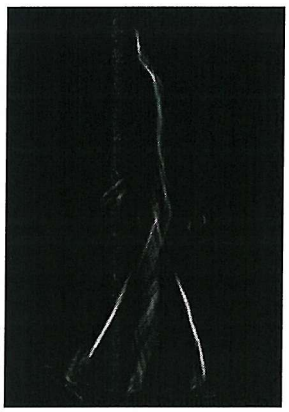

(e) symmetry of (a) using equation 4.15

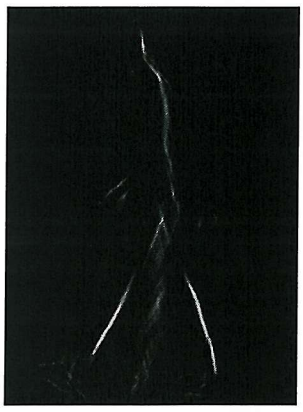

(f) symmetry of (b) using equation 4.15

Figure 4.8: Symmetry maps generated from equations 4.14 and 4.15 with $\psi = 90$, that is, using symmetry projection.

shows areas where the image is more symmetrical than the former. Hence for projective gait recognition, we will use equation 4.15 rather than equation 4.14. Further, in comparison of Figure 4.8e with Figure 4.5 it can be seen that the use of projection has filtered out some erroneous information found by the basic form of the DST.

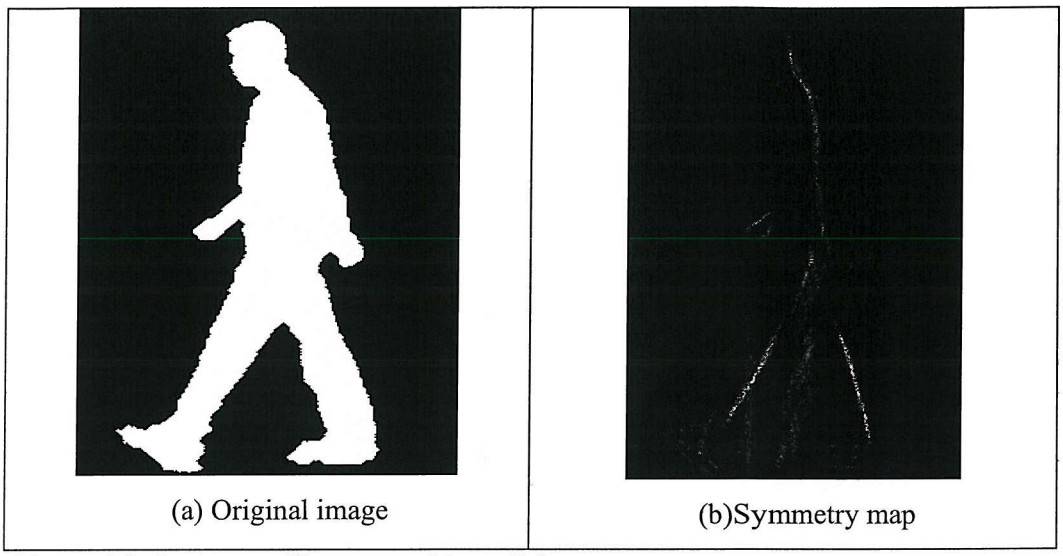

(a) Original image (b)Symmetry map

Figure 4.9: An image silhouette and its radial symmetry map

4.3.3 Radial symmetry

Radial symmetry is used to detect points that are highly symmetric in multiple distinct orientations rather than a principal one [77] by emphasising contributions in the directions normal to the main symmetry. The radial symmetry, *RS(p, ψ)* at a point *P* is defined as

$$RS(p,\psi) = M(p)\sin^2(\varphi(p) - \phi(p)) \qquad \textbf{(4.16)}$$

where $\phi(p)$ is the direction for which C(i,j) is maximal and $\varphi(p)$, the symmetry direction at the point P. For human identification, this type of symmetry can be useful in face and iris (eye) recognition. Radial symmetry has been used to detect facial features and regions of interest in a scene [77, 80]. Note that an object is said to have radial symmetry if there are many planes that divide it into two mirror images. Figure

4.9 shows an image silhouette and its corresponding radial symmetry map. The major axes of interest remain after some of the extraneous information has been removed, but now appears much more fragmentary.

4.3.4 Spatio-temporal symmetry

This new approach is an extension of the spatial approach discussed under section 4.3.1. By including temporal information in our symmetry calculations we are not recognizing people by just their body shape but also by their motion. We are the first to include time in a symmetry formulation. There are doubtless several variations possible, but here we have taken an approach that appears by results to offer some performance advantage. This naturally includes a fundamental property of motion, i.e. time. We consider the distance between points that are separated spatially (within an image) and temporally (between images) to be components of a Euclidean distance metric to give a new distance weighting function. Figure 4.10 shows two images (one $T_{j,t}$ displaced q frames from $T_{j,t-q}$, where $T_{j,t}$ and $T_{j,t-q}$ are not necessarily at the same spatial position).

The distance metric is the symmetry distance between two points separated in time and in space and can be used to replace the spatial symmetry weighting distance FD, described earlier. This gives

$$\left\|T_{i,t}-T_{j,t-q}\right\|=\sqrt{W\left\|T_{j,t}-T_{j,t-q}\right\|^2+\left\|T_{i,t}-T_{j,t}\right\|^2} \qquad \textbf{(4.17)}$$

where w is a time/space weighting function. This makes it possible to evaluate the individual contributions of spatial and temporal information in a symmetry map. When the value of w is greater than one, it implies the symmetry map will be dominated by temporal information whilst a value less than one means there is more spatial information than temporal information. Equal contributions are obtained when the value of w is 1.

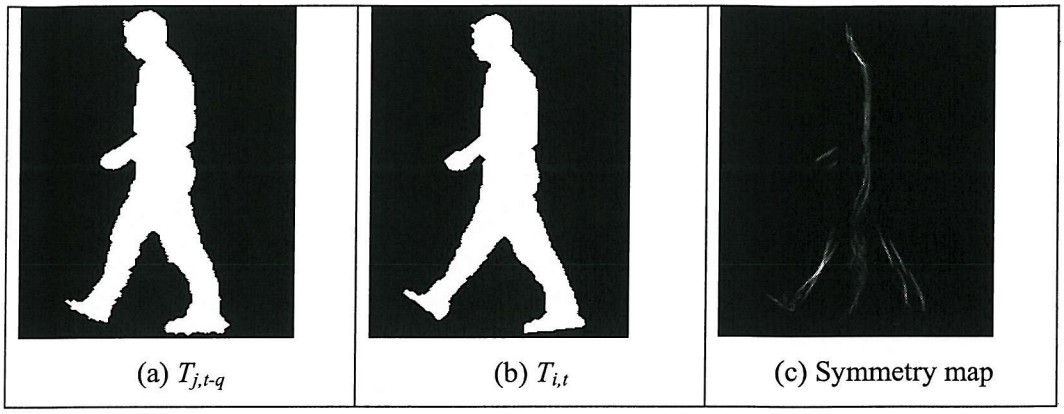

(a) $T_{j,t-q}$ (b) $T_{i,t}$ (c) Symmetry map

Figure 4.10: Generating Spatio-temporal Symmetry

Equation 4.17 can be re-written as follows:

$$\left\|T_{i,t} - T_{j,t-q}\right\| = {}^{w}\!\Big/\!\sqrt{2\pi\sigma_t}\exp\left(-\left(\frac{\left\|T_{j,t} - T_{j,t-q}\right\| - \mu_t}{2\sigma_t}\right)\right) + {}^{1}\!\Big/\!\sqrt{2\pi\sigma_s}\exp\left(-\left(\frac{\left\|T_{i,t} - T_{j,t}\right\| - \mu_s}{2\sigma_s}\right)\right) \quad \textbf{(4.18)}$$

Here, we assume variance and focus are the same for time and space $\sigma_s = \sigma_t = \sigma$ and $\mu_s = \mu_t = \mu$, and q=1 [6], so

$$\left\|T_{i,t} - T_{j,t-q}\right\| = {}^{w}\!\Big/\!\sqrt{2\pi\sigma}\exp\left(-\left(\frac{\left\|T_{j,t} - T_{j,t-q}\right\| - \mu}{2\sigma}\right)\right) + {}^{1}\!\Big/\!\sqrt{2\pi\sigma}\exp\left(-\left(\frac{\left\|T_{i,t} - T_{j,t}\right\| - \mu}{2\sigma}\right)\right) \quad \textbf{(4.19)}$$

This replaces the distance metric $FD_{i,j}$ in Equation 4.3 whilst the phase relationship remains unchanged. As such, we evaluate the symmetry relationship in time and in space. Now, recognition is based on body dynamics as well as on body shape. Figure 4.10 shows two image frames and their corresponding spatio-temporal symmetry map using the same values of σ and μ. Comparing Figures 4.5(c) and 4.10(c), it can be seen

that the spatio-temporal map shows a distribution which is centred more around the moving legs and arm, those parts of the human body that are associated with gait.

4.3.5 Extended Spatio-temporal (EST) symmetry

This approach is an extension to the spatio-temporal symmetry and as such we will refer to it as the extended spatio-temporal approach. With the spatio-temporal approach, each symmetry map is derived from two image frames. With EST, each symmetry map is derived from three image frames. Figure 4.11 shows three consecutive images from an image sequence.

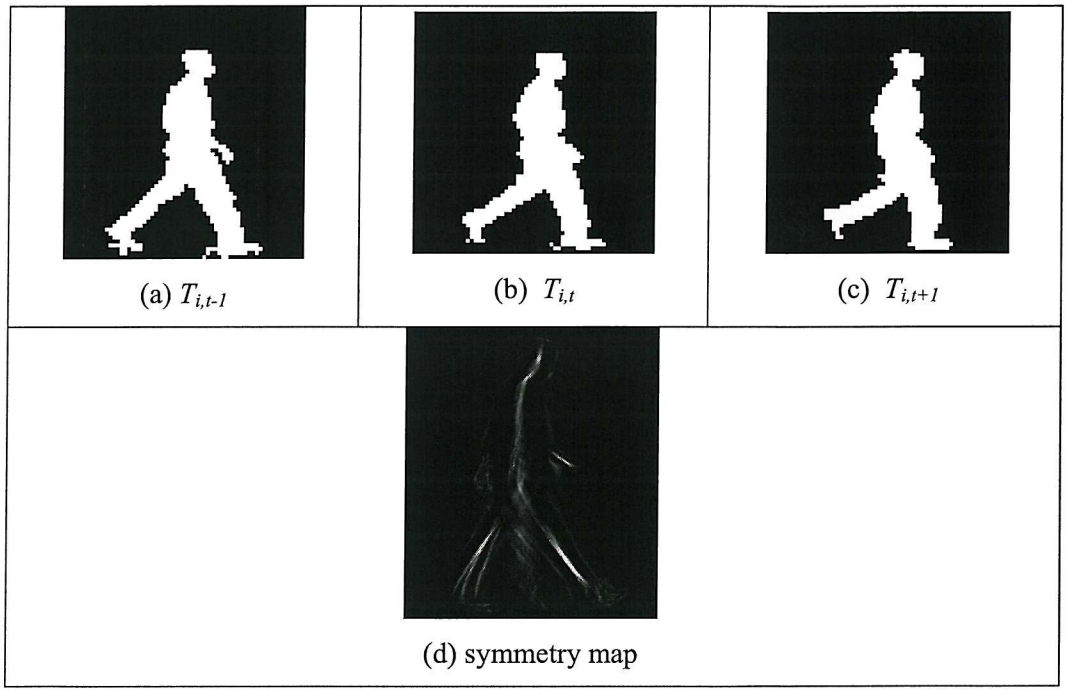

Figure 4.11: Three consecutive image frames and their extended spatio-temporal symmetry map

Here, the distance metric is the symmetry distance between points separated in time and in space to replace the *FD* in equation 4.3. For each point in the symmetry map, we average the spatial and the temporal symmetry contributions. The spatial symmetry is

calculated for each of the three spatial templates and the temporal symmetry from the pairs $T_{i,t-1}$ and $T_{i,t}$, and then $T_{i,t}$ and $T_{i,t+1}$, leading to a new distance weighting function. Let FD_a be the spatial distance metric from spatial template a, and $FD_{a,b}$ be the temporal distance metric from spatial templates a and b. Thus, the new distance metric for the extended spatio-temporal symmetry can be written as:

$$FD = W_s(FD_{T_{i,j-1}} + FD_{T_{i,j}} + FD_{T_{i,j+1}}) + W_t(FD_{T_{i,j-1}T_{i,j}} + FD_{T_{i,j}T_{i,j-1}}) \quad \textbf{(4.21)}$$

where W_S and W_t are the weighting for the spatial and the temporal components respectively. Thus, the W_S and W_t make it possible to give different weights to the spatial and the temporal components to evaluate their contributions, if necessary. For simplicity, we shall assume $W_S = W_t = 1$ as before. This therefore reduces the equation as follows.

$$FD = FD_{T_{i,j-1}} + FD_{T_{i,j}} + FD_{T_{i,j+1}} + FD_{T_{i,j-1}T_{i,j}} + FD_{T_{i,j}T_{i,j-1}} \quad \textbf{(4.22)}$$

The above formulation shows an increasing averaging associated with the symmetry computation which is likely to make it less sensitive to missing frames, occlusion and probably noise. Figure 4.11(d) shows a symmetry map obtained by using equation 4.22 slightly increasing the prominence of the legs.

4.3.6 Temporal symmetry

The computation of the temporal symmetry is very similar to the spatio-temporal approach discussed under section 4.3.4. The same distance weighting function is used with a little modification. In equation 4.19, we omit the w and the spatial component of the formula. This reduces the equation as follows.

$$FD_{\|T_{i,t} - T_{j,t-q}\|} = 1/\sqrt{2\pi\sigma} \exp \frac{(-(\|T_{i,t} - T_{j,t}\| - \mu))}{2\sigma} \quad 4.23$$

where symbols have usual meanings.

4.4 Conclusions

This chapter shows that there is more support for gait asymmetry than gait symmetry. This means that during walking both legs are not used equally suggesting that symmetry of motion can indeed be used for recognition. The studies and uses of symmetry in computer vision also provide a strong support for the use of symmetry in gait recognition. We have formulated a set of metrics that can be used to determine symmetry by the first application of symmetry analysis for automatic gait recognition. The Discrete Symmetry Transform is a basic operation with several advantages. Amongst these is the ability to extend its formulation to give specificity to time and orientation, as likely to be of advantage in application scenarios. We have shown that by novel inclusion of temporal information in our symmetry calculation, subject recognition will not only be by body shape but also body motion. We have also shown that the spatial component of our extended spatio-temporal symmetry can be omitted to leave only the temporal information and still produce good recognition rates. We have also suggested how the original formulation of symmetry projection can be modified to be useful in gait recognition.

Chapter 5

SYMMETRY EXTRACTION

To extract the symmetry of a walking human subject, image silhouettes are extracted from each gait sequence to give a template sequence. The symmetry operator uses an edge map of images in an image sequence with edge magnitude and direction as input to generate a symmetry map. It must be noted that there is a great advantage in computing symmetries using edges rather than grey levels [102] and most of the studies on symmetry analysis have been using that approach [104-108]. Edge symmetry is more significant than the region symmetry due to the importance of edges in human vision [102]. Since the symmetry computation is of the order $O(n^2)$ where n is the image size, computing symmetries on edge points will make the computations more attractive, especially for images of very large size. The symmetry map assigns symmetry magnitude and symmetry orientation to each pair of pixels or image points. These properties are derived from a distance weighting function, a phase weighting function and edge magnitudes, as given by equation 4.4.

5.1 Methods of Symmetry Extraction and gait

In this work, we extract symmetry by two different methods as alternative inputs to our approach. The main difference between these two inputs is the form in which the image frames are converted before we apply the symmetry operator. Note that in each of the forms described below, an image sequence of a subject consists of at least one gait cycle.

From similar work done by Huang *et al.* [53], combining the silhouette and optical flow information will allow better recognition rates than is achieved using the two modalities separately but our aim here is to establish whether human gait has distinct symmetrical properties that can be extracted for gait recognition.

5.1.1 Symmetry Extraction from Silhouette

Symmetry extraction from silhouettes is carried out as follows. With the SOTON database, first, the image background as in Figure 5.1(b) is computed, using a median operator. This is done by selecting at least five of the image frames such that when they are superimposed on each other no part of the subject overlaps. The median of the selected frames are then computed and the result is the image background. This is possible because the cameras used to capture the image sequences in all the databases used in this work and in most research works on gait are static and hence there is no translational motion. The computed background is then subtracted from the original image, Figure 5.1(a) to obtain the image silhouette, Figure 5.1(c). It must be noted that the image in Figure 5.1(c) has been cropped and resized to 64 x 64 pixels so as to reduce the computational requirement of the symmetry operator. The images in our databases were normalised for height and as such removes height from recognition enabling scale/distance invariance of the recognition process. Note also that each silhouette is placed in the 64 x 64 template such that the silhouette's centroid is at pixel location 32 x 32. This is then followed by the steps given under section 5.2 below. For the other databases used in this work from other institutions different techniques were used to extract the silhouettes. These methods will be covered in later chapters where appropriate.

5.1.2 Symmetry Extraction from Optical flow

The steps involved in extracting symmetries from optical flow images are not much different from that of extracting silhouettes. Here also, the optical flow images are derived from at least one gait cycle. First, the image silhouettes are extracted as given in the section 5.1.1 above to give the spatial templates. The optical flow information

used in this work, based on the algorithm proposed by Bulthoff *et al.* [109] to compute the dense optical flow field, was generated by minimising the sum of the absolute differences between image patches. The underlying assumption of the optical flow extraction algorithm is that the optical flow is due locally to a first approximation to front-to-parallel translation of the Lambertian surface. Here, the images are first filtered to remove any special effect such as changes in lighting, shadows and reflections. This is done by taking the logarithm of the brightness and then applying the Laplacian of Gaussian filter or a band pass filter. The corresponding patches for the various pixels are then compared with a finite number of shifted versions of the original image to produce a voting space. The shifted patch with the highest correlation with the *(n+1)* image's equivalent patch determines the motion of that pixel. Thus, two consecutive spatial templates (see Figure 5.2) are used to obtain one optical flow image. The images are then reversed and the process repeated. The results from the two passes are then summed so as to cancel correct results leaving only the required pixels. This helps to remove or eliminate any incorrect estimates. These processes then produce the dense optical flow fields for both the x and the y directions [110]. The magnitudes of x + y flow $\left(\left|x+y\right|\right)$ are then used.

Figure 5.2 shows samples of the optical flow images. The white pixels in the optical flow image correspond to areas where no movements were detected while light grey pixels represent an area of high amounts of motion. The darker areas on the other hand show large amounts of motion. In our case, we used the magnitude of both components $\left|x+y\right|$ as suggested by Huang *et al.* [53] that this improves the descriptive capabilities than using either the x or the y flow

Having obtained all the optical flow images of an image sequence, we then applied the symmetry operator directly to each of the images generated from spatial templates. The gait signature is then obtained by averaging all the symmetry maps of the optical flow images in an image sequence.

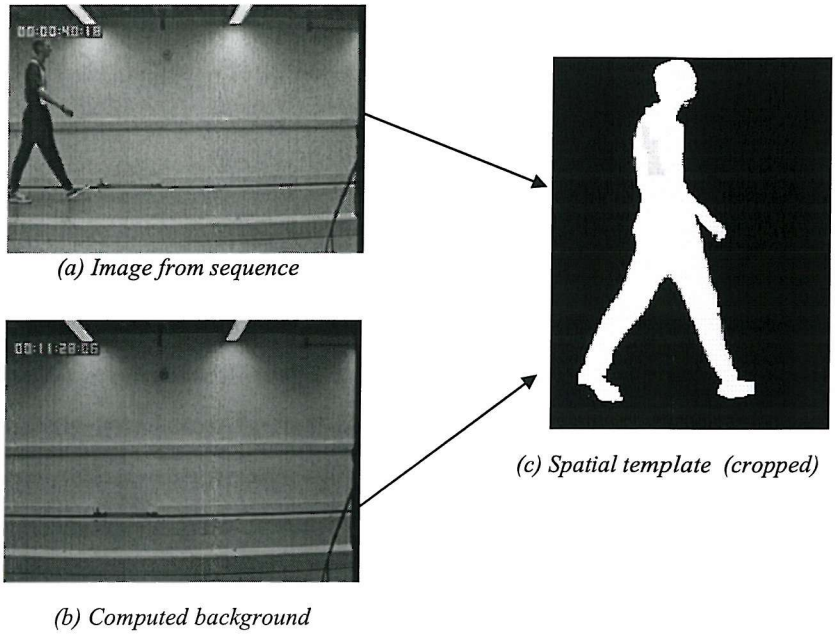

Figure 5.1: Generating a gait signature from silhouette information

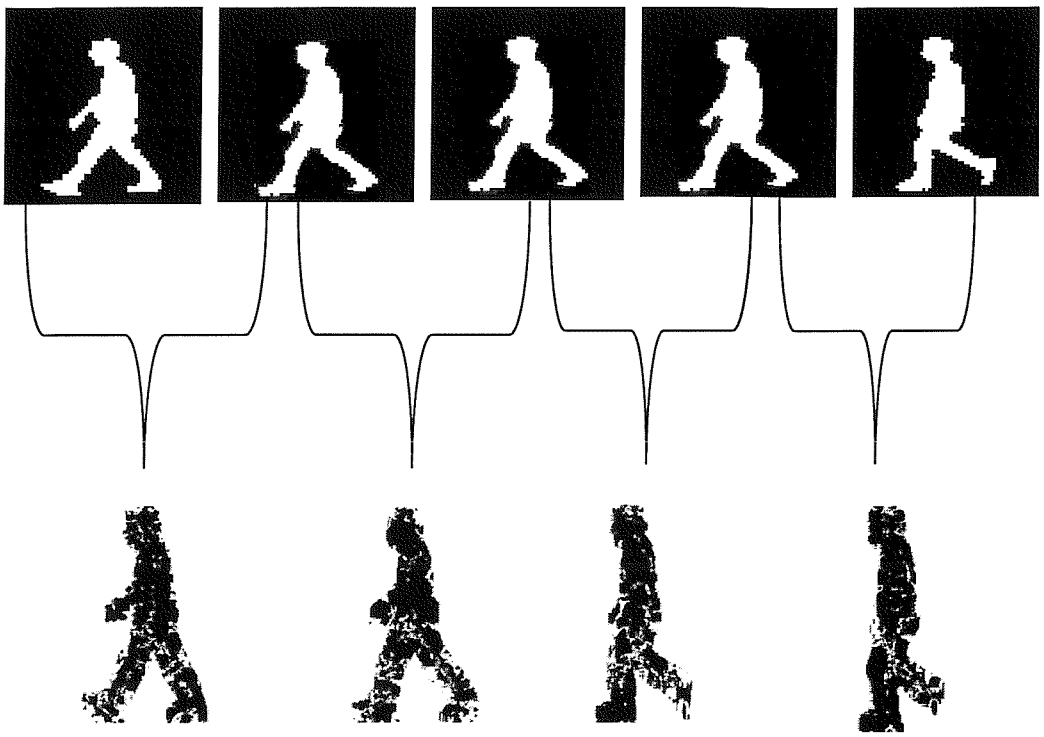

Figure 5.2: Part of optical flow images extracted from an image sequence. Two spatial templates are used to produce one optical flow image.

5.2 Deriving the Gait Signature

To extract symmetry, we need edge magnitude and direction at each image point. These can be derived by Sobel operator. We can also extract symmetry straight from optical flow images. Figure 5.1 shows how symmetry is extracted from Sobel. Note that here, for binary silhouettes, the perimeter information could be derived more easily than using the Sobel operator. However, this could remove the gradient information as needed for symmetry. We shall continue to deploy the Sobel operator acknowledging that other approaches could be used. After removing the image background and the result windowed, the Sobel operator is then applied to the image silhouette as in Figure 5.1(c) to derive its edge-map, Figure 5.1(d). The symmetry map, Figure 5.1(e), is then obtained by applying the symmetry operator to the edge map.

Similarly, in extracting symmetry from optical flow images, we apply the symmetry operator directly to the optical flow images to obtain their corresponding symmetry maps as shown in Figure 5.3.

Deriving symmetry maps from pairs of silhouettes for the spatio-temporal, temporal and the extended spatio-temporal approaches, also require that we first obtain the Sobel edge maps of the images in a sequence. For each pair of spatial templates say A and B, the $P_1(x,y)$ and $P_2(x,y)$ are taken to be image points from A and B respectively. Thus equation 4.3 is modified as follows:

$$FD_{i,j}^{A,B} = \frac{1}{\sqrt{2\pi\sigma}} \exp^{-\left(\frac{\left\|P_i^A - P_j^B\right\| - \mu}{2\sigma}\right)}, \forall i \neq j \qquad \textbf{(5.1)}$$

It must be noted that before the symmetry operator is applied to the Sobel edge map, it is normally semi-thresholded. The rationale for this is to reduce noise or remove edges with weak strength, which may be due to the background removal, if any. The threshold also has the effect of reducing computational requirement of the symmetry operator since computations are only performed on non zero pixels. The higher the threshold value the fewer the number of non-zero pixels in the edge map and hence the smaller the computational times. Having said this, care must be taken in choosing a good threshold value since a very high value will result in losing vital information.

In semi-thresholding, a reasonable minimum and maximum threshold values are chosen. All pixel values between the minimum and the maximum values inclusive are retained while all others are set to zero. Let T_{min} and T_{max}, be the minimum and the maximum threshold values respectively, then,

$$P_{x,y} = \begin{cases} P_{x,y} & T_{min,} \leq P_{x,y} \leq T_{max} \\ 0 & otherwise \end{cases} \qquad \textbf{(5.2)}$$

Figure 5.4 is a graphical representation of the semi-thresholded method. All pixels to the left of T_{min} (minimum threshold value) and those to the right of T_{max} (maximum threshold value) are set to zero. In this work, the maximum threshold value is set to 255, hence only the pixel values less than the minimum threshold value are set to zero while those greater than or equal to the minimum threshold value are retained. The minimum threshold value is manually selected depending on the range of values of the symmetry contributions within the gait signatures.

For each image sequence, the gait signature, *GS* is obtained by averaging all the symmetry maps, that is for an image sequence *i*, its gait signature GS_i is given by

$$GS_i = \frac{1}{n}\sum_{j=1}^{n} S_j \qquad \textbf{(5.3)}$$

where n is the number of symmetry maps in the sequence i and S_j, a symmetry map. Figure 5.1(f) is an example gait signature. The gait signature reveals the regions where the symmetry information are contained and the brighter the pixel the greater is its symmetry measure. Figure 5.1(f) shows that most of the symmetry information is contained in the region around the legs of the subject. Comparing Figures 5.1(e) and 5.3(c), the symmetry maps appear to be quite similar in terms of the area distribution of symmetry but the lines of symmetry are more conspicuous in the former than the latter.

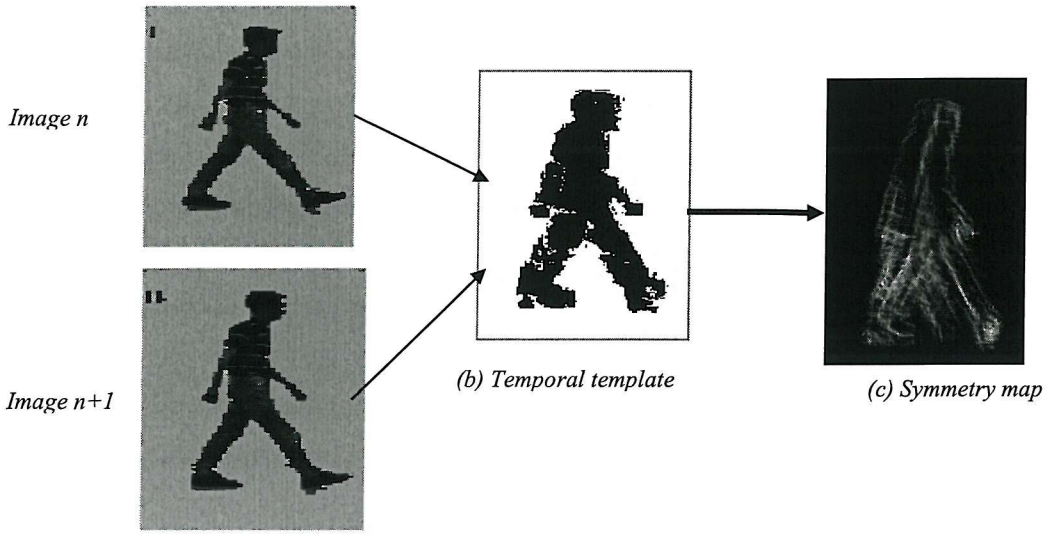

Figure 5.3: Deriving a gait signature from optical flow information

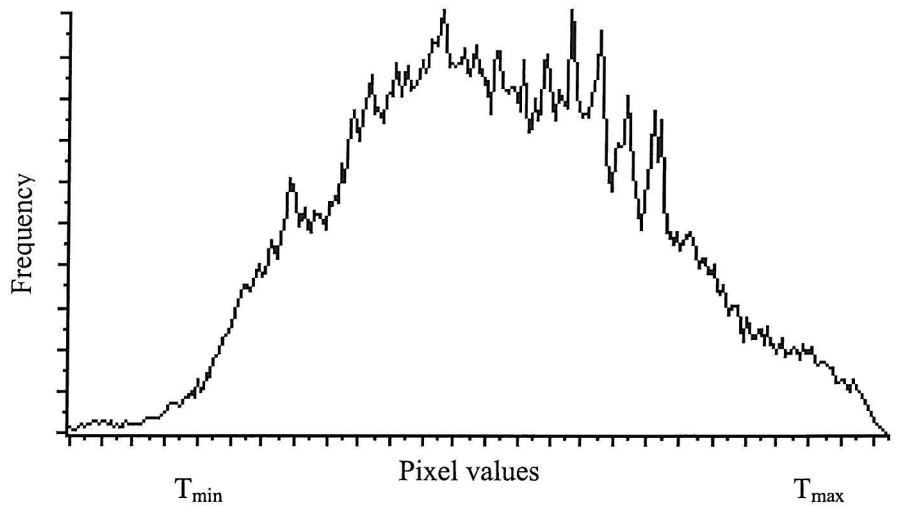

Figure 5.4: The semi-threshold technique

5.3 Separating Animal Movement

The spatial technique was first applied to demonstrate that animal movement could be separated using their symmetrical properties. This has already been reported in [5]. As

such the test sequence used comprises of three animals namely an elephant, a zebra and a bulldog. There were two image sequences for the zebra and one image sequence each of the bulldog and the elephant. Each image sequence had one walking cycle. The concern here is the distinction between quadrupeds. The symmetry operator is arranged specifically to analyse the motion of pairs of legs. As such, this indicates whether symmetry can be used to separate animals by gait.

The spatial gait signatures of these animals are shown in Fig. 5.5. Here, it can be seen visually that each of these animals is distinct and the signatures, by comparison with Figure 5.2, different from that of a human. The signatures have two for the same zebra, taken at different times. In one, the tail is moving rapidly but this did not affect the resulting symmetry map by the speed of movement and the averaging used. In fact, the Euclidean distance classification separated each of these sequences perfectly: in terms of structure, the zebra signatures,

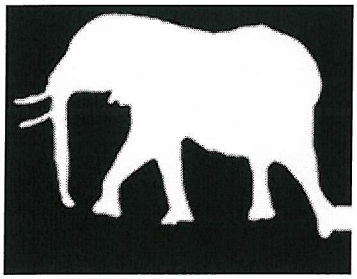

(a) elephant

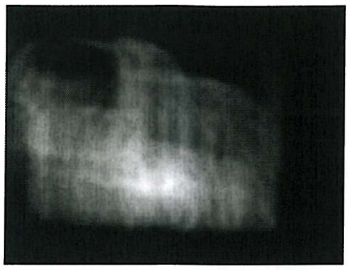

(b) gait signature for (a)

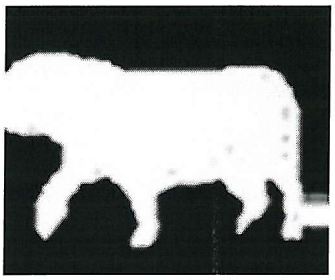

(c) Bulldog

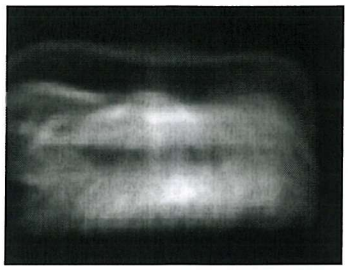

(d) Signature for (c)

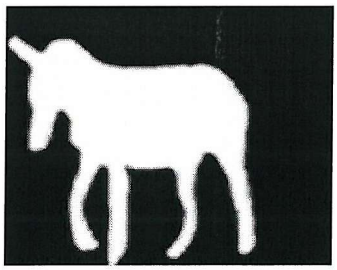

(e) Zebra 1

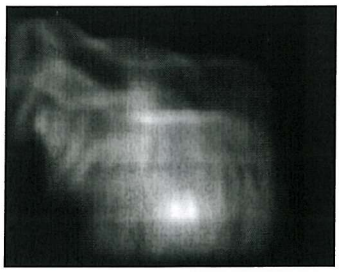

(f) Signature for (e)

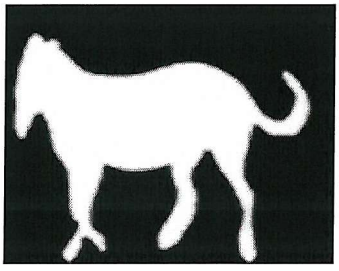

(g) Zebra 2

(h) Signature for (g)

Figure 5.5: Symmetry signatures for different animals

Figures 5.5(f) and 5.5(h) are much closer to each other than the other animals. It can be seen from the symmetry maps in Figure 5.5 that each of the different animals shows symmetry peaks at different locations within the maps. These are peaks are the regions circled. The peaks in the symmetry map of the Elephant, Figure 5.5(b) are around the legs or the lower part of the body. For the Bulldog, Figure 5.5(d) two mushy peaks are found around the legs and also at the centre of the upper body. For the zebras, Figure 5.5(f) and (h), the two focused peaks are between the centre of the legs and the upper part of the body. Though the Zebras and the Bulldog appear to have the peaks in the symmetry map around the same regions, the distributions of the peaks are completely different for the two animals.

5.4 Gait recognition

Here, steps were taken to ensure that the recognition rates are not dependent on the different speeds of movement of the subjects, noise and/or the strong edges in the images.

To ensure that the subjects are not recognised by the speed at which they walked, the image sequences were normalised before applying the symmetry operator. The normalisation was done by making each image sequence to contain one gait cycle of image frames. Gait was considered by Murray [18] as "a total walking cycle".

Having derived all gait signatures, the Fourier transform (F) is then applied to each of the gait signatures for reason of shift invariance and its descriptive capabilities; that is,

$$FT = F(GS) \tag{5.4}$$

where GS is a gait signature.

To ensure that the recognition rates are not dominated or influenced by noise and/or strong edges in the original images a low pass filter is then applied to the Fourier transform. This is achieved by selecting only the low frequencies within a circle of a specified radius, R with the DC at the centre. That is

$$FT'(u,v) = \begin{cases} FT(u,v) & if \quad (u^2+v^2) \leq R^2 \\ 0 & otherwise \end{cases} \tag{5.5}$$

where the elements of the FT' are the Fourier descriptions of the gait signatures after the low pass filtering. Equation 5.5 assumes shift of FT by $(-1)^{x+y}$ where x and y are the coordinates of an image pixel. Note that this is usually done for display purposes.

Different radii were used to determine the effect of selecting part of the Fourier coefficients. For purposes of classification or recognition, the similarity differences between the magnitudes of the Fourier coefficients of the gait signatures are then calculated using the Euclidean distance. The similarity difference of gait signatures i and j, $SMD_{i,j}$ is defined as

$$SMD_{i,j} = \sum \left\| FT^i_{x,y} - FT^j_{x,y} \right\| \tag{5.6}$$

where $FT^i_{x,y}$ and $FT^j_{x,y}$ are the Fourier coefficients of the gait signatures i and j at coordinate (x,y) respectively.

Using equation 5.6, we expect the gait signatures belonging to the same subject to give the lowest similarity difference values. The best match of subject i, $Match_i$ is therefore obtained as follows:

$$Match_i = [SMD]^N_{j=1} \quad i \neq j \tag{5.7}$$

where N is the number of gait signatures in the database.

The technique was first applied to the animal database of four image sequences belonging to four animals; two zebras (referred to as *zebra1* and *zebra2*), one bulldog and one elephant. For the purpose of distinguishing between the different animals using the Euclidean distance measure, the image sequence belonging to zebra1 is used as the test subject and the remaining three, one each of the second zebra (zebra2), elephant and the bulldog, are used as the training set. The result obtained is as shown in Table

5.1(a). The figures shown in the table are the similarity differences between the training and the test subjects obtained after Equations 5.4 and 5.6 have been applied to the gait signatures. It can be seen that taking out the DC coefficient, using all the Fourier coefficients or applying a low pass filter, the animals can be separated perfectly: zebra1 and zebra2 are the closest whilst the elephant and bulldog appear different. These show that the separation does not depend on the animal sizes or the strong edges of the images but rather the symmetry of their movement. Table 5.1(b) shows how each animal compares to the other. The best match of the elephant is to the zebras whilst that of the bulldog is to the elephant. Naturally, these results are only introductory and only on a very small dataset. We will later aim to qualify how human motion can be separated (not just from similar animal movement), and also how it might be deployed in, for example, database browsing.

Table 5.1(a): Similarity differences between the Zebra1 and the other animal and the effect of low pass filtering

Animal	**All FTs**	**All FTs – DC**	**Low pass filter (radius = 20 pixels)**
Zebra2	11106	11098	9556
Elephant	16458	15773	14502
Bulldog	24940	23560	23003

Table 5.2(b): Similarity differences between the different animals

	Zebra 1	**Zebra 2**	**Elephant**	**Bulldog**
Zebra 1	0	11858	16685	22322
Zebra 2	11858	0	16104	22579
Elephant	16685	16104	0	20823
Bulldog	22322	22579	20823	0

5.5 Conclusions

This chapter presents how gait signature can be derived from silhouette and optical flow information to be used as alternative inputs to the different approaches discussed in the earlier chapter. Also, the process of recognising the different subjects is presented. We have demonstrated that it is possible to analyse animal movement and to distinguish between different types of animals. We used the Fourier transform and the nearest neighbour approach for classification of subject resulting in the use of large number of feature vectors. However, we hope to consider other approaches such as ANOVA, Principal Component Analysis, etc. In the next chapter, we will present results on sensitivity analysis/testing. Naturally, there are other factors that benefit fine tuning such as parameter set with different approach. We have shown that symmetry can be used to describe gait. Later, we shall examine this in detail.

Chapter 6

RESULTS OF HUMAN GAIT RECOGNITION BY SYMMETRY

A number of databases are used in this work. Some of them were used to enable us make comparisons of our results with those that were obtained by others using a different approach, others enabled us to carry out performance analysis related to gait. The main sources of the databases are University of Southampton, hereafter referred to as SOTON, Carnegie Melon University (CMU) and University of California San Diego (UCSD). The SOTON data is used to evaluate the performance of the symmetry operator as the number of subjects is increased. The CMU database consists of subjects filmed front-parallel and at two different view angles. It also consists of subjects filmed walking at different speeds, slow and fast, and these will enable us to investigate the effect of walking speed on gait. Since the author was directly involved in the data capture and some of the pre-processing of the most recent version of the SOTON database, we shall consider mostly the data capture and the pre-processing of this database. Where necessary, a short description will be given concerning the other databases.

The analysis here was designed to show that symmetry is potent in gait recognition. It will also enable us to compare the performance of the different symmetry measures, to know the clustering of the gait signatures and the recognition rates on different databases. The potency is examined primarily by the correct classification rate, for this is the ultimate performance factor by which any biometric is evaluated (we have not included verification, only recognition). The correct classification also examines several factors unique to gait, such as the influence of direction of movement, speed, and different view angles on recognition capability, together with analysis investigating

choice of parameters used in application. The other aspect of research, the performance factors, aims to investigate capability with respect to current surveillance technology. In this, missing frames, addition and omission of spatial data, noise and different resolutions are used to simulate a typical surveillance camera. The results presented here were obtained from carefully selected databases from different sources. These databases have improved very much recently, both in terms of data quality and the number of databases available. The increasing sizes of the databases enable us to evaluate the effects that larger databases may have on our techniques. The same databases will later be used in investigating the performance of our techniques on gait factors.

Unless otherwise stated, the same values of σ and μ (i.e. $\sigma = 27$ and $\mu = 90$) are used so that results can be compared where necessary. It is worth mentioning that the above values of σ and μ were arrived at by extensive experimentation but we hope this can be tuned further to improve on subjects recognition. Also, for symmetry projection, unless otherwise stated, the projection angle used is 90^0 and the definition of symmetry direction is as given by equation 4.12.

The following sections give a brief description of the databases and the results obtained from the different symmetry calculations.

6.1 University of Southampton (SOTON) and University of California San Diego (UCSD) databases

In section 1.2, we described how we started by first applying the discrete symmetry operator on a small, but then state-of-the-art, database [3, 4]. We applied the spatial method described in section 4.3.1 to two different databases of spatial templates. The old SOTON database has four subjects with four image sequences each and that of UCSD six subjects with forty-two image sequences in total.

The UCSD database used here is the same one used by Little [17] and Huang [43]. Figure 6.1 shows sample image sequences from the two databases. Figure 6.1(a) shows

an image frame from an image sequence in the SOTON database and Figure 6.1(c) shows its corresponding extracted windowed silhouette. Similarly, Figure 6.1(d) is an extracted windowed silhouette of Figure 6.1(b), an image frame from an image sequence in the UCSD database. The subjects in the UCSD database are all walking at similar speeds. The distance between the camera and the subjects varies between some sequences thus the need for scale invariance in our computations. However, we did not want to make any adjustments in the image sequences so that our results can be compared with those that have used the same database. The subjects in the SOTON database are all walking at similar speeds. The direction of walk is from left to right for two image sequences and right to left for the remaining two of each subject. The USCD database was filmed outside while the SOTON was filmed indoors (in a laboratory).

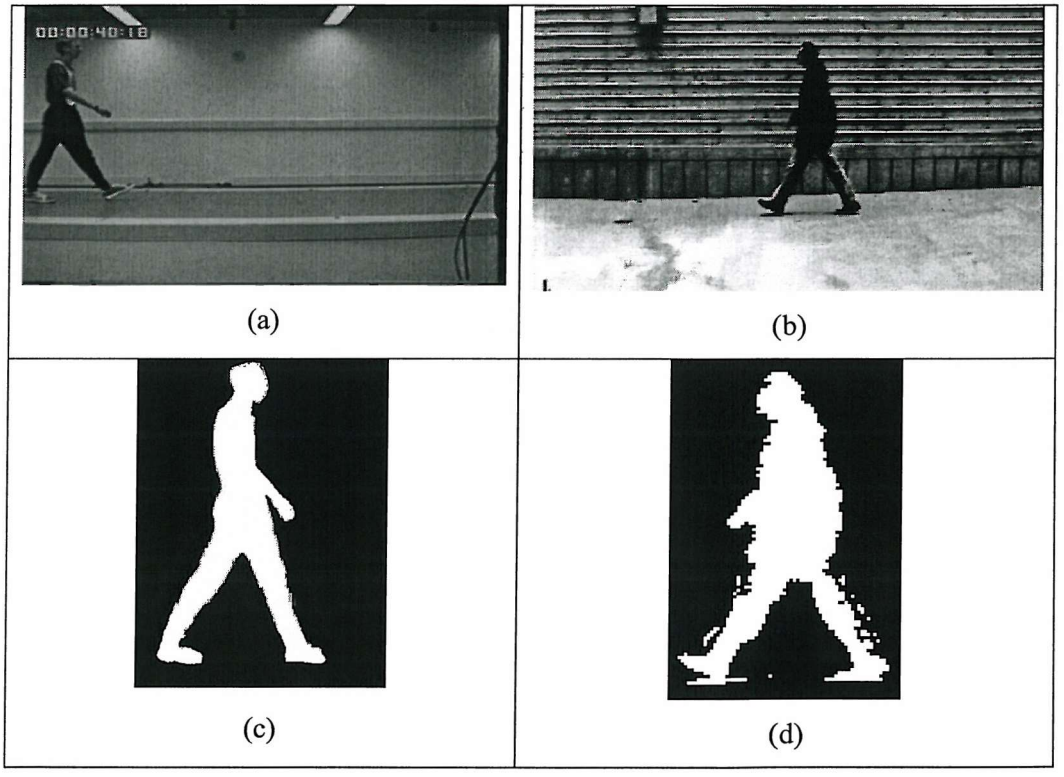

Figure 6.1: (a) and (b) are images frames from SOTON and UCSD databases respectively. (c) is the extracted and windowed silhouette of (a) with the background removed . (d) is obtained in a similar manner from (b).

For both the SOTON and the UCSD databases, we derived gait signatures for silhouette and optical flow information. These provide alternative versions of the input data for our new techniques to process. Figure 6.2 shows the gait signatures of the sixteen image sequences in the SOTON database. It can be seen that while signatures belonging to a particular subject appear very similar they differ significantly from one subject to another.

It must be noted that for the SOTON database, all gait signatures that were derived from image sequences in which the subjects were walking from left to right were all mirrored so that all gait signatures have the subject facing (walking) in the same direction before taking the Fourier Transform. This is necessary because the similarity differences are computed from the Fourier components. The mirroring would not have been necessary if the human body is vertically (perfectly) symmetric.

A low pass filter is then applied to the Fourier Transform of the gait signatures (derived from the symmetry operator). For the low pass filtering, different radii from 1 to 45 pixels inclusive were used to investigate the appropriate number of Fourier components that can be used. These values range from 0.1% to 100% of the total Fourier coefficients.

The k-Nearest Neighbour (K-NN) rule is then applied to the low pass filtered Fourier components for classification using $k = 1$ and $k = 3$. For a given database of subjects, unless otherwise stated, the same database is used as *test* set and as the *search* set. Note that for all databases used in this work, each subject has at least four image sequences. For each image sequence, T_i in the test set, we compute similarity differences between T_i and the image sequences in the search set excluding T_i (in the search set) using the Euclidean distance measure. For k =1, the image sequence in the search set with the lowest similarity difference is chosen as the match of T_i. If this match belongs to the same subject as the T_i then there is a correct classification of T_i. For $k = 3$, the three image sequences in the search set with the lowest similarity difference values are selected. The subject with the greater number of image sequences from the three sequences selected as having the lowest similarity differences are then considered as

the match for T_i. If more than one of the matches belongs to the same subject as T_i then there is a correct classification. The recognition rate is therefore the number of image sequences of correct classifications divided by the total number of image sequences in the test or the search set.

It must be noted that we could have used ANOVA or other classifiers but here k-NN is a good basic technique offering capability for comparison with other classifiers. It is worth mentioning that all those with whom we compared our results used the K-NN for classification.

The correct classification rates (CCRs) were 100% for both $k = 1$ and $k = 3$ for the SOTON database. For the UCSD database, the same approach was used for the classification. Six image sequences of each of the six subjects were used as the training set, and the seventh from each as the test data. The recognition rates for silhouette information were 97.6% and 92.9% for $k = 1$ and $k = 3$ respectively. A CCR of 92.9% was obtained for the optical flow information, for both $k = 1$ and $k = 3$.

It is worth mentioning that the lower recognition rates from the UCSD database as compared to the SOTON database was due to three of the image sequences, two from subject 5 and one from subject 3 in the UCSD database. Five of the image sequences of subject 5 appear to have been taken under the same conditions as those of the other subjects in the database. However, two of the image sequences appear to have been taken with the camera much further away from the subject than all the other image sequences. This resulted in the two image sequences being scaled down. For subject 3, in one of the image sequences, the subject's clothing was very similar to the background. This resulted in dense black spots around the legs after the segmentation. It must be noted that all image sequences of a particular database were taken under the same conditions such as lighting. This eliminates the possibility of factors such as lightning, the position of the camera, etc influencing the recognition rates. Even though some of the image sequences in the UCSD database were taken under slightly different conditions we assumed the same conditions for all the image sequences in the database for this work.

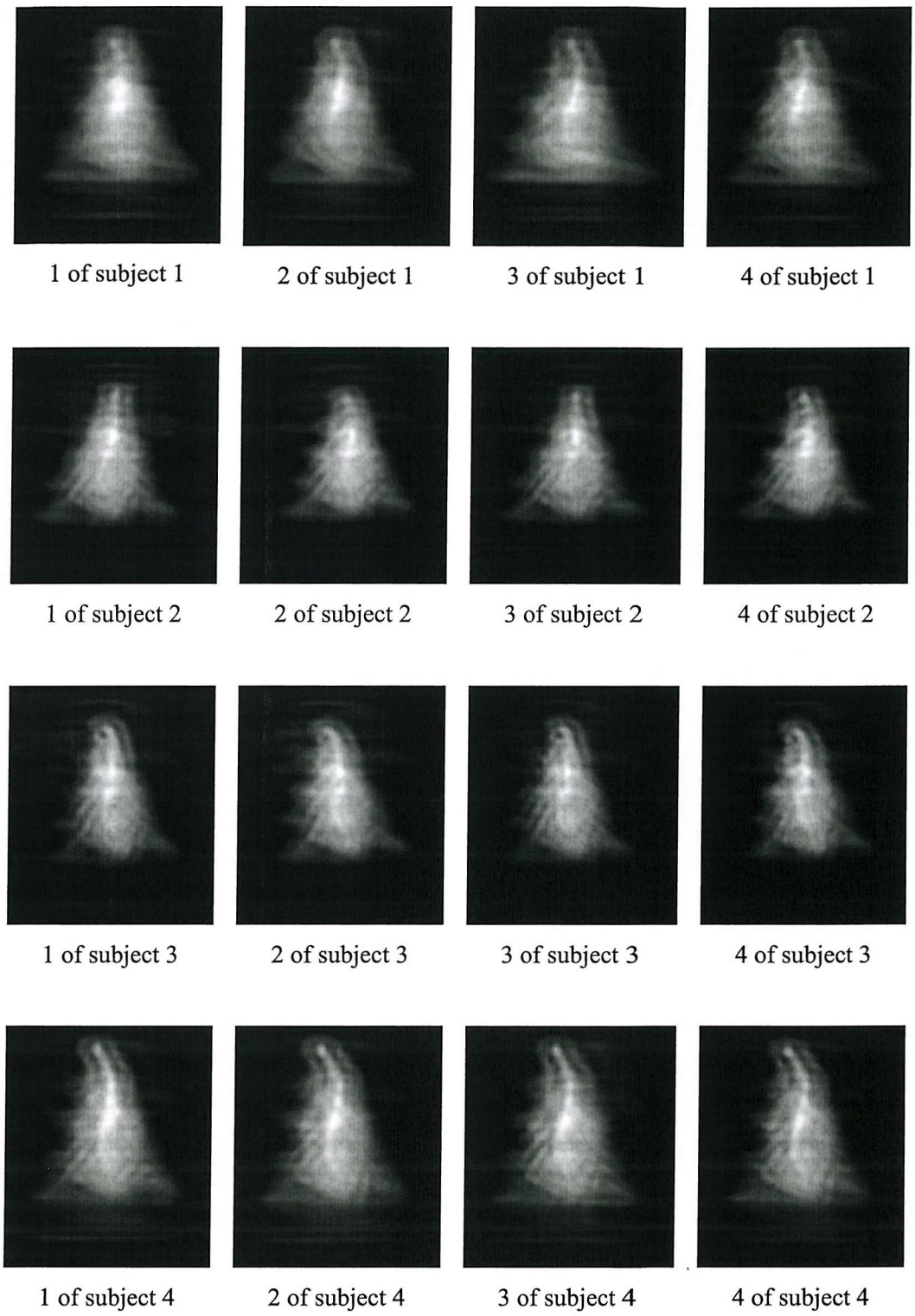

Figure 6.2: Gait signatures from the SOTON database

Table 6.1 - Initial results obtained from two disparate databases.

Database	Number of Subjects	Data Type	CCR (%)	
			$k = 1$	k = 3
SOTON	4	Silhouette	100	100
		Optic flow	100	100
UCSD	6	Silhouette	97.6	92.9
		Optic flow	92.9	92.9

Even though recognition rates of 100% were achieved for all radii values greater than 2 using the SOTON database, it was observed that selecting much smaller numbers of the Fourier coefficients may affect the recognition rates on a larger database of subjects. This is shown in Figure 6.3 from which we see that at a radius of one pixel (that is five components) the recognition rates are much higher for k=1 than for k=3. For a radius of two pixels (i.e. thirteen components) this position is reversed. The rate approaches 100% at a radius of four, in both cases. This is where more components are used. Table 6.1 shows a summary of the results obtained.

We also investigated the effect of the DC component on the recognition rates. We first applied the low pass filter to the Fourier coefficients and later removed the DC component. Note that removing the DC is a high pass filtering but this we did to investigate its effect on subject recognition. The result obtained shows that the removal of the DC component did not influence the recognition rates. This then suggests that the recognition rates obtained are not dependent on the area of the subjects. Figure 6.4 shows the trend of the calculated similarity difference values using the Euclidean distance measure of the test subject against the training subjects. The *sub11*, *sub12*, *sub13* and *sub14* are the image sequences of subject 1. The last digit in the names is the sequence number. Similarly *sub2x*, *sub3x* and *sub4x* are the image sequences for subjects 2, 3 and 4 respectively. It is clear that the shape of both curves (k = 1 and k = 3) is very similar, that is, by including or excluding the DC component has barely no

effect on the similarity difference values as there are no crossings on the graph to affect recognition rates. This was carried out on a small database of four subjects. We will investigate further on much larger databases under performance analysis of the symmetry operator in chapter 7.

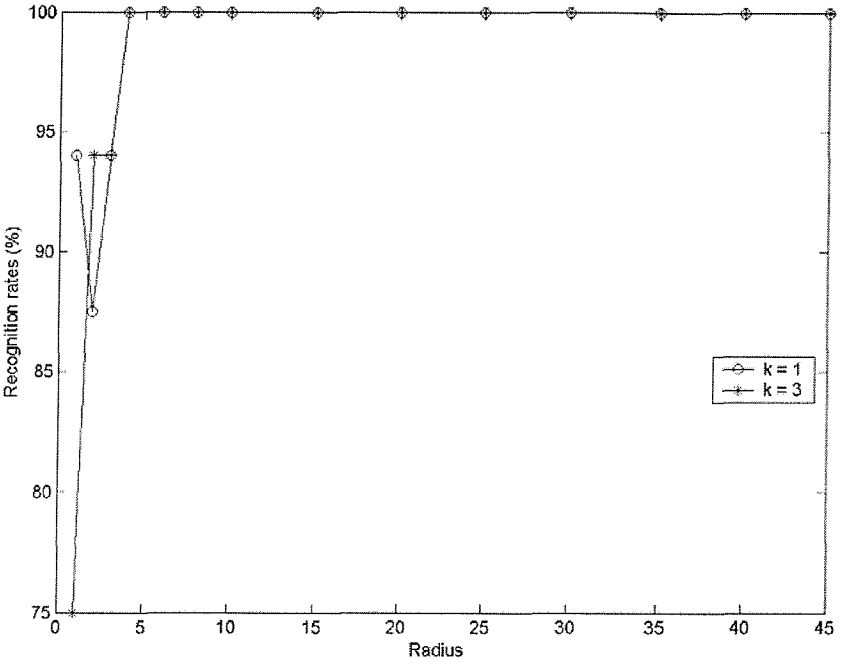

Figure 6.3: Low pass filtering result

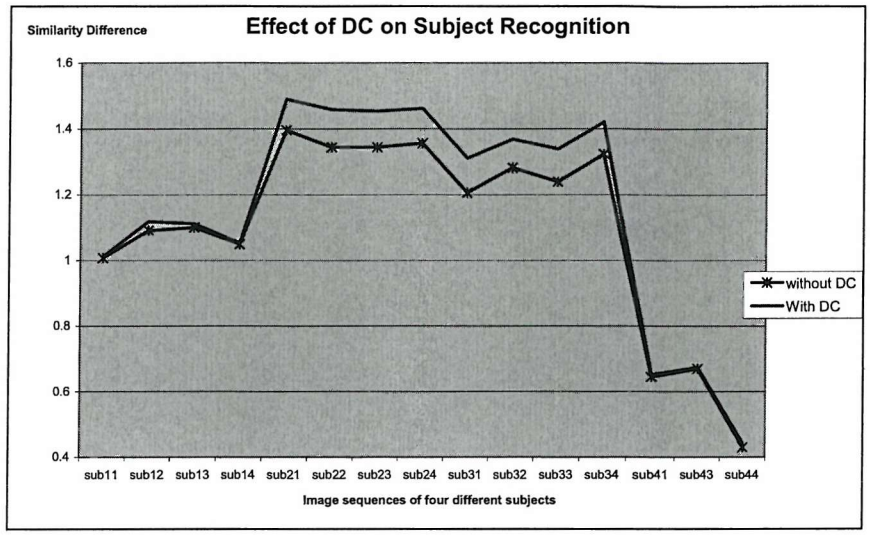

Figure 6.4: Effect of DC on subject recognition

We also investigated whether the low pass filter results in a loss of information. This was done by reconstructing the original image from the Fourier coefficients. Figure 6.5 shows some of the reconstructed images for some of the radii values used. It can be seen from the reconstructed gait signatures that not much information is lost as a result of the removal of the high frequencies in terms of structure. The only effect that this had was that the resulting signatures were blurred for smaller radii values (as expected).

Original

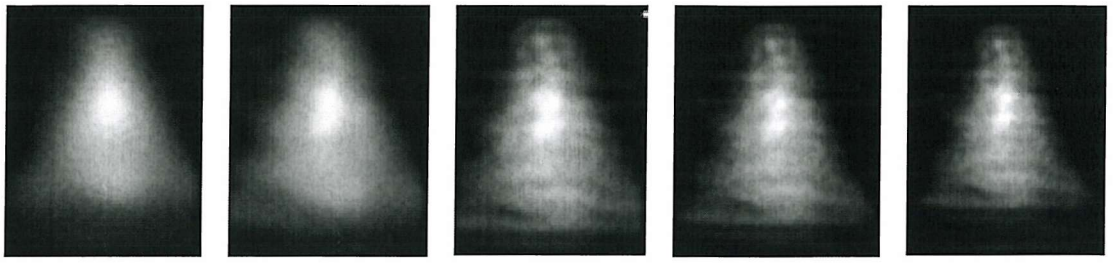

(a) 5 pixels (b) 10 pixels (c) 20 pixels (d) 30 pixels (e) 40 pixels

Figure 6.5: Reconstructed gait signatures after low pass filtering

6.2 Carnegie Mellon University (CMU) database

CMU had databases in which the subjects were made to perform four different walk patterns namely slow walk, fast walk, inclined walk and walking with a ball [111]. The databases contain the same twenty five (25) subjects filmed walking on an indoor treadmill. Six different cameras at six different positions were used in filming the subjects thus giving six different walking views. At the time of this work, not all the databases from the different walk patterns have been processed. As such, we used databases from two different views; fronto-parallel and oblique (at 45 degrees to the camera view) and at two different walk patterns (slow walk and fast walk) as these were the only ones ready for use. This means four different databases from CMU are used here. For the slow walk, the treadmill was adjusted to an average walking speed of 2.06 miles per hour and that of the fast speed was on the average 2.86 miles per hour for the subjects. We used four image sequences of each subject in each database. Each

image sequence contains one gait cycle. The descriptions of the four databases are summarised in Table 6.2. Figure 6.6 shows image frames from the two different views. Figure 6.6(a) shows a silhouette of a subject filmed fronto-parallel. Figure 6.6(b) also shows the same silhouette in Figure 6.6(a) but filmed by the camera recording at view angle of 45°. Note that the silhouettes have been windowed. From now on, we shall refer to the four databases as slow37, slow45 for slow walking filmed fronto-parallel and at 45 degrees to the camera respectively. Also, fast37 and fast45 refer to the fast walking for filming fronto-parallel and at 45 degrees to the camera respectively.

Table 6.2: The four different CMU databases. Normal means a view angle of 0 degrees and oblique refers to a view angle of 45 degrees

Name of database	**Camera**	**Walking speed**	**View angle**
CMU_037_s	037	Slow	Normal
CMU_037_f	037	Fast	Normal
CMU_045_s	045	Slow	Oblique
CMU_045_f	045	Fast	Oblique

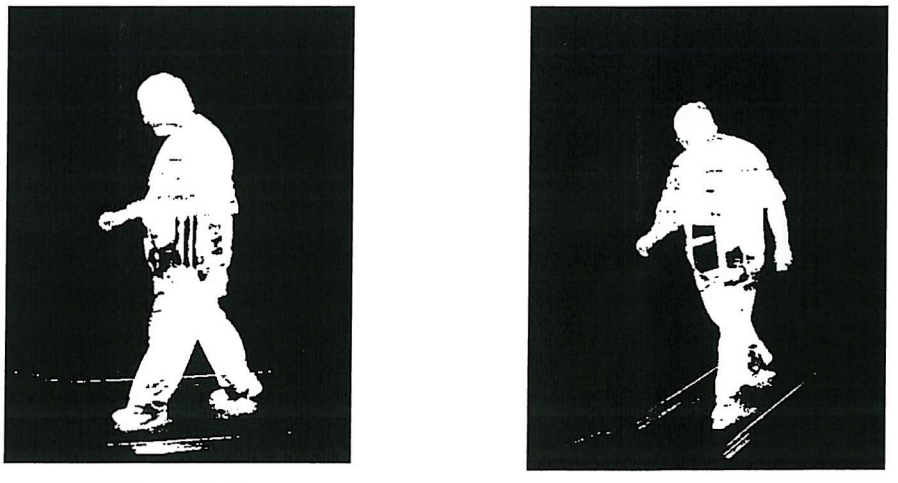

(a) Normal view (b) Oblique view

Figure 6.6: The same image frame as captured by two different cameras at two different viewing angles.

The essence of using the four databases was to investigate how well our approach performed with different walking speeds and to what extent can it tolerate different view angles. Tables 6.3 shows the recognition rates obtained from the CMU databases.

Table 6.3: Recognition rates from the fronto-parallel slow and fast walks using the various methods

Method	Slow walk		Fast walk	
	k = 1	k = 3	k = 1	k = 3
Spatial	100.0	100.0	99.0	96.0
Spatial-Temporal	100.0	100.0	99.0	96.0
Temporal	100.0	100.0	99.0	96.0
EST	100.0	99.0	99.0	96.0
Projection	100.0	100.0	98.0	96.0
Radial	95.0	96.0	96.0	88.0

It appears from table 6.3 that if all subjects in a database are filmed at roughly the same walking speeds then walking speed has barely a statistically significant effect on the recognition rates. However, this needs to be investigated further on different databases. It is also clear from the table that all the four approaches performed equally well with recognition rates exceeding 95%.

6.3 The Human Identification database (HumanID)

The HumanID database was captured at the University of Southampton for the Human ID at a distance research program sponsored by DARPA. The database consists of 50 subjects, with 4 sequences of each subject giving a total of 200 image sequences. The

silhouettes numbered 1 to 50 inclusive in appendix A shows the 50 subjects in the HumanID database. The label below each silhouette is the number used to uniquely identify the subjects. The silhouette extraction is the same as described in section 6.4.2. Thus, the HumanID database is just a subset of the most recent version of the Southampton database we started with. This we observed returned good results. We used the HumanID database so that we can offer results on the 50 subjects comparable to other approaches. The results summarised in Table 6.4 are from the temporal templates. These templates were obtained in the same manner as summarised under section 5.1.2.

Table 6.4: Recognition rates of the HID database using only the temporal templates

Metric distance	**Recognition Rates (%)**	
	k = 1	**k = 3**
Spatial	96.0	92.0
Spatio-Temporal	95.0	93.0
Temporal	95.5	93.0
EST	94.5	92.5

In [110], Zernike velocity moments were applied to the same temporal templates (optical flow images). The recognition rate obtained from using 5 moments and a much higher image resolution (690 x 400 as against our low resolution of 64 x 64) was 55.5%. However, a recognition rate of 96.0% was achieved using the Zernike velocity moments by combining the spatial templates and the temporal templates. By combining the spatial and temporal templates, better recognition rates can be achieved [53]. Thus, by using only temporal information to obtain the same recognition rate (see Table 6.4) as combining spatial and temporal templates using the Zernike velocity moments show that by performance comparison our techniques perform better.

6.4 The most recent version of the SOTON database (SOTON'02)

6.4.1 The Data capture

Most existing databases on gait contain very few subjects, usually between 4 and 25 in number. One of the objectives of the work was to establish and use a database of over 100 subjects. Each subject will have at least four image sequences and each image sequence will have at least one gait cycle, together with background and other supporting data. Given that Digital Video (DV) is now an established technology at reasonable cost we chose DV. As such, we chose to acquire imagery via good quality progressive scan and interlaced DV camcorders [112]. The database construction software was Python (and XML was used for labelling).

In order to provide an approximation to ground truth and to acquire imagery for application analysis, the subjects were filmed indoors and outdoors. However, only the indoor databases are used in this work due to time constraints. For the indoors, we also used treadmills as well as the track as these are most convenient for acquisition though there is some debate as to their effect on gait. Some studies suggest that kinetics are affected rather than kinematics, but our experience with using untrained subjects and limitations on footwear and clothing motivated us to consider the track as the most suited for full analysis. The track was prepared with the chroma-key (green, as this is an unusual clothes' colour) background illuminated by photoflood lamps, viewed normally and at an oblique angle. The design of the track was such that subjects had to walk constantly in both directions. For this work, we used the databases from the camera that filmed the subjects in fronto-parallel view. To mimic a conventional walking pattern, we set the treadmill at a constant speed and an inclination. The imagery for the large database was done with high resolution. The track data was initially segmented into background and walking and further labels were introduced for each heel strike and direction of walking. This allowed for basic analysis including manually imposed gait cycle labels. We will refer to this larger database from now on as SOTON'02, the '02 just shows the year the database was created. For further details please refer to [112].

6.4.2 Chroma-key silhouette extraction

The chroma-key approach was used to extract the silhouettes to produce the SOTON'02 database. The use of chroma-key extraction depends on the nature of data capture and the colour. The chroma-keying is the process where a subject is filmed in front of an evenly lit, bright pure coloured backdrop. For the extraction to be possible, the subject's clothing colours must be different from that of the background. Any pure colour can be used as the backdrop. With the SOTON'02 database, bright green was used as the backdrop colour as it is unlikely colour for subjects to wear. Moreover, video cameras are usually more sensitive in the green channel, and often have the best resolution and the detail in that channel due to having twice as many green pixels as red and blue in an attempt to match human vision colour sensitivity.

The powerful flood lightning in the laboratory was such that the effect of shadows was reduced to minimum with an evenly lit backdrop. To extract the subject, a luminance key is used. All pixels in the image with brightness colour over or below a chosen brightness level are replaced by another colour from a colour generator. Thus, in our case the bright green colour was replaced to remove the backdrop and the floor. An absolute error image is added around the selected colours to allow for the lightning variations due to the image backdrop. Noise is usually introduced as isolated pixels within the backdrop and these can be removed by shrink and expand operation. This leaves large objects relatively untouched.

The background subtraction applied to the SOTON'02 database is as follows. A background image is first obtained by applying a temporal-mode filter to the image sequence. By subtraction and region growing, a silhouette can be extracted by first isolating the computed background image. The background subtraction often leads to the introduction of noise or holes in the silhouette. The noise is removed by region growing. Pixels are then merged by a homogeneity criterion. The region growing algorithm is a variant of the basic split and merge method. Merging is achieved by considering pixel distribution, a variation of the algorithm proposed by Duboisson *et al.* [113]. The region growing image is then thresholded to obtain a binary silhouette which is then windowed to reduce computational time.

6.4.3 The Results obtained

The most recent versions of the SOTON databases now have at least 114 subjects each (i.e. the 50 from the HumanID version plus at least 64 new ones). Each subject has about four image sequences. In one database, 115 subjects were walking from left to right. In another database, the 114 subjects were walking from right to left while in the third database the 114 subjects were walking in both directions; left to right and right to left. In fact, the third database is just the combination of the left to right and the right to left walk databases. All the three databases mentioned here contain the same subjects (people). Appendix A shows the silhouettes of the people/subjects in the databases. The number below each silhouette is the label used to uniquely identify the different subjects.

Tables 6.5, 6.6 and 6.7 summarize the recognition rates. For both values of k, the rates are about the same for the different approaches. However, the results appear to show that more image sequences per person in a database can slightly improve the recognition rates. This is shown in Table 6.7 where each subject has eight image sequences in the database as compared to Tables 6.5 and 6.6 where each subject has four image sequences. Since we did not correct for radial distortion in the left to right and right to left walks, there is the chance that the results from the two databases would differ and this is reflected in the rates in Tables 6.5 and 6.6.

Table 6.5: Recognition rates of the left to right walk.

Method	**Recognition Rates (%)**	
	k = 1	**k = 3**
Spatial	95.2	89.9
Spatio-Temporal	95.2	90.8
Temporal	92.8	85.1
EST	95.6	90.8

Table 6.6: Recognition rates of the right to left walk.

Method	**Recognition Rates (%)**	
	K = 1	**k = 3**
Spatial	93.4	86.0
Spatio-Temporal	92.8	86.0
Temporal	92.1	85.5
EST	94.1	87.5

Table 6.7: Recognition rates of the database in which subjects walked in both directions

Method	**Recognition Rates (%)**	
	k = 1	**k = 3**
Spatial	94.6	89.6
Spatio-Temporal	94.4	89.5
Temporal	92.7	85.9
EST	95.0	90.7

6.5 Symmetry projection results

The symmetry projection as described in section 4.3.2 was applied to the SOTON'02 and the CMU databases. We first investigated the effect of ψ (the different orientations) by considering values of ψ between 0 and π inclusive. Note that the use of $|\cos(\phi(p)-\psi)|$ in equation 4.15 allows for the same recognition rates to be achieved for the same positive and negative values of ψ, that is, the rate for ψ=-π is the same as that of ψ=π. Figure 6.7 shows the recognition rates for the different values of ψ using the SOTON'02 database in which subjects walked in both directions and for k = 1. As expected, the recognition rates are higher for orientations closer to the vertical axis than those closer to the horizontal axis since the human motion is vertically skewed symmetrically. The asymmetry is inherent in the formulation of the symmetry operator as depicted by the graph. Tables 6.8 and 6.9 show a summary of the results obtained.

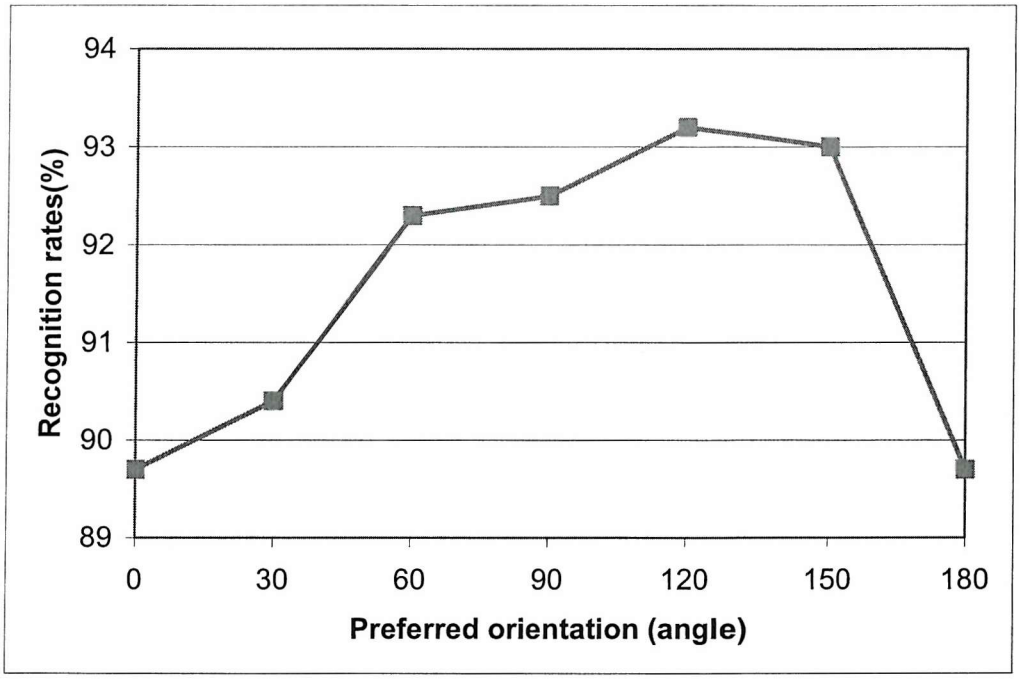

Figure 6.7: Effect of the preferred angle of orientation on projection symmetry and recognition rates

Table 6.8: Recognition rates using symmetry projection with a projection angle of 90 degrees on the SOTON database of 114 subjects

Direction of walk	**Recognition rates**	
	k=1	**k=3**
Left to right	93.5	87.3
Right to left	91.7	82.9
Both (left to right and right to left)	92.5	85.1

Table 6.9: Recognition rates using symmetry projection with a projection angle of 90 degrees on the four CMU databases of 25 subjects each

Database	**Recognition rates (%)**	
	k=1	**k=3**
Slow37	100.0	100.0
Slow45	100.0	100.0
Fast37	100.0	96.0
Fast45	100.0	97.0

The results so far in this section were obtained using the original definition of $\phi(P_k)$ in equation 4.12 and 4.13, that is, the direction of symmetry at the point P_k is given by

$$\phi(P_k) = \varphi(i, j) \tag{6.1}$$

such that $C(i,j)$ is maximal for $(i,j) \in \Gamma(P_k)$, and the symmetry at the mid point P_k given by

$$S(P_k) = [M(P_k), \phi(P_k)] \tag{6.2}$$

We now show by experimental results that by modifying equation 6.1 as follows gives a better representation of $\phi(P_k)$ from the different $\varphi(i,j)$ and hence better recognition rates.

$$\phi(P_k) = \frac{1}{m}\sum_{1}^{m}\varphi(i,j) \tag{6.3}$$

where m is the number of pairs of edge points contributing to the symmetry magnitude, $M(P_k)$ as in equation 6.2.

Table 6.10: Recognition rates using equation 6.3 instead of equation 4.12

Direction of walk	**Recognition rates (%)**	
	k = 1	**k = 3**
Left to right	95.4	89.9
Right to left	93.4	86.0
Both (left to right and vice-versa)	94.7	89.6

(a) Recognition rates using the SOTON'02 database

Database	**Recognition rates (%)**	
	k = 1	**k = 3**
Slow37	100.0	100.0
Slow45	100.0	100.0
Fast37	99.0	96.0
Fast45	100.0	99.0

(b) Recognition rates from the CMU databases

Comparing Table 6.10(a) and Table 6.8, we can see that recognition rates are much higher in Table 6.10(a) than in Table 6.8 for all the SOTON'02 databases for both values of k. The increase of about 2% is very significant as the recognition rates are already high. However, from Table 6.9 and 6.10(b) there are no significant differences

in recognition rates using the CMU databases. This may be due to the fact that most of the rates (100%) cannot be improved and the others are also already very high.

6.6 Radial symmetry results

The radial symmetry as described in section 4.3.3 was applied to the SOTON'02 database and the recognition rates are shown in Table 6.11. Comparing results of radial symmetry with the other symmetry approaches presented in this work, it appears the radial symmetry does not work very well. It might work better on performance analysis which addresses whether the technique can handle practical concerns, to be analysed in the following chapter.

Table 6.11: Recognition rates using radial symmetry.

Direction of walk	**Recognition rates**	
	k =1	**k=3**
Left to right	84.4	65.8
Right to left	76.1	59.2
Both (left to right and right to left)	80.9	65.7

6.7 Conclusions

We have applied the different approaches to different databases of different sizes. The results presented show that the symmetry of human motion can indeed be used to recognise people by the way they walk. Most of the existing approaches were tested on smaller databases usually containing up to 30 subjects. On much larger databases from different sources, the performances of the different approaches were very good. The results also show that by including temporal information in the symmetry calculations improvements in performance have been realised. There was no statistically significant effect from using a larger database. Recognition rates of over 95% were achieved from using smaller databases and from two different larger databases from two different

institutions. It is also clear that the modification to the symmetry projection computations could prove useful in gait recognition as well. Further tests on much larger databases will still be required to really appreciate the use of symmetry in gait recognition. We have also shown that by changing the definition of equation 6.3, subject recognition can be improved.

In this chapter, we have shown how we have been using increasing database sizes. When this work first started, most of the contemporary database had up to 5 subjects. With time, this has increased to about 30 subjects. At present, the SOTON'02 is the largest gait database of its kind. We have found that using these different databases as the number of subjects has increased, the recognition rates from our new techniques have remained very much the same. This indicates that the performance of our new techniques has not really been affected by the increasing size of the database which is very encouraging if the techniques are to be used in real life applications. From the results obtained from the SOTON'02 and the CMU databases, the recognition rates for $k = 1$ is always greater than that of $k = 3$. This suggests that the distribution of the gait signatures is not well clustered and this may require further analysis.

Chapter 7

PERFORMANCE ANALYSIS OF SYMMETRY OPERATOR

For symmetry approaches to assist in the advancement of this research, they need to perform well under different environments and conditions. In this regard, many published recognition approaches address few factors of practical consequence. It is important to know the conditions under which the gait recognition problem is solvable, the important factors affecting a person's gait and the research approaches that appear promising for improving the performance of gait-based recognition [45]. We also need to know how well our approaches compare with some of the existing approaches, using a common database. With these points in mind, we have evaluated the performance of the Symmetry operator by looking at (i) gait factors such as the effect of walking speeds and the direction of walking and (ii) performance factors or generalisation capabilities such as addition/missing spatial data, missing image frames, noise, different image resolutions, direction of walk and different view angles. Different databases are used here depending on the type of analysis being considered.

In most of the analysis, the test will be carried out on both a smaller and a larger database to enable comparisons with other techniques and also to ascertain how an increase in database size can affect our results. With the smaller database, the test analysis will be applied only to the image sequence being used as the test sequence. This will answer questions such as how will the techniques perform given for example a noisy image sequence to be recognised from a database of *clean* image sequences. For the larger database, the test will be applied to all image sequences in the database.

The results of these experiments are as presented in the following sections. It must be noted that the tests on performance and generalisation capability were carried out after

the extraction of the silhouette from the sequence. This is because it is difficult to add, for example real noise to an image; hence what we did was an attempt to look at noise and occlusion in the worse case. With powerful noise removal algorithms, noise can easily be reduced to minimum in most cases to eliminate its effect. Moreover, the issue of noise is not really to do with signal noise but may be due to the poor performance of segmentation/detection algorithms under less favourable illumination conditions. Therefore carrying out the performance analysis on the extracted silhouette appears to be reasonable.

7.1 Gait factors

7.1.1 Effect of speed on gait by symmetry analysis

We investigated the effect of speed on gait by our methods using the CMU data. To do this we use a *gallery* and a *probe* set. A gallery is set of gait signatures representing subjects in a database to be used to recognise from unknown gait signatures. The unknown gait signatures constitute the probe set. The unknown signatures need not necessarily have to have a corresponding signature in the gallery set, but here, every signature in the probe set has a corresponding signature in the gallery set and that these will represent gait signatures from different image sequences of the same subject.

For example, we used *slow37* to probe *fast37* and vice versa as these two databases contain image sequences for which the subjects were filmed fronto-parallel. Similarly, *slow45* is used to probe *fast45* and vice versa as both of these databases contain image sequences the subjects were filmed walking at an oblique of 45° to the camera. In each table, the number of classification tests performed is 10000 (the 100 image sequences in gallery multiplied by the 100 image sequences in probe). Tables 7.1 to 7.4 show the recognition rates obtained by applying the spatial, spatio-temporal, temporal and the extended spatio-temporal approaches respectively.

Table 7.1: Recognition rates using the spatial approach

Probe and Gallery	**Recognition rates**	
	k=1	**k=3**
Slow37 and fast37	75.0	76.0
Slow45 and fast45	71.0	70.0
Fast37 and slow37	70.0	68.0
Fast45 and slow45	76.0	73.0

Table 7.2: Recognition rates using the spatio-temporal approach

Probe and Gallery	**Recognition rates**	
	k=1	**k=3**
Slow37 and fast37	75.0	74.0
Slow45 and fast45	70.0	69.0
Fast37 and slow37	71.0	67.0
Fast45 and slow45	75.0	72.0

Table 7.3: Recognition rates using the temporal approach

Probe and Gallery	**Recognition rates**	
	k=1	**k=3**
Slow37 and fast37	68.0	65.0
Slow45 and fast45	70.0	65.0
Fast37 and slow37	67.0	65.0
Fast45 and slow45	76.0	69.0

Table 7.4: Recognition rates using the extended spatio-temporal approach

Probe and Gallery	Recognition rates	
	k=1	k=3
Slow37 and fast37	70.0	68.0
Slow45 and fast45	69.0	69.0
Fast37 and slow37	73.0	67.0
Fast45 and slow45	77.0	68.0

From the results shown in Tables 7.1 to 7.4 for the different approaches, it can be seen that the performance of the symmetry operator is not affected by the speed at which subjects walk. This is due to the averaging within the symmetry calculations. This may be very useful in real application as people do not normally walk at constant speeds in carrying out their daily activities. It must be noted that here we cannot compare recognition rates from different databases but only performances of different approaches. This also explains why we did not evaluate performance rates between different databases such as slow45 and SOTON'02.

7.1.2 Effect of direction of movement on symmetry analysis

Here we used the SOTON'02 databases as we have two databases in which for one the subjects were walking from left to right and in the other from right to left. From Tables 6.5 and 6.6, it can be seen that the recognition rates are quite similar for the different values of k for the four different approaches, suggesting that the direction of walk has no significant effect on the recognition rates if all subjects in the database are filmed walking in the same direction. However, further tests carried out appear to suggest that the direction of walk to some extent affects gait recognition. This may be due to the fact that as we walk in front of a camera, different parts of our body are occluded from the camera's view depending on which side of the body faces the camera, thus affecting the symmetry of motion. As such, we now record different leg (from different side,

left/right of the individual), introducing concepts of asymmetry discussed earlier. Here, we use the right to left gait database to probe the left to right gait database and vice-versa. In Table 7.5, 'Left and Right' means the left to right gait database was used as the probe and the right to left database as the gallery. It must be noted that in using a left to right walk database to probe a right to left walk gait database and vice-versa requires that all gait signatures in one of the databases be mirrored so that subjects in both databases will have the same direction of walk.

Table 7.5: Recognition rates on direction of motion

	Left and Right		**Right and Left**	
	K = 1	k = 3	k = 1	k = 3
Spatial	65.0	53.1	60.0	47.4
Spatio-temporal	66.6	55.5	63.3	49.3
Temporal	56.4	45.6	51.1	38.9
Extended Spatio-temporal	68.4	57.5	66.6	54.7

The results in Table 7.5 are not as good as one would have expected by comparing them with those of Tables 6.5 and 6.6. One of the reasons may be the fact that after mirroring gait signatures from one of the databases we did not do any radial correction. If this is done then we will not be able to make correct comparisons with others who have used the same databases without any pre-processing or modifications. A test carried out on a small database of subjects has confirmed that radial correction can improve recognition rates.

7.1.3 Effect of different view angle on symmetry analysis

To investigate the effect of different view angles, we used the CMU database. Here, for both walking speeds, we used the fronto-parallel (Slow37 and Fast37) database as the probe and the oblique view (Slow45 and Fast45) database as the gallery. It must be noted that at the time of this work, we could not get databases in which the subjects were filmed

at smaller view angles. The only database we could use to carry out this test was the CMU database in which the subjects were filmed fronto-parallel and at a view angle of 45 degrees. The results obtained from the tests are shown in Table 7.6(a). The recognition rates are less than 15% for the different approaches. It is therefore clear from the table that at a view angle of 45 degrees, it is almost impossible to recognise a subject from his/her fronto-parallel video footage by symmetry without viewpoint correction. Further tests will be required to ascertain the view angle at which a subject can still be recognised from a fronto-parallel video footage.

Even though the recognition rates in Table 7.6 (a) are very low, they are just more than chance rate for correct subject classification (4.0%) and also the chance rate for correct sequence classification (far less than 1%). On a database of N subjects the chance rate for correct subject classification is $1/N$, and for m (independent) sequences of N subjects the chance rate of 100% correct classification is $1/N^m$.

However, it is clear from Table 7.6(b) that if all subjects in a database are filmed walking from the same view angle then the view point has no statistically significant effect on the recognition. Comparing the results in Tables 6.3 and 7.6(b), it can be seen that the recognition rates for the fronto-parallel slow walk and that of the oblique view are about the same. However, there are only slight differences in the corresponding rates for the fast walk. The similarities in the overall rates show that for a complete gait cycle, gait is invariant to speed. In future, we will apply the techniques to databases of smaller view angles and make the approaches view invariant.

Table 7.6: Recognition rates using the CMU databases

Symmetry approach	Slow37 and Slow 45		Fast 37 and Fast 45	
	k = 1	k = 3	k = 1	k = 3
Spatial	7.0	6.0	6.0	7.0
Spatio-temporal	7.0	4.0	9.0	7.0
Temporal	8.0	5.0	12.0	8.0
Extended Spatio-temporal	5.0	4.0	8.0	5.0

(a) From different view angles

Method	Slow walk		Fast walk	
	K = 1	k = 3	k = 1	k = 3
Spatial	100.0	100.0	100.0	99.0
Spatio-Temporal	100.0	100.0	100.0	99.0
Temporal	100.0	100.0	100.0	98.0
EST	100.0	100.0	100.0	99.0
Projection(1)	100.0	100.0	98.6	96.0
Projection(2)	100.0	100.0	99.0	96.0
Radial	95.0	96.0	96.0	88.0

(b) From view angle of 45 degrees

7.2 Performance factors and generalisation capability

7.2.1 Missing frames

The evaluation, aimed to simulate time lapse, was done by considering a consecutive number of frames as missing, i.e. by omitting them from the computation of symmetry. This was applied to both the old and the SOTON'02 databases. For the old SOTON database, the missing frames approach was applied to only the test data. Figure 7.1(a) shows the gait signature when every other frame was considered missing starting with image frame 2 using the old SOTON. Figure 7.1(b) shows the gait signature when every other two consecutive frames were considered missing, that is frames (2, 3), (5, 6), (8, 9), etc were treated as missing. This means only frames 1, 4, 7, 10, etc from image sequences are used. Similarly, considering 3 consecutive frames as missing means we used only frames 1, 5, 9, 13, etc. This was repeated for 4, 5, 6, 7 and 8 consecutive frames being considered as missing. The percentages in Figure 7.1 are the corresponding percentages of image frames considered as missing.

The results showed no effect on the recognition rates for both k=1 and k=3 using the CCR. This is due to the averaging associated with symmetry operator's evidence gathering. Figure 7.2 shows the general trend of deviation of the best matches of each subject from the test subject. The *sub 1*, *sub 2*, *sub 3* and *sub 4* are the best match of subject 1, subject 2, subject 3 and subject 4 of the test data respectively. Figure 7.3 shows that as more frames are omitted, the resulting gait signature tends to deviate from all other gait signatures by approximately the same margin and is still closest to other gait signatures of the same subject.

Carrying out the same evaluation using the SOTON'02 database, the missing frames approach was applied to all image sequences in the database. Figures 7.3 and 7.4 show the recognition rates obtained from the different techniques using $k = 1$ and $k = 3$ respectively. The figures show that by having similar image frames missing in all image sequences, recognition rates are not much affected depending on the percentage of frames missing. From Figures 7.3 and 7.4, it is clear that by considering up to 75%

of the image frames (that is using about 3 image frames on average) as missing recognition rates of over 60% are obtained for both k =1 and k = 3 except for radial symmetry. We also see that by increasing the number of missing frames from 50% to about 85% does not lead to drastic fall in recognition rates. The average number of image frames in a sequence is about 28. It appears radial symmetry is very much affected by having missing frames in a sequence. For example, by considering 50% of the frames as missing, the recognition rates from the radial symmetry fell by about 24% whilst that of the other forms of symmetry fell by less than 3% for $k = 1$, and about the same for $k = 3$.

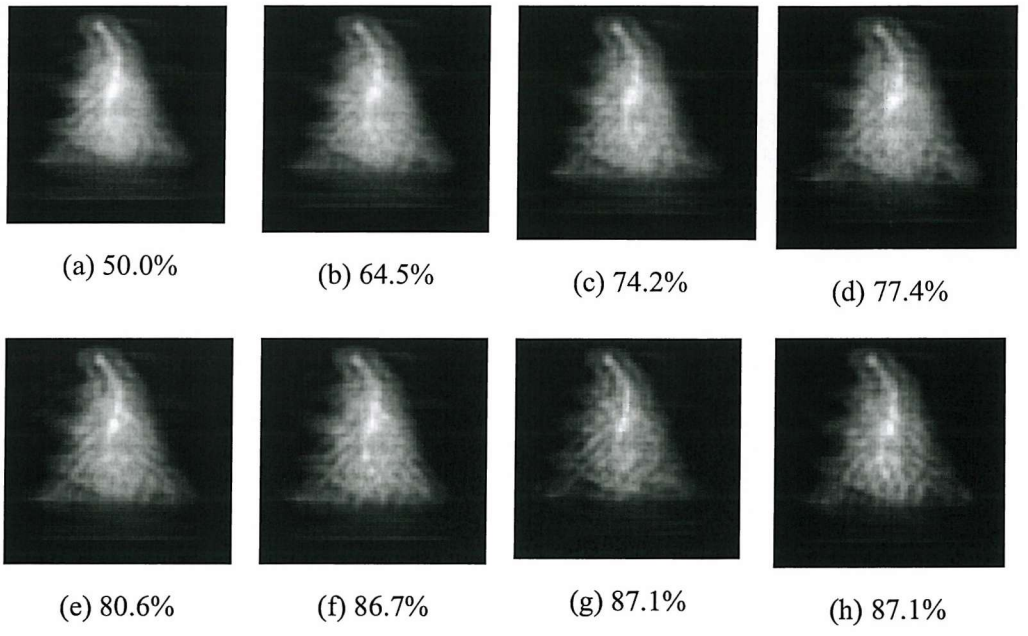

Figure 7.1: Gait signatures from missing frames using old SOTON database

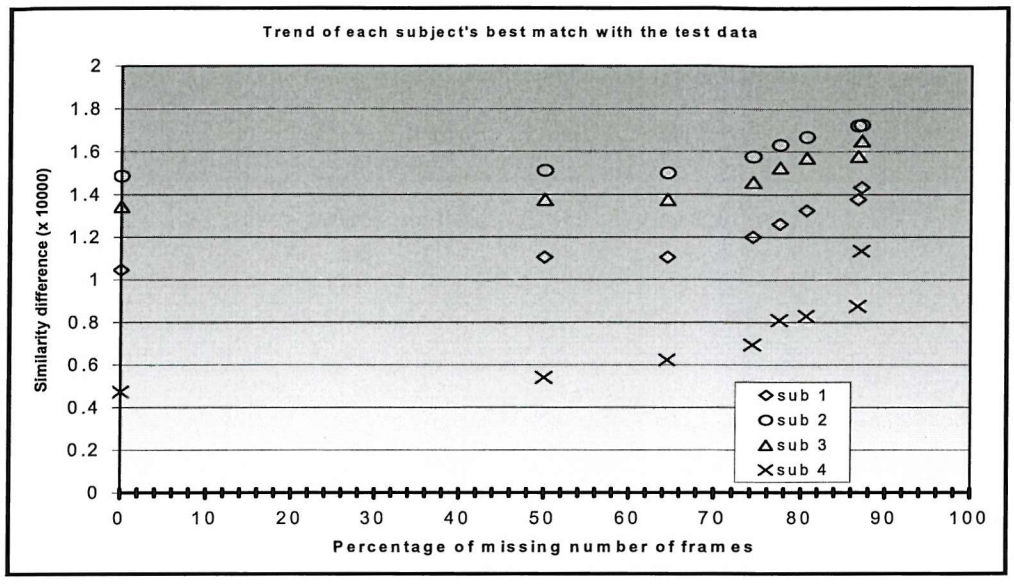

Figure 7.2: Effect of missing image frames

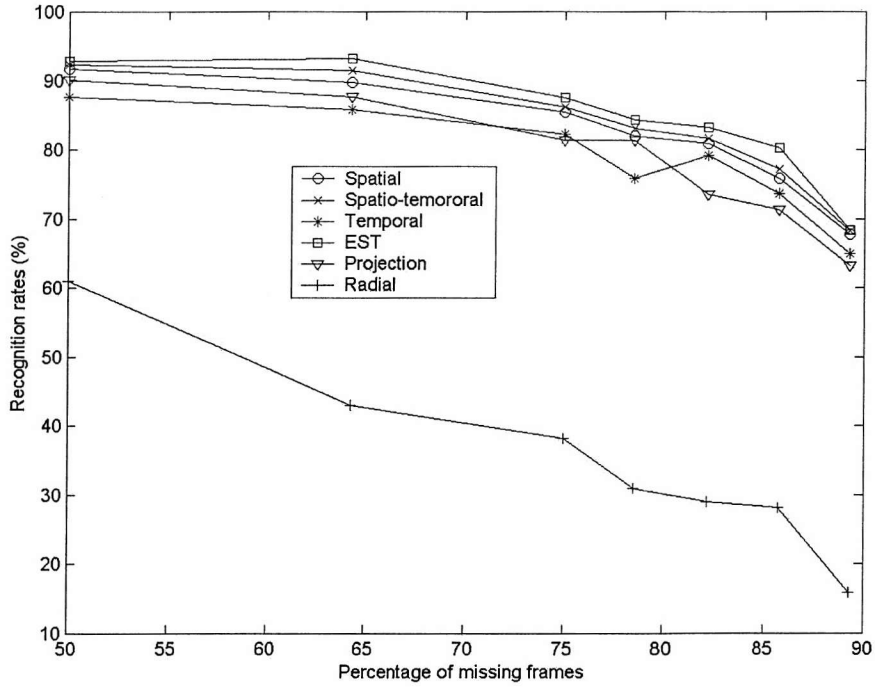

Figure 7.3: Effects of missing frames on recognition rates using $k = 1$

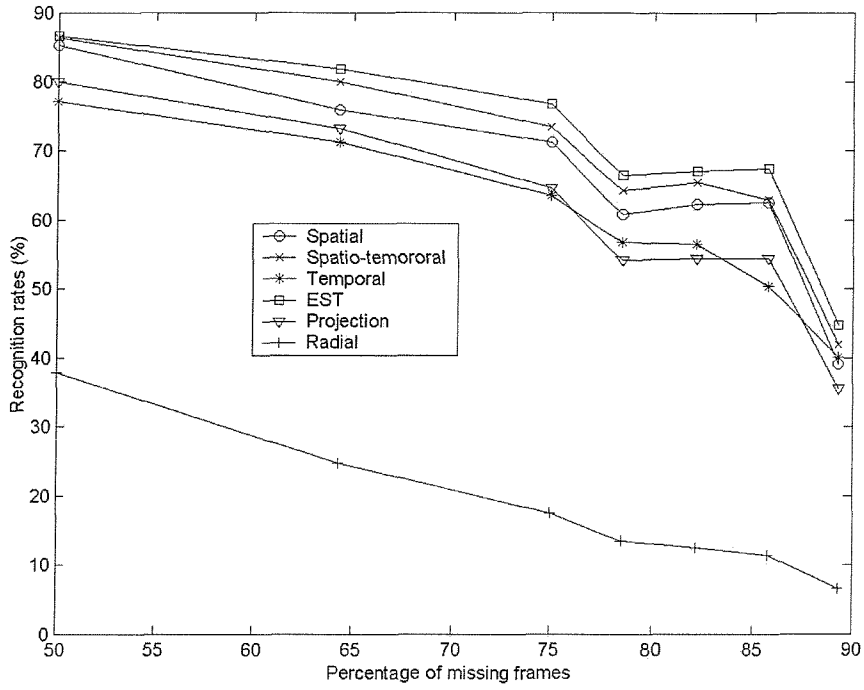

Figure 7.4: Effects of missing frames on recognition rates using $k = 3$

7.2.2 Addition or removal of spatial data

The evaluations were done on both the old SOTON and the SOTON'02 databases by masking with a rectangular bar of different widths of up to 35 pixels in steps of 5 in each image frame at the same position. These tests were done to see the effect of removing or adding spatial data on the recognition rates. If the object has the same colour as the bar, then that illustrates addition of spatial data whilst an object with a different colour from the bar illustrates omission of data. By omitting spatial data, we reduce the effect of the main axis of symmetry resulting from the human body with the resulting symmetry map being derived mainly from the legs and the arms which are the main parts of the human body associated with gait.

For the old SOTON database, the masking was applied to only the test subject with bar sizes of 5, 10 and 15. The area masked was on the average, 13.2, 26.3 and 39.5% of the

image silhouette in each image frame. The bar either had the same colour as the image silhouette or as the background. The masking was applied before the Sobel operator. These are shown in Figure 7.5. In both cases, recognition rates of 100% were obtained for a bar size of 5 pixels for both $k = 1$ and $k = 3$. For a bar size of 10 pixels, Figure 7.5(g) failed but 7.5(b) gave correct recognition for $k = 3$ and not $k = 1$. For bar sizes of 15 and above, the test data could not be recognised as the subject is occluded in almost all the image frames in the sequence. Here we used the spatial symmetry approach.

For the SOTON'02 database, the masking was applied to all image sequences in the database. The results obtained were very encouraging as recognition rates of over 70% were obtained for all techniques except the radial symmetry, with bar sizes of up to 25 pixels, that covers up to about 80% of the silhouette in most of the image frames. Here, we used spatial, spatio-temporal, extended spatio-temporal, temporal, projection and radial symmetry approaches. The results are shown in Figures 7.6 and 7.7 for missing and addition of spatial data respectively. Apart from radial symmetry, the fall in recognition rates is gradual with increasing bar width showing how the approaches can tolerate addition and removal of spatial data. For radial symmetry, the recognition rate approaches that of chance with increasing bar width. Appendix C and D show a gait cycle of a subject with image frames masked with black and white rectangular bars of widths 25 pixels respectively.

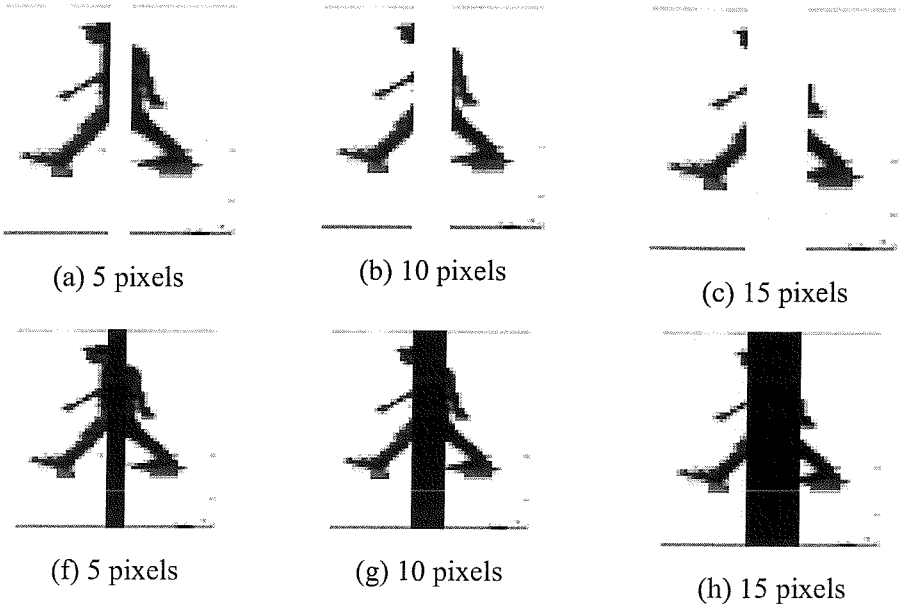

(a) 5 pixels (b) 10 pixels (c) 15 pixels

(f) 5 pixels (g) 10 pixels (h) 15 pixels

Figure 7.5: Addition or removal of spatial data

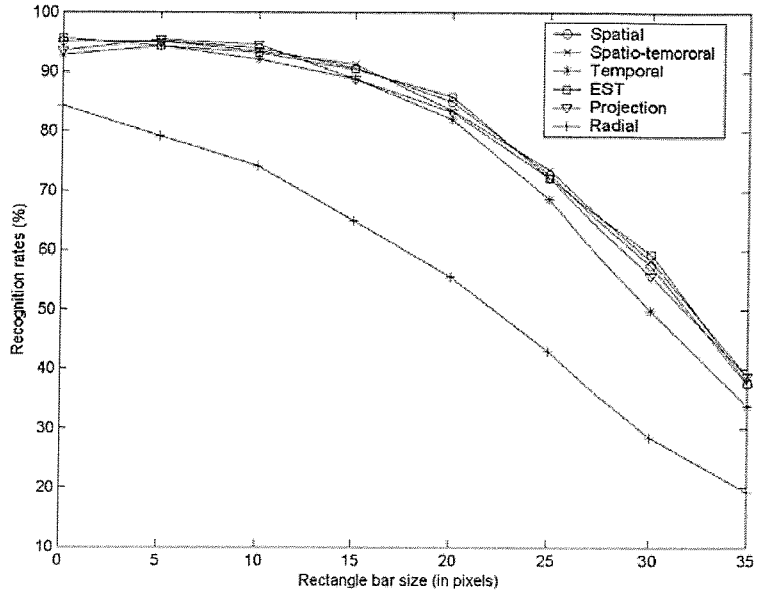

(a) For $k = 1$

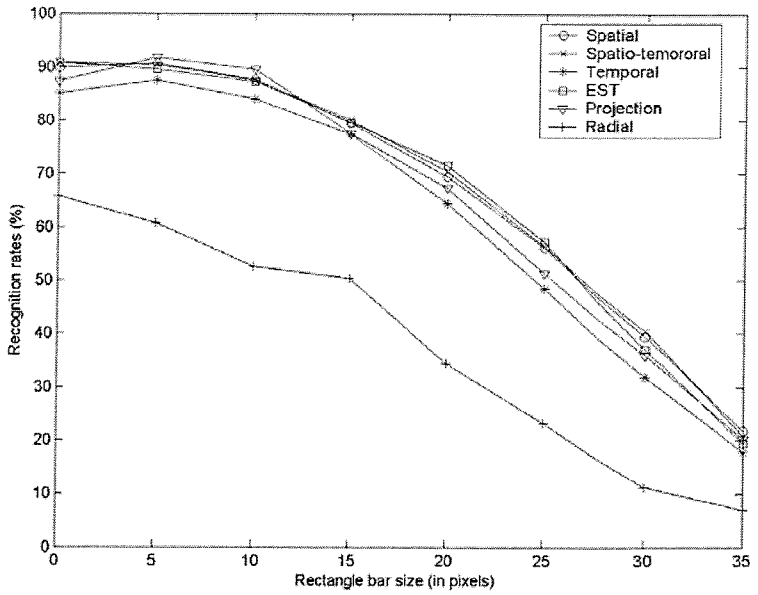

(b) For $k = 3$

Figure 7.6: Effect of missing spatial data on recognition rates

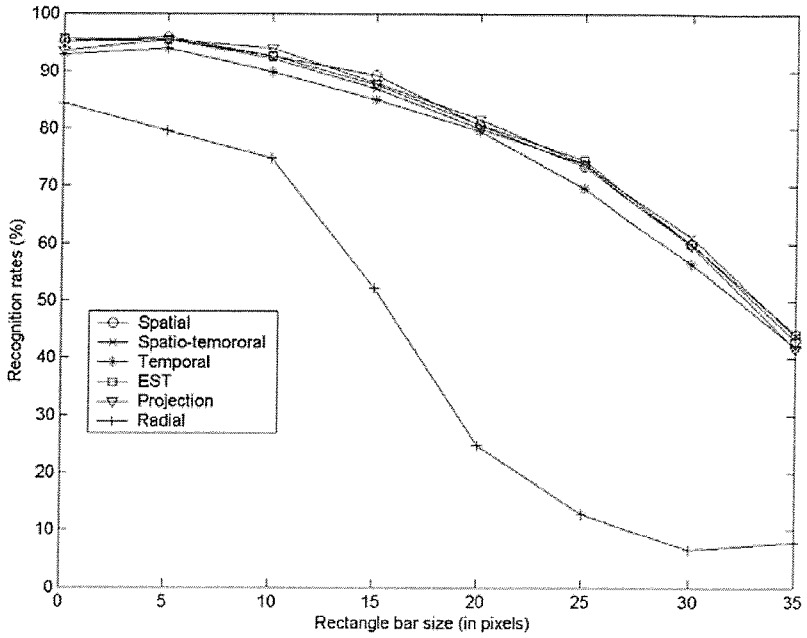

(a) For $k = 1$

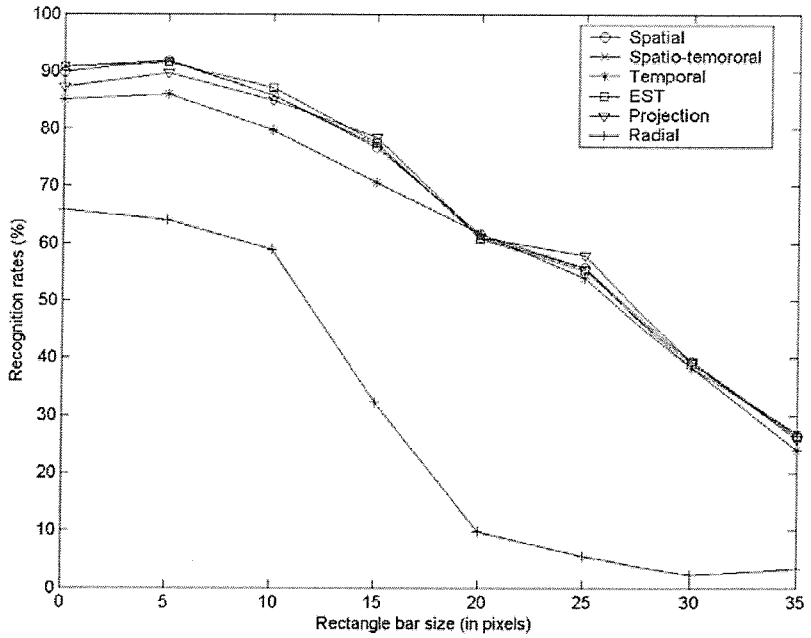

(b) For $k = 3$

Figure 7.7: Effect of adding spatial data on recognition rates

Table 7.7 shows the recognition rates obtained by using equation 6.3. Again, it is clear from the results that better recognition rates are obtained as compared to the corresponding rates (for projection symmetry) shown in Figures 7.7.

Table 7.7: Recognition rates obtained from different noise levels using equation 6.3

Bar colour	Rectangular bar width (in pixels)											
	10		15		20		25		30		35	
	k = 1	k = 3	k = 1	k = 3	k = 1	K = 3	k = 1	k = 3	K = 1	k = 3	k = 1	k = 3
Black	93.9	87.7	90.6	79.2	84.7	70.0	72.6	56.1	57.7	39.9	37.3	21.5
White	92.5	85.5	89.3	76.8	80.3	61.4	73.9	56.1	59.7	39.5	42.8	26.8

7.2.3 Noise

The symmetry operator is able to handle noise by the averaging associated with its evidence gathering and our experimentation has confirmed that using symmetry can tolerate some, but naturally not excessive, additive salt and pepper noise as consistent with silhouettes. We added 10% to 70% (inclusive) of salt and pepper noise to each image frame of the test subject and compared the resulting signature with those of the training subjects in the database. The noise is added before the Sobel operator. Figure 7.8 shows samples of the first six noise levels used. The evaluation was carried out under different two conditions.

For the first condition, we used the same values of σ and μ (see equation 4.3) as earlier. With a noise level of 5%, the recognition rates for both $k = 1$ and $k = 3$ were 100%. With 10% added noise, the test subject could still be recognised correctly for k=1 but not for k=3, i.e. CCR of 100% and 0% respectively. With added noise levels of 20% and above, the test subject could not be recognised for both $k = 1$ and $k = 3$.

For the second condition, the values of σ and μ were made relatively smaller (2 and 10 respectively). The recognition rates were not affected for both $k = 1$ and $k = 3$ for added noise levels even exceeding 60% Figure 7.9 shows how the best matches of each subject deviated from the test subject as more noise is added using the second condition. The reduction in the values of σ and μ was to ensure that closer points are given higher distance values than the distant points. This is because the distribution of the noise resulted in having most pairs of the noise as the distant points.

The above test showed that if we have noisy subjects to recognise from a database of 'clean' subjects, then we can achieve very good recognition rates. A further test was carried out by adding different noise levels to all image sequences in the SOTON'02 database. Appendix G shows a pseudo code of the algorithm used for adding the artificial noise. Table 7.8 shows the recognition rates on the different approaches by adding different amounts of noise to the image sequences.

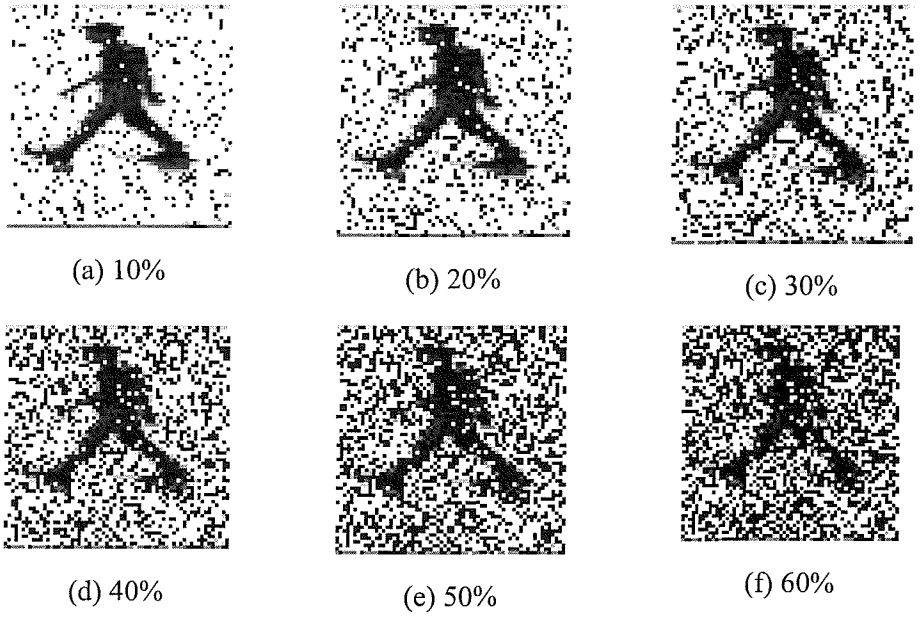

(a) 10% (b) 20% (c) 30%

(d) 40% (e) 50% (f) 60%

Figure 7.8: Noisy data

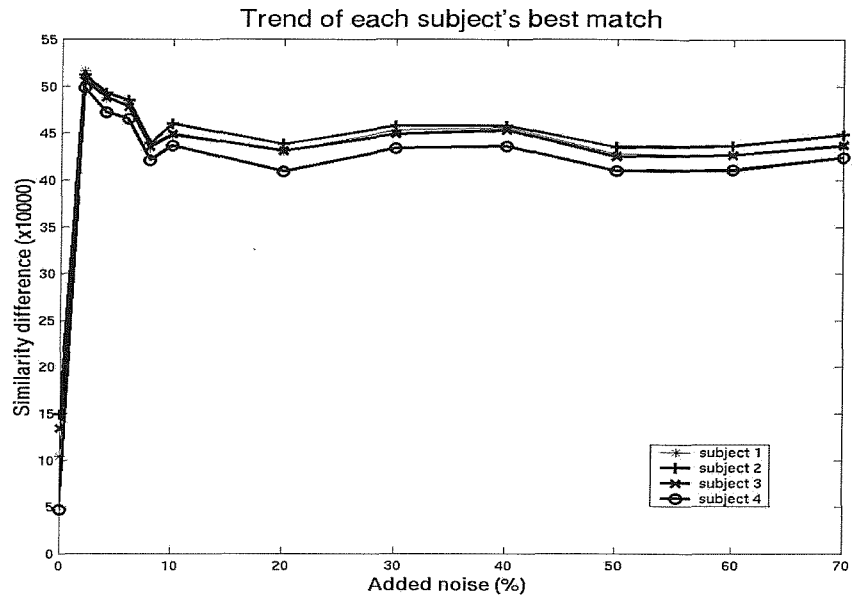

Figure 7.9: Effect of noise using the old SOTON data. This figure shows the similarity differences between each subject's best match and the test data.

Table 7.8: Effect of noise using SOTON'02 database

Symmetry approach	Recognition rates (%)							
	10%		20%		30%		40%	
	k = 1	k = 3	k = 1	k = 3	k = 1	K = 3	K = 1	k = 3
Spatial	75.0	61.6	48.9	32.7	27.4	10.8	14.3	3.3
Spatio-temporal	75.9	61.8	48.0	30.3	26.8	10.5	15.1	4.4
Temporal	72.8	55.3	44.7	28.3	31.6	14.3	14.5	5.0
EST	71.3	54.0	42.5	24.3	23.5	6.6	11.8	4.0
Projection	51.8	34.4	18.0	7.5	3.7	0.0	1.5	0.0
Radial	4.8	0.9	1.5	0.0	0.7	0.0	0.0	0.0

Table 7.9 Recognition rates from projection symmetry using projection angle of 90°, equation and different noise levels

Recognition rates (%)							
10%		20%		30%		40%	
k = 1	k = 3	k = 1	k = 3	k = 1	k = 3	k = 1	k = 3
75.2	61.2	47.6	33.1	26.8	10.8	14.7	2.9

The results in Table 7.9 show the recognition rates obtained by using equation 6.3 in place of equation 4.12. It can be seen that the recognition rates are higher than the projection symmetry rates in Table 7.8. For noise levels up to 30%, the increase in recognition rates is on average about 20% for both values of k which is very encouraging. This confirms our earlier observation that using equation 6.3 rather than equation 4.12 improves the performance of the symmetry projection. It is clear that this modification makes the symmetry projection to perform just as well as the best approaches (that is spatio-temporal symmetry and the extended spatio-temporal) in Table 7.8.

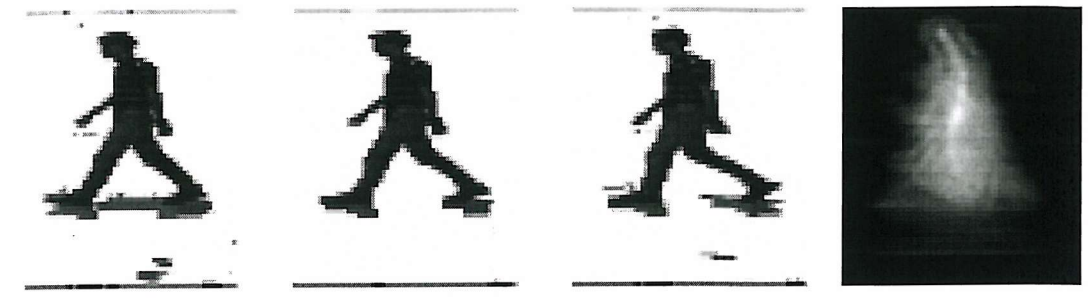

(a) 64 x 64

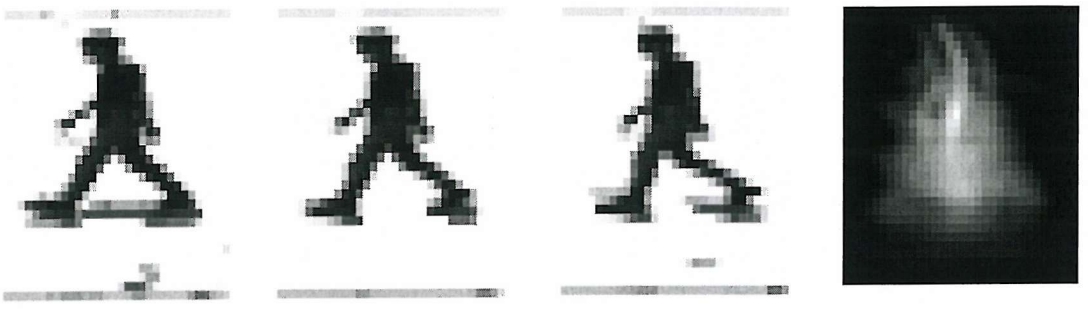

(b) 32 x 32

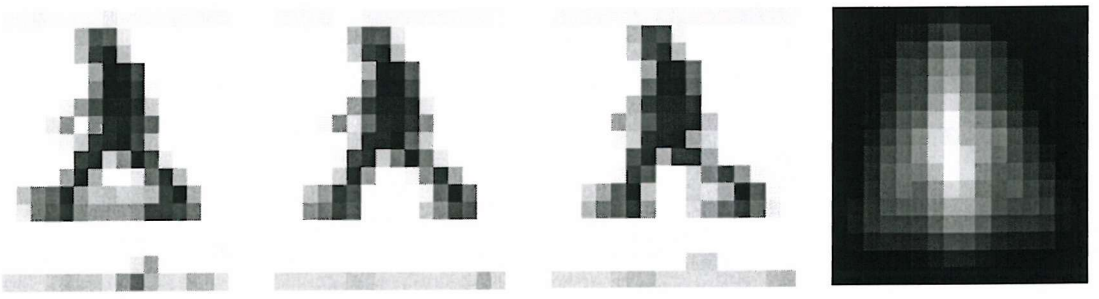

(c) 16 x 16

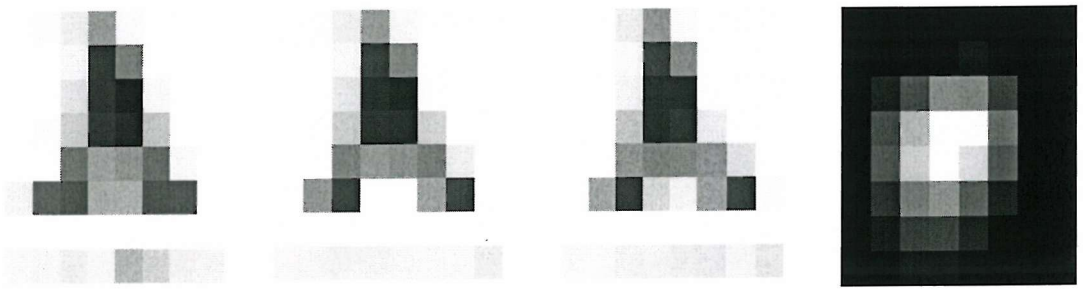

(d) 8 x 8

Figure 7.10: Different resolution images. Images have been enlarged to the same size to reveal loss of detail as resolution decreases

7.2.4 Low resolution and Scaling

Investigation was also conducted on low resolution images using the SOTON'02 database in which the subjects were walking from right to left. For each image resolution, all image frames in the database were resized to the same size. This was done to simulate both poor images and scaling. We did this by resizing (scaling) the original image sequences before deriving the corresponding gait signature. Figure 7.10 shows the three different image sizes used, that is 32x32, 16x16 and 8x8 pixels. The images in the figure have been enlarged to the same size to reveal the loss of detail. It can be seen that as the images are made smaller, a considerable amount of information is lost. In Figure 7.10(d), the gait signature showed no resemblance to the other gait signatures in the figure. In [4, 6], only the test subject was resized. This showed that even in that case, recognition rates of over 95% could still be achieved for image sizes up to 16 x 16 pixels. Table 7.10 shows the results presented in [4, 6].

Table 7.10: Recognition rates from low resolution images using spatial approach

Image size	**#subj.(#seq.)**	**Classification rate (%)**	
		k = 1	**k = 3**
64×64	28(4)	97.3	96.4
32×32	28(4)	97.3	92.9
16×16	28(4)	84.0	67.0
8×8	28(4)	57.1	33.0

Images are usually normalised to 64×64 to reduce computational demand. Reduction in resolution by half to 32×32 changes recognition performance little. Using the same values of σ and μ, except for the radial symmetry, recognition rates of over 90% were obtained for $k = 1$ and over 80% for $k = 3$ for the 32 x 32. In fact, further reduction to 16×16 is where no other biometric could be perceived, but where recognition by gait still occurs to some extent (one far better than random performance). For the 16 x 16 images, recognition rates of over 80% and 70% were obtained for $k = 1$ and $k = 3$

respectively. For the 8 x 8 images, the recognition rates were below 50% for both values of *k*. Looking at the image quality in Figure 7.10(c), it could be argued that the symmetry operator is able to handle low resolution images or scaling to a large extent. This is due to the averaging associated with the symmetry operator. Table 7.11 shows the results obtained after applying the different image resolution to all image sequences in the SOTON'02 database. Again, we see an increase (of about 2.5% on average) in the recognition rates obtained from the projection symmetry approach using equation 6.3.

Table 7.11: Recognition rates (%) on low resolution images using SOTON'02 database

Symmetry approach	**32 x 32**		**16 x 16**		**8 x 8**	
	k = 1	k = 3	k = 1	K = 3	k = 1	K = 3
Spatial	93.4	88.2	87.9	75.2	39.7	18.2
Spatio-temporal	94.3	88.2	87.9	75.7	38.8	19.3
Temporal	91.7	84.9	85.1	72.8	39.3	17.8
EST	93.4	88.2	88.4	76.1	38.8	20.4
Projection	92.8	86.0	82.0	70.8	40.1	18.6
Radial	55.5	35.6	23.9	8.6	13.8	4.0
Projection (equation 6.3)	93.6	88.2	87.7	76.3	40.6	19.3

7.2.5 Appropriate number of Fourier components

The investigation into the appropriate number of Fourier components (feature vectors) to be used for recognition was carried out using the CMU databases. In selecting the appropriate number of components, we first define a circle of radius, R. This circle has the same centre as that of the Fourier components matrix. Thus, for our 64 x 64 Fourier components matrix, the centre of the circle will be at (32 x 32). We know that for

Fourier components, the low frequencies are at the corners with the high frequencies around the centre of the matrix. Having defined our circle, we then select all frequencies that lie outside the circle from the components matrix. This is illustrated in Figure 7.11.

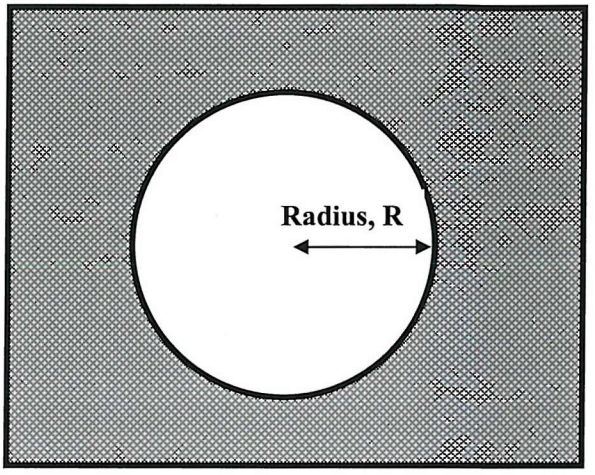

Figure 7.11: How Fourier components are selected

The shaded part shows the Fourier components that are selected for a circle of radius R. The components that lie outside the circle must satisfy the following expression.

$$\left(x-\tfrac{w}{2}\right)^2+\left(y-\tfrac{h}{2}\right)^2>R^2$$

where x and y are the row and column of a component, w and h are the number of rows and columns of the Fourier component matrix respectively

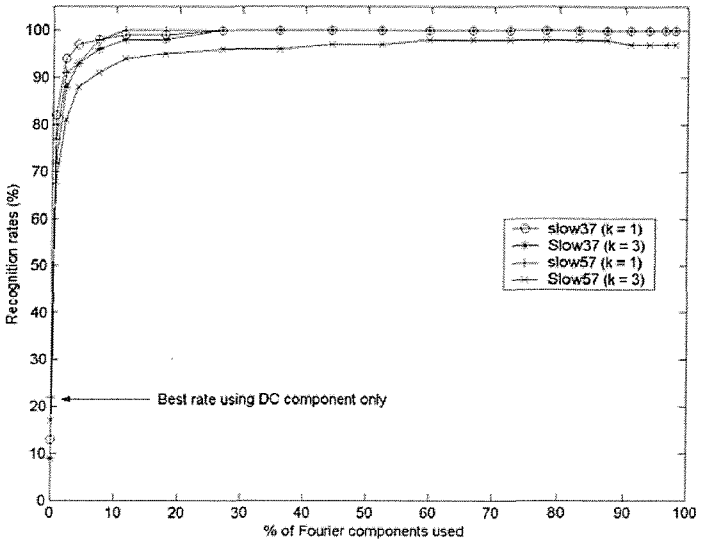

Figures 7.12: The effect of the percentages of the Fourier components selected on the recognition rates using the CMU slow walk databases.

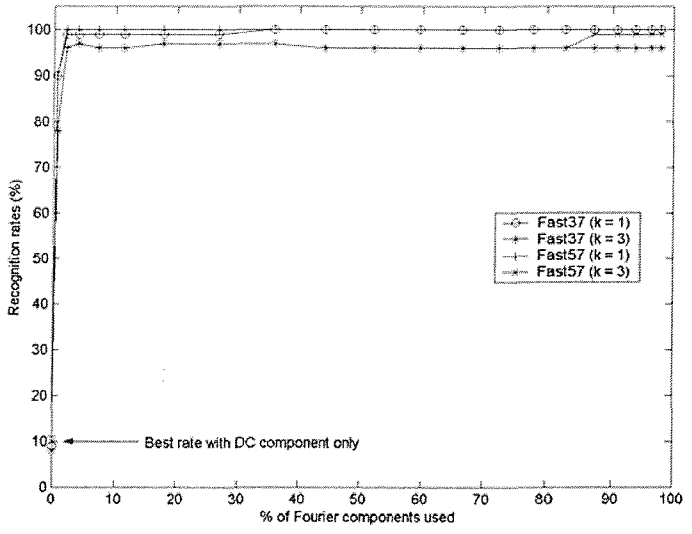

Figures 7.13: The effect of the percentages of the Fourier components selected on the recognition rates using the CMU fast walk databases.

As we can see from Figures 7.12 and 7.13, selecting as few as 4% of the Fourier components gives a recognition rate of at least 88%.

7.2.6 Comparison with other techniques

As mentioned earlier, gait would benefit from an established database on which to compare different approaches and new developments. In the absence of such an acceptable standard database, we compared our techniques with some of the current approaches that have used the same databases as used in this work. The results are as follows.

(i) *Velocity Moments*: In [57], velocity moments were applied to both the UCSD and the old SOTON data. Recognition rates of 100% from both the spatial and the optical flow information were obtained using Velocity moments from the old SOTON database. The spatial symmetry approach used in this work also gave the same recognition rates from using the same classifier. The recognition rates from the USCD database were also very similar. However, whilst we considered image size of 64 x 64, that is at very low resolution, [57] used silhouette size of 128 x 128 pixels to achieve the same results.

(ii) *Area Masks and Moment based descriptors:* In [114], the two techniques; Area Masks and Moment based descriptors were applied to the SOTON'02 databases. In both techniques, recognition rates of approximately 70% were obtained as against recognition rates of over 90% from our new techniques using the same classifier for our feature vectors. The tables below show how our techniques and that of [114] fell in performance analysis from noise and low resolution images as well. From Table 7.12, it is clear that though recognition rates from our approaches appear to fall slightly faster as more noise is added, the recognition rates are still better for all noise levels considered. Also from Table 7.13, it is clear that for image resolutions of 16 x 16 and above, our approach performed better.

Table 7.12: Comparison of our techniques, Area Masks and Moment based descriptors using different noise levels of up to 40%

Percentage noise added	Spatial	Spatio-tempora	Area Masks	Moments
0	95.2	95.2	71.9	68.3
10	75.0	75.9	66.0	47.6
20	48.9	48.0	48.1	24.6
30	27.4	26.8	25.2	11.1
40	14.3	15.1	6.0	-

Table 7.13: Comparison of our techniques, Area Masks and Moment based descriptors using different image resolutions

Image size	Spatial	Spatio-temporal	Area Masks	Moments
64 x 64	95.2	95.2	71.9	68.3
32 x 32	93.4	94.3	69.2	64.4
16 x 16	87.9	87.9	60.3	52.1
8 x 8	39.7	38.8	47.3	27.6

(iii) *Zernike Velocity Moments:* In [115], the Zernike Velocity moment was applied to the HumanID database. The recognition rate was 55.5% percent using the temporal templates and $k = 3$ while we obtained recognition rates of over 90% for both values of k. Again, our image resolution was by far lower than that used in [115].

(iv) The institutions involved in the DARPA project (Automatic Gait Recognition for Human Identification at a Distance) focussing specifically on gait, tested their respective techniques on the CMU databases. Table 7.14 shows the recognition rates from some of

the institutions. Here, the slow walk database was used as the gallery and the fast walk as the probe. All institutions used the nearest neighbour approach for classification.

Table 7.14: Results from institutions involved in the DARPA project focussing specifically on gait [116]

Institution	**Recognition rate (%)**
CMU	76
MIT	65
GT	45
UM	32

The CMU approach [60] involves extracting key frames from a walking sequence. First, the silhouette in each key frame is extracted and normalised. They are then compared to the training silhouette of each subject using a template matching algorithm. MIT's approach [117] uses shape information to extract feature vectors for recognition. For each frame in a sequence, the silhouette is first extracted and then segmented into seven regions. Statistics such as the centroid, aspect ratio and orientation are then computed and averaged over a sequence. The gait signature is therefore the concatenation of the mean features for each region. The GT approach [55] uses four static and stride parameters that are recovered from a gait cycle. The UM technique [118] is a dynamic approach that uses the changes in the contour of the human body during walking to train a Hidden Markov Model for each subject in a database.

Our new techniques; spatial and temporal gave recognition rates of up to 76% (see Table 7.1 and Table 7.3 respectively). The temporal approach gave 75% recognition rate. However, our extended spatio-temporal symmetry gave a recognition rate of 77% (see Table 7.4), thus, on average, we obtained recognition rate of 76% which equals that of CMU and better than that of the other institutions indicating that our new techniques have good performance. It must be noted that while we used image sequences of low resolutions (64x64), the other institutions used higher resolution images.

A recent review of current advances in automatic gait recognition [119] stated "It is of note that symmetry has the most potent performance,...." suggesting that the use of symmetry has a great potential in automatic gait recognition.

7.3 Conclusions

The analysis on performance factors or generalisation capability shows that the symmetry operator has the capability to handle noise, occlusion, missing frames and poor resolution images. Much of this ability derives from the averaging processes inherent in the operator. The most potent performance appears to be derived by extended spatio-temporal symmetry approach whereas the radial symmetry approach appeared to have the least generalisation capability for both values of k. The analysis on gait factors such as direction of walk and walking speed gave encouraging results. However, more work needs to be done to improve on view point invariance. Comparing our main approaches with other existing approaches also showed that our approaches in most cases perform very well.

The results show that some of the subjects (image sequences) in the SOTON'02 databases failed to be recognized correctly. There are a number of reasons for this, notable among these are subjects scratching their heads, stopping during filming, turning to face the camera, etc during filming. Appendix F shows some of the image sequences that failed to be recognized by our techniques. Each row is 5 successive image frames taken from an image sequence of the subject whose number is indicated below the sequence(s). It can be seen that for subject 067 apart from stopping most of the time, she was not swinging the arms (row 1) as she does in her normal walk and in some sequences she was found to be scratching and holding the head (rows 2 and 4) and also halting at times during the filming (row 4). None of the image sequences of this subject did match any of the others of the same subject. It can also be seen that for subject 054, in some sequences he had blobs (row 1) around the feet and in other sequences he appears to have a carrier bag on his back (row 2). Subject 110 appears to be dancing, stopping and walked at an angle the camera plane of view. Subject 29 stopped walking and turned to face the camera for a while. Some of these sequences

could have either been removed from the database or could have been corrected manually (where possible, for example the blobs) but then we needed to compare our results with those who have earlier on used the same databases without any modifications or removals. These problems will be looked at in the future.

We also see that starting with small databases and then moving on to much larger databases did not significantly affect the performance of our new techniques. It is therefore clear that symmetry has practical advantages and further testing on much larger databases and improvements in performance is necessary.

Chapter 8

Conclusions and further work

8.1 Overall Conclusions

The aim of this work is to determine whether the view from psychological literature concerning the symmetry of human motion can be applied to automatic recognition. We have therefore presented, as a starting point, a new approach to automatic gait recognition. The extensive experimentation using various-sized databases from different sources has shown that both animal and human gait in particular appears to have distinct symmetrical properties that can be extracted for recognition.

The symmetry operator, essentially, forms an accumulator of points, which are measures of the symmetry between image points to give a symmetry map. By using the symmetry operator, the Fourier Transform and a simple nearest-neighbour approach, the results have produced very good recognition rates for both $k = 1$ and $k = 3$ on a small database of four subjects. Using the same databases as in other works, we have achieved very comparable recognition rates. Also, using the largest database of its kind (the SOTON'02 database) gave recognition rates of over 95%. We started with the spatial approach at a time when symmetry analysis was completely new to gait analysis and then a novel extension to include temporal information so that subject recognition is not based on the body shape but also by human motion. The spatio-temporal approach was further enhanced to give the extended spatio-temporal approach. All these approaches gave very promising and comparable results on both smaller and larger databases, the largest analysis yet on gait databases.

We have also shown that symmetry projection, in particular, can be used to good effect in gait recognition. With symmetry projection, we have shown that by modifying the

symmetry magnitude formulation and also by redefining the corresponding symmetry direction, subject recognition can be improved greatly. Further analysis and parameter tuning may improve the performance of the symmetry projection and radial symmetry.

The symmetry operator has been shown able to handle missing spatial data, missing image frames, and to some extent noise. Thus, it will prove very useful when applied to poorly extracted sequences, partially occluded and missing frames in image sequences for gait recognition. Moreover, unlike other more standard approaches where adding an additional subject to an existing database requires that the entire database be reprocessed, our approaches only require a gait signature to be generated for the new addition and then be classified thus saving a considerable amount of time in generating feature vectors all over.

The development of symmetry has therefore, continued to support the contention that human walking can indeed be used for gait recognition. Performance analysis shows that the formulation of the symmetry operator can be arranged to recognise people from low-resolution imagery where other biometrics are obscured.

8.2. Further Work

The results presented in this work show that the symmetry operator appears to have considerable potential in automatic gait recognition. It has also been shown to enjoy support and practical advantages. However, the computational cost associated with the operator is very high. It would therefore appear appropriate to devote some effort to reducing computational demand, perhaps by using a frequency domain implementation of the symmetry operator. Naturally we also aim to increase the size of the database of subjects and also carry out more evaluation on the performance analysis.

At the time of thesis, most of the existing databases contain video footage of subjects filmed walking normal to the cameras plane of view. For practical applications we will need to consider subjects walking at different angles to the cameras plane of view. A test carried out suggests that it may be possible to describe subjects walking at small

angles towards the camera and not at high angles. Further analysis will be needed to prove this and also to make our approaches view invariant. We will investigate the effect of subjects walking at different inclinations. This is useful for recognising people walking up or down on a hill, etc. We will also investigate the effect of different conditions such as load carrying, clothing, shoes, etc. The databases used in this work were mostly captured under controlled environment such as lighting, background, walking path, etc. Further tests will be required to investigate the potential of our techniques in an uncontrolled environment. Also, most of the databases used in this work were captured indoors, future work will concentrate more on outdoor databases.

We will also look at other types of time formulation of our approaches. The recognition rates obtained by using a left to right walk to probe a right to left walk and vice versa were lower than recognition rates obtained from using databases in which the direction of walk is the same for all subjects. This is not peculiar to our techniques and needs to be investigated further so as to improve subject recognition for different directions of walk. Currently, the main suspicion is that this concerns radial distortion correction, and we shall work on this in the future.

The methods of subject classification also need further consideration. Performance analysis showed that using about 4% of the feature vectors is just enough to give the same recognition rate as using the entire feature vectors (4096 for 64 x 64 images). By using an approach such as Principal Component Analysis, it is possible to reduce the dimensionality of the feature space. As such, it might prove beneficial to deploy methods of feature set selection to prune the symmetry features. As this is the first use of symmetry for spatio-temporal image classification, these factors (amongst others) await refinement by application in a greater range of scenarios.

Appendix

Appendix A – Database Overview

The table below shows a spatial template for each of the subjects in the SOTON'02 database. The number below each silhouette refers to the label used to uniquely identify each subject. Numbers 82 and 93 are missing from the database because of insufficient numbers of sequences were captured for both subjects.

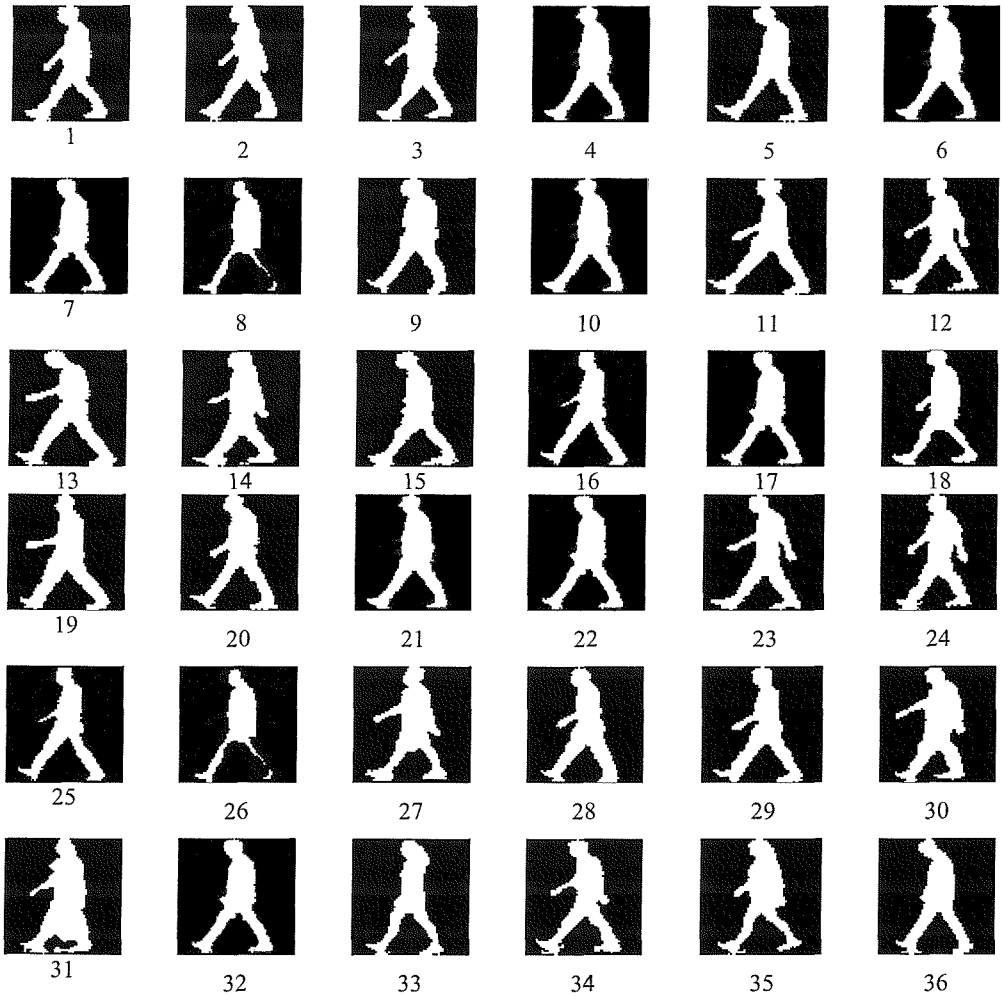

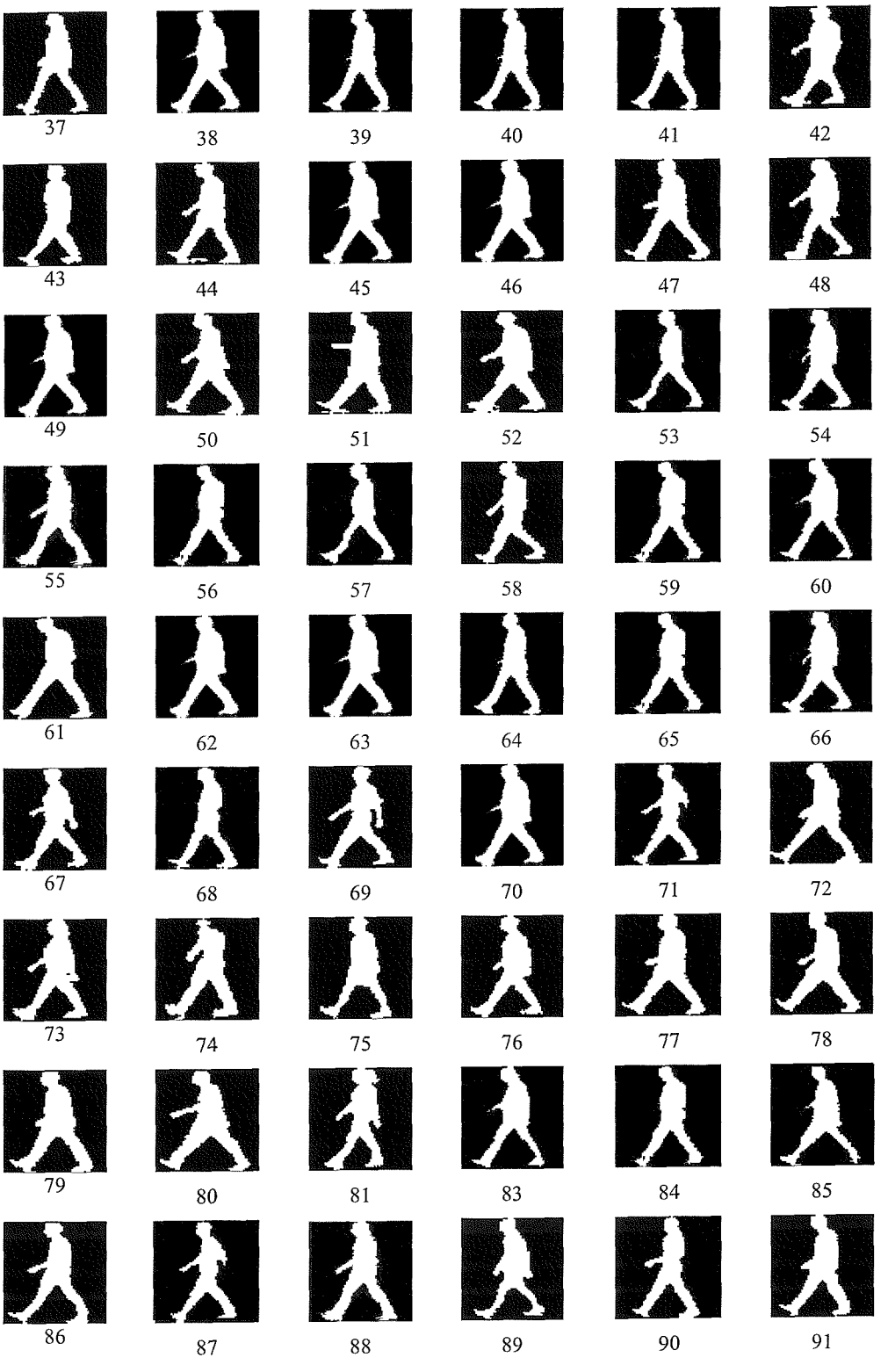
37
38
39
40
41
42
43
44
45
46
47
48
49
50
51
52
53
54
55
56
57
58
59
60
61
62
63
64
65
66
67
68
69
70
71
72
73
74
75
76
77
78
79
80
81
83
84
85
86
87
88
89
90
91

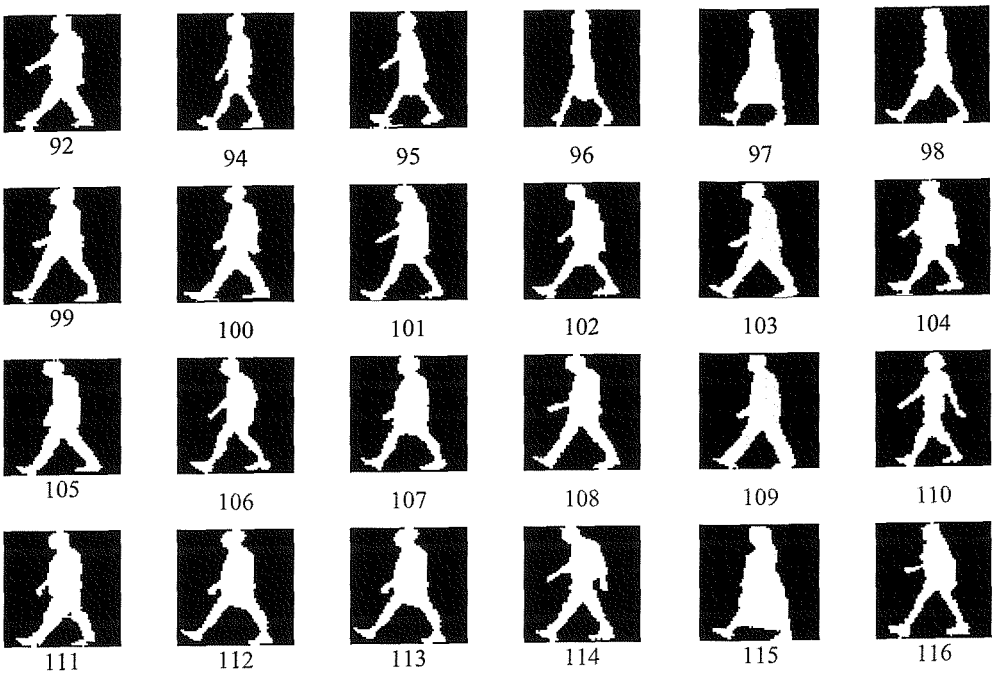
92
94
95
96
97
98
99
100
101
102
103
104
105
106
107
108
109
110
111
112
113
114
115
116

Appendix B - A gait cycle

A gait cycle is the time interval between successive instances of initial foot-to-floor contact 'heel strike' for the same foot, that is a gait cycle starts and ends with the heel strike of the same foot

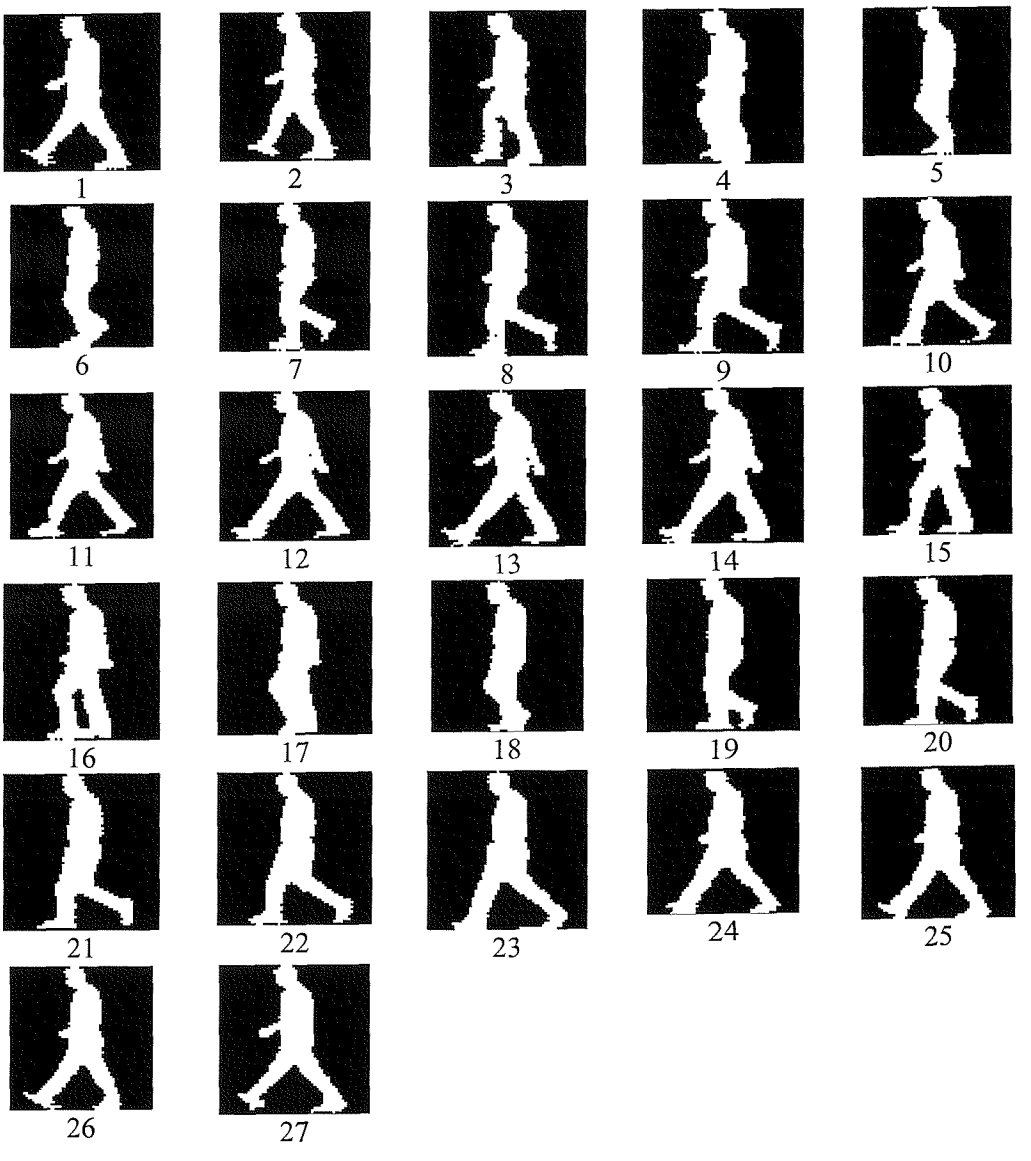

Appendix C – Image frames masked with a black rectangular bar of width 25 pixels

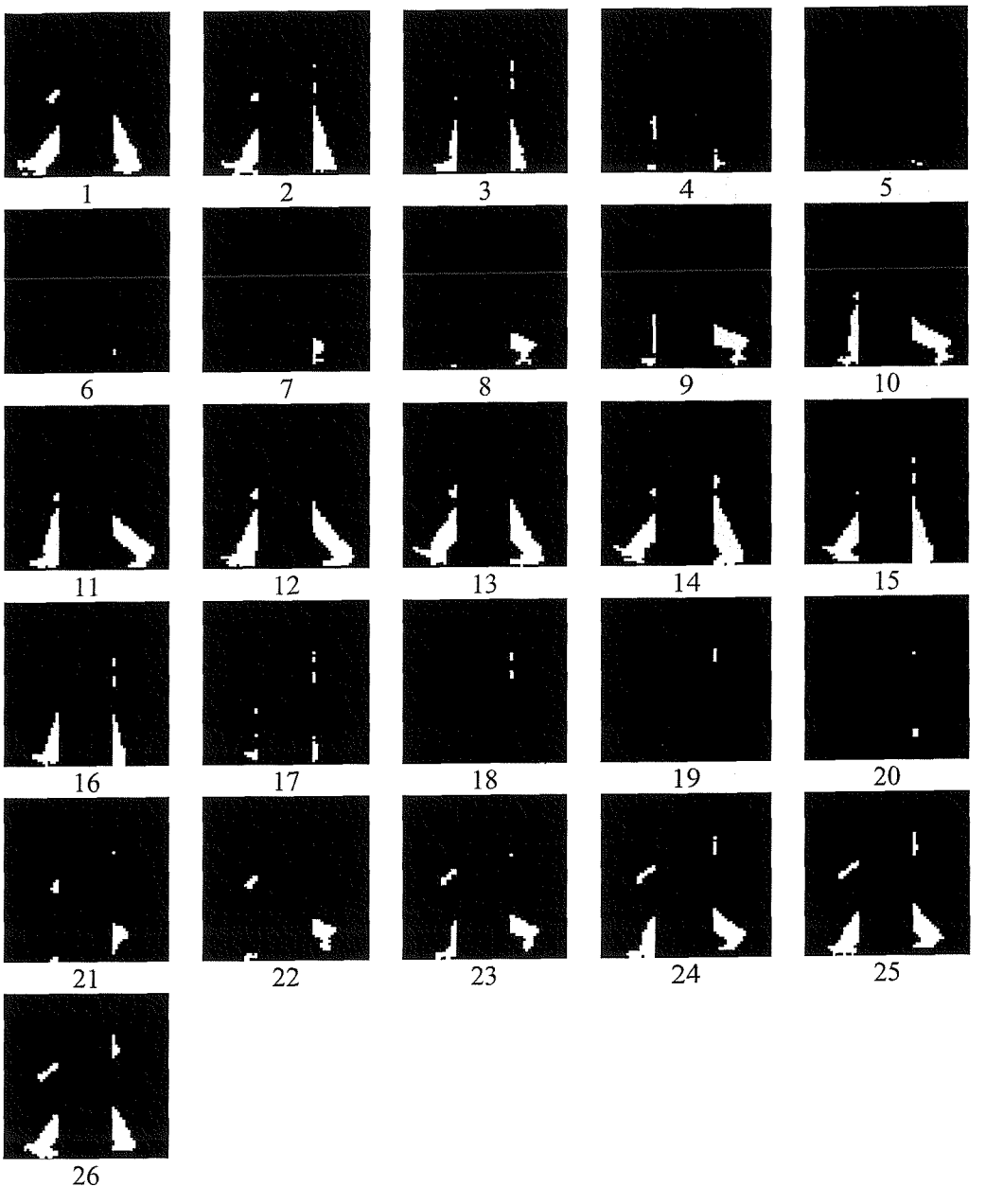

Appendix D – Image frames masked with a white rectangular bar of width 25 pixels

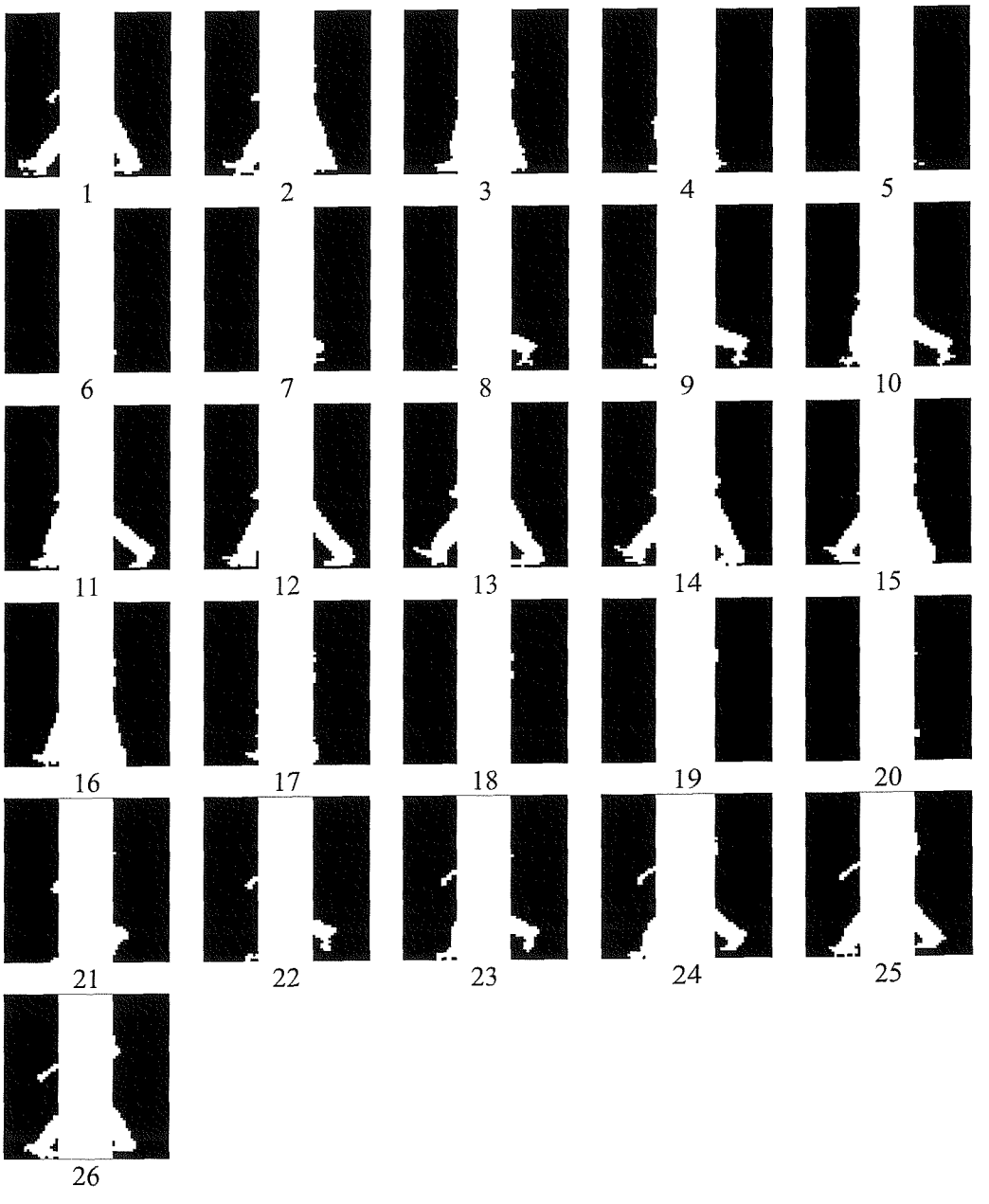

Appendix E – A gait cycle with about 75% missing frames

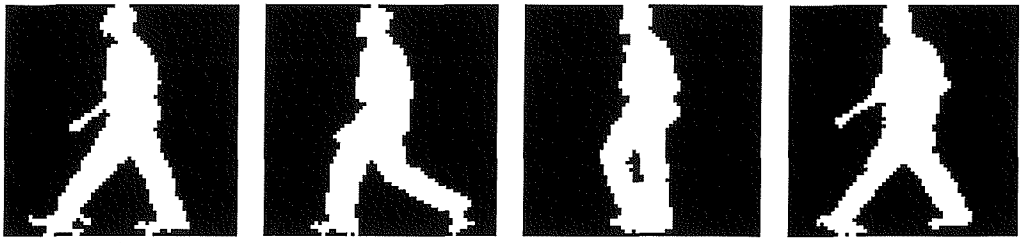

This is a gait cycle with about 75% missing frames. The above shows the situation where every seven consecutive image frames as missing. The numbers under the image frames are the frame numbers within the sequence.

Appendix F –Some image sequences that failed recognition

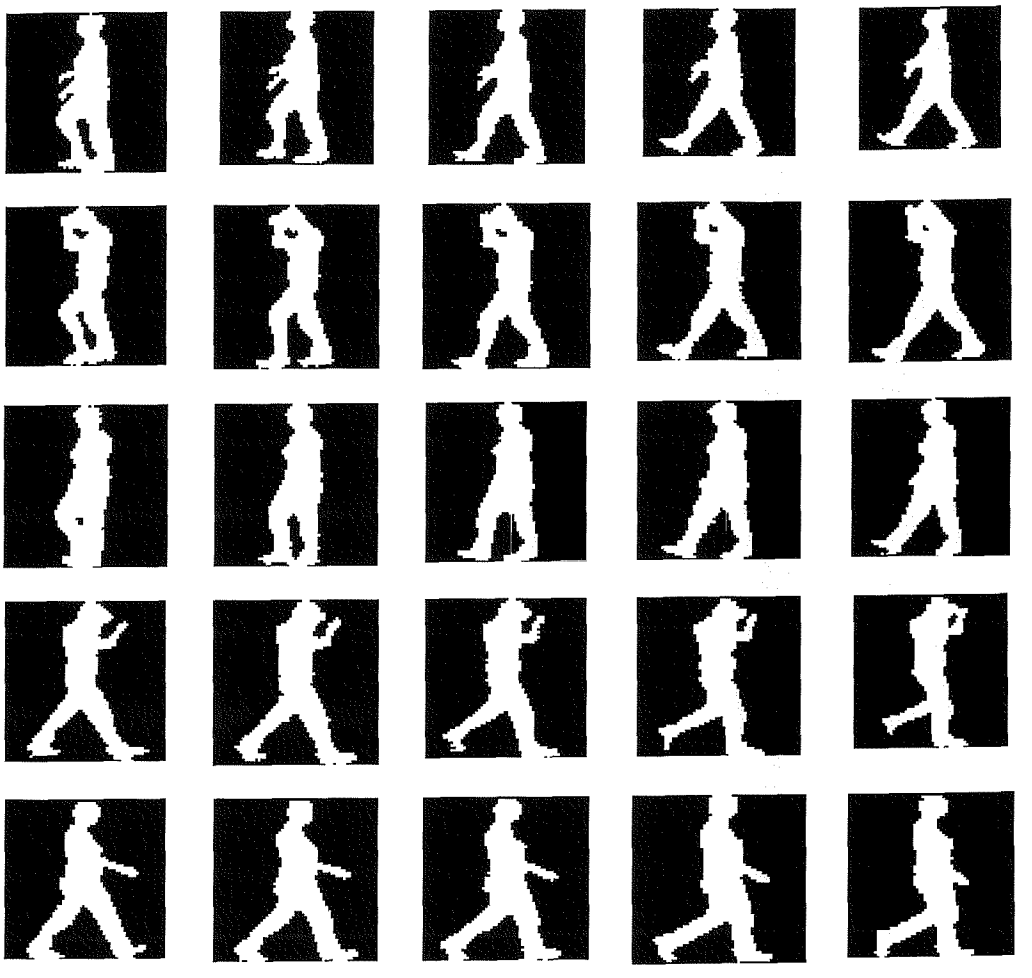

(a) Subject 067

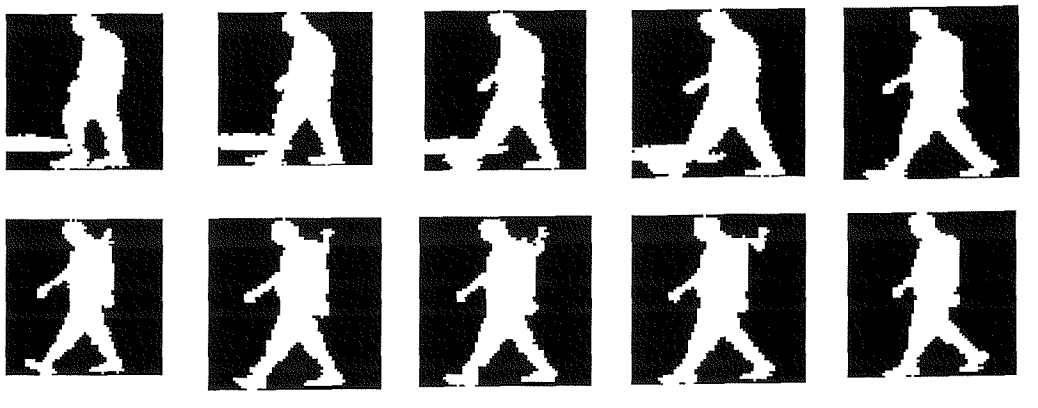

(b) Subject 054

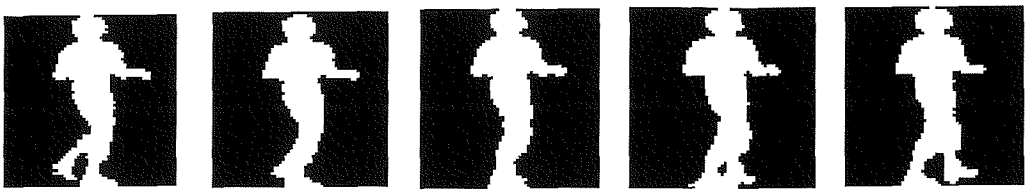

(c) Subject 110

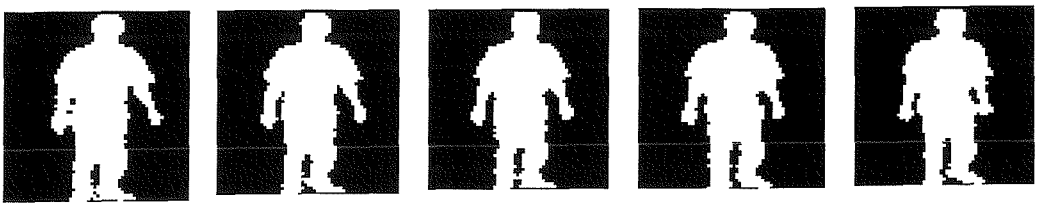

(d) Subject 29

Appendix G – Noise algorithm

The following pseudo code defines the algorithm used in adding artificial noise to image frames for evaluating performance of the symmetry operator with respect to noise. *NoiseLevel* defines the percentage of noise to be added to the image frames. A *NoiseLevel* of 50% means that half the pixels in image are flipped from their previous binary value. *Rand* 1 and *rand2* are random numbers.

```
For each image frame in a sequence;
    For each pixel(x,y) in image;
      Generate random number, rand1
      Generate random number, rand2
      If rand1 <= NoiseLevel
        If rand2 <= 0.5 then
          Pixel(x,y) ← 1;
        Else
            Pixel(x,y) ← 0;
    Return image sequence;
```

References

1. Pratt, D., *Some Aspects of Modern Orthotics.* Physiol Meas., 1994. **15**(1): p. 1-27.

2. Sadeghi, H., et al., *Symmetry and Limb Dominance in Able Bodied Gait: A Review.* Gait and Posture, 2000. **12**: p. 34-45.

3. Hayfron-Acquah, J.B., M.S. Nixon, and J.N. Carter, *Automatic Gait Recognition via the Generalised Symmetry Operator.* BMVA Workshop Understanding Visual Behaviour, 2001.

4. Hayfron-Acquah, J.B., M.S. Nixon, and J.N. Carter, *Automatic Gait Recognition by Symmetry Analysis.* Proc. Audio-and-Video-Based Biometric Person Authentication, 2001: p. 272-277.

5. Hayfron-Acquah, J.B., M.S. Nixon, and J.N. Carter, *Recognising Human and Animal Movement by Symmetry.* Proc. IEEE International Conference on Image Processing, 2001: p. 290-293.

6. Hayfron-Acquah, J., M. Nixon, and J. Carter, *Human Identification by Spatio-Temporal Symmetry.* 16th International Conference on Pattern Recognition, 2002: p. 632-635.

7. Cutting, J.T., D.R. Proffitt, and L.T. Kozlowski, *A Biomechanical Invariant for Gait Perception.* Journal of Experimental Psychology: Human Perception and Performance, 1978: p. 357-372.

8. Dingwell, J. and B. Davies, *A Rehabilitation Treadmill With Software Providing Real-Time Gait Analysis and Visual Feedback.* Transactions of ASME, Journal of Biomechanical Engineering, 1996: p. 253-255.

9. Griffin, M., S. Olney, and I. McBride, *Role of Symmetry in Gait Performance of Stroke Patients with Hemiplegia.* Gait Posture, 1995. **3**: p. 132-142.

10. Bigun, J., *Pattern Recognition by Detection of Local Symmetry.* Pattern Recognition and Artificial Intelligence, 1988: p. 75-90.

11. Bigun, J., *Pattern Recognition in Images by Symmetries and Coordinate Transformations.* Computer Vision and Image Understanding, 1997: p. 290-307.

12. Blum, H. and R.N. Nigel, *Shape Description Using Weighted Axis Symmetry.* Pattern Recognition, 1978. **10**: p. 169-180.

13. Bonneh, Y., D. Reisfeld, and Y. Yeshurun, *Quantification of Local Symmetry: Application for Texture Descrimination.* Spatial-Vision, 1994. **8**(4): p. 515-530.

14. Marola, G., *On Detection of the Axis of Symmetry and Almost Symmetric Images.* IEEE Transactions on Pattern analysis and Machine Intelligence, 1989. **11**(1): p. 104-108.

15. Cunado, D., et al., *Gait Extraction and Description by Evidence-Gathering.* Proc. Audio and Video based Biometric Person Authentication, 1999: p. 43-48.

16. Cutting, J.E. and L.T. Kozlowski, *Recognizing Friends by Their Walk: Gait Perception Without Familiarity Cues.* Bulletin of the Psychonomic Society, 1977. **9**(5): p. 353-356.

17. Little, J.J. and J.E. Boyd, *Recognising People by Their Gait: the Shape of Motion.* Videre, International Journal of Computer Vision, 1998. **14**(6): p. 83-105.

18. Parsons, C.J. and M.S. Nixon, *Introducing Focus in the Generalized Symmetry Operator.* IEEE Signal Processing Letters, 1999. **6**(3): p. 49-51.

19. Stevenage, S.V., M.S. Nixon, and K. Vince, *Visual Analysis of Gait as a Cue to Identity.* Applied Cognitive Psychology, 1999(13): p. 513-526.

20. Reisfeld, D., H. Wolfson, and Y. Yeshurun, *Context-Free Attentional Operators: The Generalized Symmetry Transform.* International Journal of Computer Vision, 1995. **14**: p. 119-130.

21. Murray, M.P., A.B. Drought, and R.C. Kory, *Walking Patterns of Normal Men.* Journal of Bone Joint Surgery, 1964. **46-A**(2): p. 335-360.

22. Murray, M.P., *Gait as a Total Pattern of Movement.* American Journal of Physical Medicine, 1967. **46**(1): p. 290-332.

23. Nixon, M., et al., *Automatic Gait Recognition: BIOMETRICS - Personal Identification in Networked Society*, A. Jain, R. Bolle, and S. Pankanti, Editors. 1999, Kluwer Academic Publishers. p. 231-249.

24. Johansson, G., *Visual Perception of Biological Motion and a Model for its Analysis.* Perception Psychophysics, 1973. **14**(2): p. 201-211.

25. Dittrich, W., *Action Categories and the Perception of Biological Motion.* Perception, 1993. **22**: p. 15-22.

26. Bingham, G., R. Schmidt, and L. Rosenblum, *Dynamics and the Orientation of Kinematic Forms in Visual Event Recognition.* Journal of Experimental Psychologoy: Human Perception and Performance, 1995. **21**(6): p. 1473-1493.

27. Kozlowski, L.T. and J.E. Cutting, *Recognizing the Sex of a Walker From a Dynamic Point-Light Display.* Perception and Psychophysics, 1977. **21**(6): p. 575-580.

28. Akita, K., *Image Analysis of Real World Human Motion.* Pattern Recognition, 1984. **17**(1): p. 73-83.

29. H-J Lee, L. and Z. Chen, *Determination of 3D Human Body Structures From a Single View.* Computer Vision, Graphics, and Image Processing, 1985. **30**: p. 148-168.

30. Guo, Y., G. Xu, and S. Tsuji, *Understanding Human Motion Patterns.* Proceedings 12th International Conference on Pattern Recognition, 1994. **2**: p. 325-329.

31. Dockstader, S., K. Bergkessel, and A. Tekalp, *Feature Extraction for the Analysis of Gait and Human Motion.* 16th International Conference for Pattern Recognition, 2002: p. 5-8.

32. Hogg, D., *Model-Based Vision-A Program to See a Walking Person.* Image and Vision Computing, 1983. **1**(1): p. 5-20.

33. Rohr, K., *Incremental Recognition of Pedestrians from Image Sequences.* Proceedings Conference Computer Vision and Pattern Recognition, 1993: p. 8-13.

34. Kurakake, S. and R. Nevatia, *Description and Tracking of Moving Articulated Objects.* Systems and Computers in Japan, 1994. **25**(8): p. 16-26.

35. Kauth, R., A. Pentland, and G. Thomas, *Blob: An Unsupervised Clustering Approach to Spatial Pre-processing of MSS Imagery.* Proceedings 11th International Symposium on Remote Sensing of the Environment, 1977: p. 1309-1317.

36. Azarbayejani, A., et al., *Pfinder: Real-time 3-D tracking of Human Body.* IEEE Trans. on PAMI, 1997. **19**(7): p. 780-785.

37. Campbell, L. and A. Bobick, *Recognition of Human Body Motion Using Phase Space Constraints.* 1995, MIT Media Lab Perceptual Computing Report 309.

38. Gavrila, D. and L. Davis, *3-D Model Based Tracking of Humans in Action: A Multi-View Approach.* Proceedings International Conference Computer Vision and Pattern Recognition, 1996: p. 73-80.

39. Bhanu, B. and J. Han, *Individual Recognition by Kinematic-Based Gait Analysis.* Proc. 16th International Conference on Pattern Recognition, 2002. **3**: p. 343-347.

40. Bobick, A. and A. Johnson, *Gait Recognition using Static, Activity-specific Parameters.* IEEE Computer Vision and Pattern Recognition, 2001. **1**: p. 423-430.

41. Cunado, D., M.S. Nixon, and J.N. Carter, *Automatic Gait Recognition via Model-Based Evidence Gathering.* Proc. AutoID99: IEEE Workshop on Automated ID Technologies Summit, 1999: p. 27-30.

42. Foster, J., M. Nixon, and A. Prugel-Bennett, *New Area Based Metrics for Automatic Gait Recognition.* Proc. British Machine Vision Conference 2001, 2001: p. 233-242.

43. Huang, P.S., C.J. Harris, and M.S. Nixon, *Recognising Humans by Gait via Parametric Canonical Space.* Artificial Intelligence in Engineering, 1999. **13**: p. 359-366.

44. Lee, L. and W. Grimson, *Gait Analysis for Recognition and Classification.* Proc. 5th IEEE Face and Gesture Recognition, 2002: p. 155-162.

45. Philips, P., et al., *The Gait Identification Challenge problem:Data Sets and Baseline Algorithm.* International Conference for Pattern Recognition, 2002: p. 385-388.

46. Shutler, J.D., M.S. Nixon, and C.J. Harris, *Statistical Gait Recognition via Temporal Moments.* 4th IEEE Southwest Symposium on Image Analysis and Interpretation, Texas, 2000: p. 291-295.

47. Wang, L., W. Hu, and T. Tan, *A New Attempt to Gait-Based Human Identification.* Proc. 16th International Conference on Pattern Recognition, 2002. **1**: p. 115-119.

48. Yam, C.-Y., M.S. Nixon, and J.N. Carter, *Extended Model-Based Automatic Gait Recognition of Walking and Running.* Proc. 3rd Audio- and Video-Based Biometric Person Authentication, 2001: p. 284-294.

49. Niyogi, S.A. and E.H. Adelson, *Analyzing and Recognizing Walking Figures in XYT.* Proc. Computer Vision and Pattern Recognition, 1994: p. 469-474.

50. Nash, J., J. Carter, and M. Nixon, *Extraction of Moving Articulated-Objects by Evidence Gathering.* Proc. British Machine Vision Conference, 1998. **2**: p. 609-618.

51. Yam, C.-Y., M.S. Nixon, and J.N. Carter, *Gait Recognition by Walking and Running: A Model-based Approach.* Proc. 5th Asian Conference on Computer Vision, 2002: p. 1-6.

52. Murase, H. and R. Sakai, *Moving Object Recognition in Eigenspace Representation: Gait Analysis and Lip Reading.* Pattern Recognition Letters, 1996. **17**: p. 155-162.

53. Huang, P.S., C.J. Harris, and M.S. Nixon, *Human Gait Recognition in Canonical Space using Temporal Template.* IEE Proc. Vision Image and Signal Processing, 1999. **146**(2): p. 93-100.

54. BenAbdelkader, C., J. Cutting, and L. Davis, *Motion-based Recognition of People in EigenGait Space.* Proc. 5th IEEE Face and Gesture Recognition, 2002: p. 378-384.

55. Johnson, A.Y. and A.F. Bobick, *A Multi-View Method for Gait Recognition Using Static Body Parameters.* 3rd International Conference AVBPA, 2001: p. 301-311.

56. Shutler, J.D., M.S. Nixon, and C.J. Harris, *Statistical Gait Recognition via Velocity Moments.* IEE Electronics and Communications, Colloquium, Visual Biometrics, London, 2000: p. 1-5.

57. Shutler, J., M. Nixon, and C. Harris, *Zernike Velocity Moments for Description and Recognition of Moving Shapes.* British Machine Vision Conference 2001, 2001: p. 705-714.

58. Foster, J., M. Nixon, and A. Prugel-Bennett, *New Area Measures for Automatic Gait Recognition.* BMVA Workshop Understanding Visual Behaviour, 2001.

59. Foster, J.P., M.S. Nixon, and A. Prugel-Bennett, *New Area Based Measures for Gait Recognition.* Proc. Audio- and Video-Based Biometric Person Authentication, 2001: p. 312-317.

60. Collins, R., R. Gross, and J. Shi, *Silhouette-based Human Identification from Body Shape and Gait.* 5th IEEE Face and Gesture Recognition, 2002: p. 366-371.

61. Phillips, P.J., et al., *Baseline Results for the Challenge Problem of Human ID Using Gait Analysis.* Proc 5th Automatic Face and Gesture Recognition, 2002: p. 137-143.

62. Herzog, W., et al., *Asymmetries in Ground Reaction Force Patterns in Normal Human Gait.* Medical Science Sports Exerc., 1982. **21**(1): p. 110-114.

63. Soudan, K., *Standardization of Gait Kinematic Data Using a Gait Symmetry Index and Fourier analysis.* In: Biomechanics: Principles and Applications, Development in Biomechanics, 1982. **1**: p. 135-140.

64. Hesse, S., et al., *Asymmetry of Gait Initiation in Hemiparetic Stroke Patients.* Arch. Phys. Med. Rehab., 1997. **78**(7): p. 719-724.

65. Gundersen, L., et al., *Bilateral Analysis of the Knee and Ankle During Gait: An Examination of the Relationship Between Lateral Dominance and Symmetry.* Phy. Ther., 1989. **69**(8): p. 640-650.

66. Gabbard, C., *Coming to Terms with Laterality.* Journal of Psychology, 1997. **131**(5): p. 561-564.

67. Giakas, G. and V. Baltzopoulos, *Time and Frequency Domain Analysis of Ground Reaction Force During Walking:an investigation of Variability and Symmetry.* Gait Posture, 1997. **5**: p. 189-197.

68. Menard, M., et al., *Comparative Biomechanical Analysis of Energy-storing Prosthetic Feet.* Arch. Phys. Med. Rehab., 1192. **73**(5): p. 451-458.

69. Hamill, J., B. Bates, and K. Knutzen, *Ground Reaction Force Symmetry During Walking and Running.* Research Quarterly, 1984. **55**: p. 289-293.

70. Chou, L., S. Song, and L. Draganich, *Predicting the Kinematics and Kinetics of Gait Based on the Optimum Trajectory of the Swing Limb.* Journal of Biotech, 1995. **28**(4): p. 377-385.

71. Wall, J. and G. Turnbull, *Gait Asymmetries in Residual Hemiplegia.* Arch. Phys. Med. Rehab., 1986. **67**: p. 550-553.

72. Perttunen, J., *Foot loading in Normal Pathological Walking*, in *Faculty of sports and Health Sciences*. 2002, PhD thesis, University of JYVASKYLA.

73. Singh, I., *Function Asymmetry in the Lower Limbs.* Acta Anatomica, 1970. **77**: p. 131-138.

74. Rosenrot, P., *Asymmetry of Gait and the Relationship to Lower Limb Dominance.* Proc. of the special conference of the Canadian Society of Biomechanics, 1980: p. 26-27.

75. Wheelwright, E., et al., *Temporal and spatial parameters of gait in children, I: normal control data.* Dev. Med Child Neurol, 1993. **35**(2): p. 102-113.

76. Dickey, J. and D. Winter, *Adaptations in Gait resulting from Unilateral Ischaemic Block of Leg.* Clinical Biomech., 1992. **7**: p. 215-225.

77. Reisfeld, D., H. Wolfson, and Y. Yeshurun, *Robust Detection of Facial Features by Generalised Symmetry.* Proc. int'l Conf. Pattern recognition, 1992: p. 117-120.

78. Edelman, S., D. Reisfeld, and Y. Yeshurun, *Learning to Recognise Face From Examples.* In second European Conference on Computer Vision, 1992: p. 787-791.

79. Leyton, M., *Symmetry, Casuality, Mind.* MIT Press, Cambridge, MA, 1992.

80. Reisfeld, D., H. Wolfson, and Y. Yeshurun, *Detection of Interest Points Using Symmetry.* In Proceedings of the 3rd International Conference on Computer Vision, 1990: p. 62-65.

81. Brady, M. and M. H Asada, *Smoothed Local Symmetries and thier Implementation.* Int. J. Robotics Research, 1984. **3**(3): p. 36-61.

82. Marola, G., *Using Symmetry for Detecting and Locating Objects in a Picture.* Computer Vision Graphics Image Processing, 1989: p. 175-195.

83. Oh, W.G., M. Asada, and S. Tsuji, *Model Based Matching Using Skewed Symmetry Information.* Proc 9th International Conference on Pattern Recognition, 1988: p. 1043-1045.

84. Ponce, J., *On Characterizing Ribbons and Finding Skewed Symmetries.* Computer Vision, Graphics, and Image Processing, 1990. **52**: p. 328-340.

85. Reisfeld, D., *Generalised Symmetry Transforms:Attentional Mechanisms and Face Recognition.* 1993, Tel-Aviv University: Tel-Aviv.

86. Fogel, I. and D. Sagi, *Gabor Filters as Texture Discrimnination.* Biological Cybernatics, 1989. **61**: p. 103-111.

87. Krose, B., *Local Structure Analyzers as Determinants of Preattentive Texture Discrimination.* Biological Cybernatics, 1987. **55**: p. 289-298.

88. Rubenstein, B. and D. Sagi, *Spatial Variability as a Limiting Factor in Texture Discrimination Tasks: Implecations for Performance Asymmetries.* Journal of Opt. Soc. America, 1990. **7**: p. 1632-1643.

89. Malik, J. and P. Perona, *Preattentive Texture Discrimation with Early Vision Mechanisms.* Journal of Opt. Soc. America, 1990. **7**(5): p. 923-932.

90. Bergen, J. and E. Adelson, *Early Vision and Texture Perception.* Nature, 1988. **333**: p. 363-364.

91. Buf, J. and F. Heitger, *A Neural Network for Detecting Symmetry Orders.* In Proc. 7th Int. Conf. on Image Analysis, Bari, Italy, 1993.

92. Loy, G. and A. Zelinsky, *A Fast Radial Symmetry Transform for Detecting Points of Interest.* 7th European Conference on Computer Vision, ECCV 2002, 2002. **1**: p. 358-368.

93. Gesu, V. and C. Valenti, *The Discrete Symmetry Transform in Computer Vision.* Technical Report DMA 011 95, Palermo University, 1995.

94. Lin, C.-C. and W.-C. Lin, *Extracting Facial Features by an Inhibitory Mechanism Based on Gradient Distributions.* Pattern Recognition, 1996. **29**(12): p. 2079-2101.

95. Minor, L. and J. Sklansky, *Detection and Segmentation of Blobs in Infrared Images.* IEEE Trans. on Systems, Man & Cybernatics, SMC, March 1981. **11**(3): p. 194-201.

96. Sela, G. and M. Levine, *Real-Time Attention for Robotic Vision.* Real-Time Imaging, 1997. **3**: p. 173-194.

97. Sun, Q., W. Huang, and J. Wu, *Face Detection Based on Color and Local Symmetry Information.* In proc. of 3rd IEEE International Conference on Automatic Face and Gesture recognition, 1998: p. 130-135.

98. Li, Y. and H. Kabatake, *Extraction of Facial Sketech Image Based on Morphological Processing.* In Proc. of the 4th IEEE International Conference on Image Processing, 1997. **3**: p. 316-319.

99. Loy, G. and A. Zelinsky, *A Fast Radial Symmetry Transform for Detecting Points of Interest.* 7th European Conference on Computer Vision, 2002. **1**: p. 358-368.

100. Gesu, V. and C. Valenti, *The Discrete Symmetry Transform in Computer Vision*, in *Technical Report DMA 011 95.* 1995, Palermo University.

101. Bonneh, Y., D. Reisfeld, and Y. Yeshurun, *Texture Descrimination by Local Generalised Symmetry.* In Proceeding of the 4th International Conference on Computer Vision, 1993: p. 461-465.

102. Kiryati, N. and Y. Gofman, *Detecting Symmetry in Grey Level Images: The Global Optimization Approach.* International Journal of Computer Vision, 1998. **29**(1): p. 29-45.

103. Sun, J., et al., *The Influence of Surface Slope on Human Gait Characteristics: A study of Urban Pedestrians Walking on an Inclined Surface.* Ergonomics, 1996. **39 (4)**: p. 677-692.

104. Zabrodsky, H., S. Peleg, and D. Avnir, *Symmetry as a Continous Feature.* IEEE Trans. Pattern Anal. Machine Intell., 1995. **17**: p. 1154-1166.

105. Nalwa, V., *Line-Drawing Interpretation: Bilateral Symmetry.* IEEE Trans. Pattern Anal. Machine Intell., 1989. **11**: p. 1117-1120.

106. Parui, S. and D. Majumder, *Symmetry Analysis by Computer.* Pattern recognition, 1983. **16**: p. 63-67.

107. Gool, L.V., et al., *Symmetry from Shape and Shape from Symmetry.* Int. J. Robotics Research, 1995. **14**: p. 407-424.

108. Attalah, M., *On Symmetry detection.* IEEE Trans. Computing, 1985. **34**: p. 663-666.

109. Bluthoff, H., J. Little, and T. Poggio, *A Parallel Algorithm for Real-Time Computation of Optical Flow.* Letters to Nature, 1989. **337**(9): p. 549-553.

110. Shutler, J., *Velocity Moments for Holistic Shape Description of Temporal Features*, in *Department of Electronics and Computer Science.* 2002, PhD Thesis, University of Southampton: Southampton, England.

111. Gross, R. and J. Shi, *The CMU motion of body (MOBO) Database.* Technical Report, CMU-RI-TR-01-18, 2001.

112. Shutler, J. and M. Grant, *The Large Southampton Human ID Gait Database.* Technical Report, ISIS Research Group, ECS, University of Southampton, 2002.

113. Dubuisson, M.-P. and A. Jain, *Contour Extraction of Moving Objects in Complex Outdoor Scenes.* International Journal of Computer Vision, 1995. **14**(6): p. 83-105.

114. Foster, J., *Automatic Gait recognition via Area Based Metrics*, in *Department of Electronics and Computer science.* 2002, PhD thesis, University of Southampton: Southampton, England.

115. Shutler, J., *Velocity Moments for Holistic Shape description of temporal Features*, in *Electronics and Computer Science Department.* 2002, University of Southampton: Southampton.

116. Johnson, A., *A New Method for Human Identification Using Static, Activity-Specific Parameters*, in *School of Electrical and Computer Engineering.* 2002, PhD thesis, Georgia Institute of Technology: Georgia.

117. Shakharovich, G., L. Lee, and T. Darell, *Interated face and gait recognition from multiple views.* In IEEE Conference on CVPR, 2001.

118. Kale, A., V. Kruger, and R. Chellappa, *Hidden Markov models for the recognition of gait.* 2001, University of Maryland: Maryland.

119. Nixon, M., et al., *New Advances in automatic Gait Recognition.* Elsevier Information Security Technical Report, At press.